4930

NATIONAL LIBRARY

OTTAWA

BIBLIOTHÈQUE NATIONALE

OTTAWA

NAME OF AUTHOR..Norman E. Davison.....

TITLE OF THESIS..The Reaction Mechanism.....
..of the ^{16}O+d Reactions.....
.....

UNIVERSITY..University of Alberta.....

DEGREE...Ph.D.....YEAR GRANTED..1969.....

Permission is hereby granted to THE NATIONAL LIBRARY OF CANADA to microfilm this thesis and to lend or sell copies of the film.

The author reserves other publication rights, and neither the thesis nor extensive extracts from it may be printed or otherwise reproduced without the author's written permission.

(Signed) Norman E. Davison

PERMANENT ADDRESS:

c/o L'Institut de Recherche
Nucleaire, St.
Strasbourg-Cronenbourg
France

DATED. October 16. 19

NL-91

THE UNIVERSITY OF ALBERTA

THE REACTION MECHANISM OF THE ^{16}O + d REACTIONS

by

© Norman Edgar Davison

A THESIS

SUBMITTED TO THE FACULTY OF GRADUATE STUDIES

IN PARTIAL FULFILLMENT OF THE REQUIREMENTS FOR THE DEGREE

OF DOCTOR OF PHILOSOPHY

DEPARTMENT OF PHYSICS

EDMONTON, ALBERTA

Fall, 1969

UNIVERSITY OF ALBERTA

FACULTY OF GRADUATE STUDIES

The undersigned certify that they have read, and recommend to the Faculty of Graduate Studies for acceptance, a thesis entitled THE REACTION MECHANISM OF THE ^{16}O + d REACTIONS submitted by Norman Edgar Davison in partial fulfillment of the requirements for the degree of Doctor of Philosophy.

(Supervisor)

External Examiner

Date October 15, 1969

ABSTRACT

The reactions $^{16}O(d,d)^{16}O$, $^{16}O(d,p)^{17}O$ and $^{16}O(d,n)^{17}F$ have been studied in the deuteron energy range 4.00 to 6.00 MeV in order to determine to what extent current theories can satisfactorily describe these reactions. The deuteron elastic scattering data were analyzed to obtain optical model parameters suitable for the energy range of the present work. It was found that the theoretical curves from both the optical and DWBA model fit the experimental data significantly better when the deuteron optical model potentials had been obtained using a spin-orbit potential in the analysis of the elastic scattering data. Spectroscopic factors obtained for the ground and first excited states of ^{17}O and ^{17}F using the DWBA theory are in satisfactory agreement with theoretical predictions and with values obtained by previous workers. Small, but nonzero, spectroscopic factors have been calculated for the states at 3.058 and 3.846 MeV excitation in ^{17}O using data measured in this work and in previous experiments. The sum of the calculated direct interaction and compound nucleus cross sections is in good agreement with experimental data for all states studied whether they were populated primarily by direct or compound nucleus reactions. The calculated compound nucleus lifetimes are in agreement with values obtained from the analysis of the fluctuations in the yield curves. It was thus found that the combined DWBA and Hauser-Feshbach theories and the optical model give a good description of the energy averaged properties of the ^{16}O + d reactions between 4.00 and 6.00 MeV.

ACKNOWLEDGEMENTS

In the course of several years, one must inevitably learn some physics. However, this is not the most important aspect of graduate studies. The most lasting effect of any staff member or student on another is in the development of research habits. In this context, I am especially indebted to my supervisor Dr. W.J. McDonald. He has displayed a combination of thoroughness, objectivity and ability to tell students that they are wrong without injuring their self-confidence, that I hope I can emulate in the future.

Dr. G.C. Neilson and Dr. G. Roy have made many suggestions toward this project. They have been particularly helpful when I have become too involved in a narrow problem, and have been unable to "see the forest for the trees".

Mr. Jim Easton has not hesitated to express his opinions concerning the proper way to write computer programs. He has extricated me from some more or less serious situations, and has convinced me that others would not have arisen if I had followed his advice in the first place.

Physics can not be all work and no play. Messrs. Jan Bogaards, Georges Carola, Bob Humphries and Bill Saunders have amply demonstrated this through numerous sessions that enabled all of us to survive the tensions of obtaining a degree. It must also be noted that the data used in this thesis would have been of much lower quality had it not been for the vigilance of my fellow students.

The experimental portions of this work would not have been carried out at all if Messrs. Jock Elliott, Lars Holm, Ron Popik, Paul Karvonen and Con Green had not spent a great deal of time maintaining the accelerator and electronics. In many instances, Jock gave up his weekends to get the accelerator working for us.

The typing of the thesis was done by Miss Elsie Hawirko. Her attitude toward this undertaking is exemplified by the fact that she began work on her first day back from holidays. Whereas many people drag through the first week after their vacations, Elsie worked late on the first day. Her enthusiasm has helped get this thesis done on time.

The financial assistance of the National Research Council of Canada and the University of Alberta are gratefully acknowledged. Extra teaching duties inevitably entail much time lost in reorganizing ones thoughts and notes. The financial assistance given me has greatly helped my work and peace of mind.

Finally I would like to thank my wife Nancy for her patience and her encouragement on days when everything was going wrong. Married students are "expected" to thank their wives, but I feel that Nancy has been far above average in her acceptance without complaint of odd working hours and last minute changes in plans that meant much to both of us.

TABLE OF CONTENTS

LIST OF TABLES

LIST OF FIGURES

CHAPTER 1

INTRODUCTION

The study of (d,n) and (d,p) stripping reactions has produced a wealth of nuclear structure information not easily obtainable in other ways. The angular momentum transferred to the residual nucleus (the ℓ-value) is easily determined in many cases, and a somewhat more involved analysis allows the experimenter to determine the spectroscopic factor which is important in assessing the applicability of various nuclear models. The analysis of stripping reactions is fairly straightforward when competing reaction mechanisms contribute only a negligible portion of the total cross section.

For much of the work of current interest, competing reactions are not negligible. Determination of the spectroscopic factor frequently involves considering the effect of compound nucleus reactions even when the stripping pattern is strong. It is thus necessary to investigate in detail the accuracy of results obtained using current compound nucleus calculations.

An even more crucial need for a study of reaction mechanisms is provided by the current interest in stripping reactions which must proceed through a small part of the wavefunction. Such a situation arises, for instance, in the study of isospin forbidden transitions. The direct interaction cross section may be quite small, and indeed

of the same order of magnitude as the cross section from competing reactions.

It may be argued that such work is best carried out at higher energies where compound nucleus reactions are relatively much weaker. However, previous work has shown considerable structure in the $^{16}O(d,p)^{17}O$ yield curve (Al 67) in the vicinity of 12 MeV deuteron energy, and even studies of the reaction $^{52}Cr(d,p)^{53}Cr$ at 11 MeV (Al 66) were somewhat affected by compound nucleus processes. In addition, work at higher energies is frequently limited by technical problems not encountered to the same extent at lower energies. For instance, the energy resolution of a neutron time-of-flight spectrometer decreases as the neutron energy rises, and the background in charged particle studies increases rapidly with energy.

Previous studies have touched on various aspects of the reaction mechanisms found associated with stripping reactions, but there has been a singular lack of attempts to construct a self-consistent picture describing compound nucleus reactions and direct interactions simultaneously. There is not much question as to the ability of the current theories to allow the determination of ℓ-values in light nuclei, but whether more detailed information is obtainable is open to question. Since the study of direct interactions is potentially a very useful tool for studying nuclear structure, it is likely that efforts to improve the reliability of calculations will continue. Concurrently, it will be necessary to investigate limitations in the application of the theory. This will include not only a study of direct interactions,

but studies also of compound nucleus reactions, interference effects and other small effects which may turn up in detailed studies.

In the experiment reported in this thesis, the optical model parameters describing the elastic scattering of deuterons from oxygen in the energy range 4.00 to 6.00 MeV were obtained. Then using previously reported optical model parameters for the neutron and proton, an attempt was made to simultaneously describe several features of the compound nucleus and direct interactions. In addition, an attempt was made to determine if the combined compound nucleus and direct interaction mechanisms could account for all the features observed.

In chapter 2, the theory behind this study is outlined. As several excellent review articles exist on most of the topics considered, the theories are not considered here in great detail.

Although several reactions have been studied in this work, it is difficult to consider them separately. Consequently, the experimental techniques used in obtaining all the data are discussed in chapter 3. The analysis and discussion of the results are presented in chapter 4. Finally in the fifth chapter, the results are summarized and conclusions are drawn. Suggestions are made concerning ways in which the present study could be extended.

CHAPTER 2

THEORY

2.1 Optical Model

The study of nuclear physics frequently involves a situation in which a complex nucleus is bombarded by a projectile. Ideally, we would like to consider all the 2-body forces between the nucleons of the nucleus and projectile when trying to describe the reaction. This approach is much too complicated in most cases. The approximation that the many-body problem may be reduced to the interaction of two structureless bodies interacting through an average potential is known as the optical model. The form of the optical model potential used in this work is:

$$U(r) = V_C(r) - Vf(x_R) + iW_V f(x_I) + 4i\, W_S \frac{d}{dx_I} f(x_I) - \frac{V_{SO}}{r_{SO}} \frac{d}{dr_{SO}} f(x_{SO}) \vec{\ell}\cdot\vec{s} \qquad 2.1$$

In the preceeding, $f(x) = (1+e^x)^{-1}$, and is known as the Woods-Saxon form factor. In addition, the symbols

$$x_R = \frac{r - r_R A^{\frac{1}{3}}}{a_R} \quad ; \quad x_{SO} = \frac{r - r_{SO} A^{\frac{1}{3}}}{a_{SO}} \quad ,$$

and $$x_I = \frac{r - r_I A^{\frac{1}{3}}}{a_I}$$ are used.

a_I, a_R and a_{SO} are diffuseness parameters, and r_I, r_R and r_{SO} are radius parameters of the Woods-Saxon form factors. The meanings of each of the symbols used

are given in Appendix B, and are discussed further below.

In analogy with light interacting with a translucent material, there are 2 basic types of potential:

(a) refractive forms. The wavelength of the incident particle is changed, but the total flux is unaltered. Such potentials are symbolized by V's in expression 2.1.

(b) absorptive forms. Particles in the incident beam disappear in some unspecified manner. Absorption into the target to form a compound nucleus, breakup and other inelastic reactions are among the means whereby particles are lost. This type of potential is symbolized by the W's in expression 2.1.

The Woods-Saxon form factor has been chosen primarily because it is a relatively simple mathematical form capable of representing two important nuclear properties. Firstly, the nearly constant value of f(x) for small values of x reflects the saturation properties of nuclear forces. The nuclear density is nearly constant over the majority of the nuclear volume. Secondly, the value of a_R gives the diffuseness of the nuclear surface. It has been known since the early days of the shell model that the shape of the nuclear potential lay somewhere between the parabola of the harmonic oscillator and the square well. More recently, the effect of the diffuseness on nuclear reactions has been made apparent. The relative number of particles reflected or absorbed at the nuclear surface is strongly affected by the surface diffuseness (Vo 62).

The term $V_C(r)$ is the Coulomb potential of a uniformly charged sphere. The radius is usually chosen to be the same as the radius of

the refractive or real well. With the present accuracy of calculations and experiments, there seems to be little need to consider refinements such as the neutron excess in the nuclear surface or the surface diffuseness.

The potential $Vf(x_R)$ is the most important of the refractive potentials. It is meant to represent the sum of all the spin-independent 2-body forces between the nucleons of the nucleus and the projectile. Since the range of the nucleon-nucleon force is small, the spacial distribution of the real potential will resemble that of the nucleons in the nucleus. The radius may be somewhat larger than the electron scattering radius of the nucleus, but few other refinements are necessary (Pr 62a).

The potential acting on a single nucleon in the vicinity of the nucleus is now known to have approximately the following parameters for the real well (Ro 66, Vo 68).

$$V = 53 \text{ MeV}$$

$$r_R = 1.25 \text{ fm}$$

$$a_R = 0.65 \text{ fm}$$

The situation is not as well understood for the complex projectiles. The deuteron is the best studied of the complex projectiles, but great uncertainties exist for some of its parameters. The well depth V is believed to be of the order of the sum of the well depths for the neutron and proton. This value is obtained when the spacial extent of the neutron and proton making up the deuteron is considered along with the 2-body interaction of the proton and neutron with the nucleus. Calculations

by Perey and Satchler (Pe 67) indicate that the well depth should be of the order of 85 MeV or 110 MeV, but are not able to distinguish between the two cases.

Little is known about the spin-orbit potential V_{SO}. Firstly, it is weak as compared with the potential V, and secondly, it makes itself felt only through the fact that if affects different spin states to a different extent. In the case of medium weight and heavy nuclei, if the spin-orbit potential is omitted from the analysis of elastic scattering data, the other optical model parameters can be adjusted to compensate for the omission. To this extent, the study of elastic scattering from many nuclei is not suitable for the determination of V_{SO}. In stripping reactions, and polarization phenomena, however, this compensation may not be adequate, and a spin-orbit potential must be included explicitly. The serious difficulty is that as stated above, the presence of spin-orbit forces requires the modification of some of the other parameters in the optical model potential (Le 64). Thus it is not valid to determine the optical model potential in the absence of spin orbit forces from elastic scattering, and then to arbitrarily add on a spin-orbit potential. Nevertheless this procedure is frequently used because of the absence of reliable measurements of the potential V_{SO}.

The parameters of the absorptive potential are rather uncertain especially in the case of the deuteron. The well depth as determined by various workers is sometimes 10 to 12 MeV and sometimes 4 to 6 MeV for bombarding energies in the vicinity of 6.00 MeV, and the radius is

less certain. Possibly part of the uncertainty arises because absorption is caused by a variety of processes. Direct interactions tend to take place at larger radii than does absorption to form the compound nucleus (Vo 68). Consequently, if the direct interactions predominate we may expect a larger value of r_I. Conceivably, the Woods-Saxon form and its derivative are not appropriate since they make no provision for absorption at two different radii.

In order to calculate the differential cross section for elastic scattering, we begin with a plane wave decomposed into partial waves on the basis of the orbital angular momentum ℓ. When the wave approaches the nucleus, part of it is reflected, and part is absorbed. Exactly how much of each process occurs is calculated by solving the Schrödinger equation for one partial wave at a time. For each partial wave, we obtain a reflection coefficient η_ℓ and a phase shift δ_ℓ. The scattering amplitude is then given by $S_\ell = \eta_\ell e^{2i\delta_\ell}$. The calculation of the angular distribution is then just a matter of geometry which, although tedious, is well understood (Bl 52).

The optical model potential thus obtained should vary only slowly with energy. Shape elastic scattering requires only a very short time - of the order of 10^{-23} seconds. The uncertainty principle then shows that variations of yield with energy must have widths of the order of 5 to 10 MeV. Consequently, when optical model parameters are determined from experimental data taken at several energies over a range of 2 or 3 MeV, they should be quite similar, or show at most only a slow variation with energy. In practice, much more rapid variations of yield with energy are

frequently seen. These are attributed to the compound nucleus interactions which proceed much more slowly. Since elastic scattering via the compound nucleus mechanism is a fundamentally different process than shape elastic scattering, its effects should be removed before an attempt is made to calculate the optical model parameters. Some workers have allowed significant variations in the optical model parameters as a function of energy in the hope that they may thus be compensating for the presence of compound nucleus reactions. However, as will be discussed later in this chapter, the fluctuations of yield with energy observed in one channel bear little relation to those observed in another. Therefore such parameters are not likely to produce satisfactory results if they are subsequently used in the analysis of stripping reactions.

2.2 Direct Interactions

The name "direct interactions" embraces a wide range of reaction mechanisms all with the characteristic that they proceed very rapidly-with a time scale of the order of 10^{-23} seconds. In this section, direct interactions will be considered in the context of deuteron stripping. Only the perturbation approach will be considered (Sa 64), as it is the basis of the distorted wave Born approximation or DWBA theory used in this work. Within this picture, direct interactions are considered as occurring in a single step. The initial state of the system passes into the final state without the intermediary of an entity such as the compound nucleus.

Let us symbolize the reaction by A(a,b)B. For the cases of deuteron

stripping,

A ~ target nucleus;

a ~ deuteron;

b ~ neutron or proton for (d,n) or (d,p) stripping respectively, and

B ~ residual nucleus.

It is also useful to introduce the particle x, the transferred particle. In terms of this particle,

$$a = b + x \ ;$$

$$B = A + x \ .$$

The interaction which causes the direct reactions is usually pictured as being weak. Mathematically this means that direct reactions can be treated as a perturbation to be added to the elastic scattering. The use of perturbation theory implies that the cross section will simply be proportional to

$$|\langle \psi_f | V | \psi_i \rangle|^2 \qquad 2.2$$

In this expression, ψ_i is the wavefunction describing both the internal and relative motions of a and A; ψ_f is the wavefunction describing the internal and relative motions of the pair b and B, and V is the potential that causes the interaction. It is usually taken to be the neutron-proton interaction potential V_{pn}.

The relative motion of a pair of particles, say a and A, is taken to be the same as that in elastic scattering. Thus the wavefunction for the relative motion is easily calculated from the optical model potentials

obtained from elastic scattering. The apparently formidable task of describing the internal motion of the nuclei A and B is greatly simplified by the assumption that B = A + x. In fact, when the overlap of the wavefunctions for the nuclei A and B is calculated in this approximation, only the wavefunction of the captured particle remains. Thus nearly all the physics of the interaction is left in an entity called the form factor:

$$\psi_x \, V_{pn} \, \psi_a$$

Here ψ_x is the wavefunction of x in B, and ψ_a is the wavefunction describing the internal motion of the deuteron.

The matrix element in expression 2.2 involves a 6-dimensional integral over the separations $\vec{r}_{aA}$ between a and A, and $\vec{r}_{bB}$ between b and B. Unfortunately, the power of modern computers does not allow us the luxury of going beyond 3 dimensions. For several years, calculations were performed in the zero range approximation (Ba 62). The assumption was made that the potential V_{pn} was of very short range so that the product $V_{pn} \, \psi_a$ could be replaced by a delta function multiplied by a constant. This approximation has the effect of reducing the integral to 3 dimensions. However, any tensor terms in V_{pn} and the d-state of the deuteron are neglected. The implication is also made that the particle b appears exactly where a disappears. Since the deuteron is a large diffuse particle, this latter point is unsatisfactory. An approach known as the local energy approximation (Pe 64) was found to allow the mathematical simplifications of the zero range approximation, and also to simulate many of the effects of a proper finite range calculation. It consists

of multiplying the zero range form factor by a constant correction factor (Bu 64). The finite size of the deuteron is simulated, but the tensor forces and deuteron d-state are still neglected. If it is eventually desired to introduce these latter two points, it will be necessary to carry out a full scale 6-dimensional integration.

Realistic nuclear forces are usually thought to be nonlocal. The particle interacts with the potential not only at the center of its wavepacket, but over all space. The result is that the simple term $\psi(r)V(r)$ in the Schrödinger equation must be replaced by $\int\psi(r')V(r,r')d^3r'$. Thus nonlocality corrections also introduce an extra 3 dimensions into the calculation of the elastic scattering wavefunctions. Since nonlocality reduces the amplitude of the elastic scattering waves in the nuclear interior (Le 64), it helps to simulate part of the effect of the exclusion principle. The local energy approximation again allows the most important effects to be accounted for while retaining the mathematical simplicity of the local approximation. In this case, the wavefunctions of the local approximation are multiplied by a constant depending on the real well depth and the range of the nonlocality (Hj 65).

Stripping reactions have been quite useful because they frequently allow the determination of the angular momentum transfer or ℓ-value. The most common case in which only one ℓ-value is allowed is the one of interest in this work - zero spin for the target nucleus. Restricting ourselves to this case, we note that in stripping reactions the parity change is $(-1)^{\ell}$ (Au 64), and the final state spin is $J = \ell \pm 1/2$. Thus only one ℓ-value is capable of leading to the correct spin and parity of the final state.

A stripping reaction, by allowing the determination of the ℓ-value, gives the parity of the final state, and restricts the spin to $\ell \pm 1/2$.

In the 2s-1d shell nuclei, many spins and parities are known. Interest is thus shifting to the use of stripping reactions to extract more subtle features of nuclear structure. Because of its complexity, the nucleus must be interpreted in terms of models. The shell model is one of the most useful because it allows a great number of nuclear configurations to be expressed in terms of a relatively small number of states known as the single particle states. These are customarily designated by symbols such as $1d_{\frac{5}{2}}$, $2p_{\frac{1}{2}}$ etc. which give the spin-parity (J^{π}) and oscillator number of the state (Pr 62b). The single particle states arise quite naturally in the ideal case of a single particle moving in a spherically symmetric central potential. Some nuclei approximate the ideal case, and many nuclear properties are then found to be quite similar to those associated with the single particle state.

In a slightly more complicated case, the core may be pictured as deformed, but otherwise inert. In this case, several single particle states may be mixed together, each with its own amplitude. By way of example, consider the first excited state of ^{21}Na (Bu 68). It has a spin-parity (J^{π}) of $5/2^{+}$, and is the second member of a rotational band built on the ground state. The intrinsic portion of the wavefunction is given by:

$$\psi = \alpha(1d_{\frac{5}{2}}) + \beta(2s_{\frac{1}{2}}) + \gamma(1d_{\frac{3}{2}})$$

where α, β and γ can be calculated, for example, within the Nilsson model

(Ni 55). Since the state has $J^{\pi} = 5/2^{+}$, the single particle component of the wavefunction is $\alpha(1d_{\frac{5}{2}})$, and a quantity known as the spectroscopic factor is found to be proportional to $|\alpha|^2$ (Sa 58).

The general case may also be treated in a similar manner. It is possible within the fractional parentage formalism (Sh 63) to express any nuclear wavefunction in terms of any other configuration plus some sort of "residual configuration". In particular, it is possible to calculate how much of a given wavefunction looks like a single particle state plus an inert core. In this case, the amplitude of the single particle plus core state is known as the coefficient of fractional parentage. The spectroscopic factor is equal to the square of the coefficient of fractional parentage.

Direct interactions are ideally suited for measurement of spectroscopic factors. The single step nature of the reaction implies that the only component of the final state wavefunction that can participate in the reaction is the one having the captured particle in a single particle state with the same spin and parity as the final state. Participation of other single particle states or collective states would require more complicated interactions between the projectile and target, or between the residual nucleus and outgoing particle. If the spin of the target nucleus is zero, only one ℓ-value is allowed. Thus, if we assume that first order perturbation theory is adequate to describe direct interactions, the experimental cross section is found to be proportional to the spectroscopic factor. Within the DWBA theory, calculations are performed in the extreme single particle limit. That is, the captured particle is assumed

to be in a purely single particle state, and the core is assumed to be completely inert. If only one ℓ-value is allowed, it is found that the ratio of the experimental cross section to the calculated cross section is equal to the spectroscopic factor.

2.3 Compound Nucleus

Hauser-Feshbach Calculations

The compound nucleus model was originally proposed to account for the large number of narrow resonances observed in the scattering of low energy neutrons from heavy nuclei (Vo 62 and references therein). The large number of resonances implied that very complicated states were being formed, and the width of the resonances indicated a lifetime of the order of 10^{-15} seconds. The model proposed that the incident neutron was absorbed into the target exciting the compound nucleus to just above the neutron emission threshold. The relatively long lifetime of the compound nucleus was explained by assuming the energy of the incident neutron was distributed over a great number of the possible states in the compound nucleus. Thus a relatively long time was required before sufficient energy was concentrated on a single particle to allow it to escape from the compound nucleus.

In the case of deuteron scattering, the compound nucleus is excited to several MeV above the particle emission threshold. Therefore, the lifetime is much shorter (about 10^{-20} seconds in this work). By use of the uncertainty principle, it can be shown that such a lifetime corresponds

to a width of about 50 keV for the structure observed in the yield curve.

It is not difficult to calculate the average properties of compound nucleus reactions within the context of the optical model (Bo 62, Vo 68). In fact, the presence of the absorptive potential in the optical model indicates that a certain portion of the incident flux will be absorbed into the target nucleus. Calculations are carried out using methods quite similar to those used in the calculation of the elastic scattering angular distributions (Sm 65). The essential difference is that the results are interpreted in terms of absorption of the incident particles instead of reflection.

Although the process of the decay of the compound nucleus looks quite different from the formation, the two processes are closely related by the concept of detailed balance or time reversal. In fact, except for some statistical factors, the cross sections are the same. Thus if we have a compound nucleus, say ^{18}F, and wish to calculate the probability that it will emit a proton, and leave the residual nucleus ^{17}O in its ground state, we turn the problem around, and consider protons incident on ^{17}O. Once the probability of the ^{17}O nucleus absorbing a proton to form ^{18}F is known, the original problem of decay of the compound nucleus can be easily solved.

In practice, the absolute cross section is calculated only in the case of formation of the compound nucleus. The probability of populating any given final state can be expressed as the product of two terms. The first is the probability that the compound nucleus will be formed in the first place. The second term is the relative probability of decay to the

state of interest as opposed to decay into any of the other states available. The fact that relative decay probabilities are extensively used means that many of the inaccuracies of an absolute calculation tend to cancel out.

The symmetry about 90° which is frequently assumed to be characteristic of compound nuclear reactions is really justified in only two cases (Bl 52).

(1) The reaction proceeds through only one state in the compound nucleus.

(2) The reaction excites a statistically large number of states in the compound nucleus.

For most of the nuclei in the 2s-1d shell, the number of compound nucleus levels excited will lie somewhere between these two extremes. Consequently, a differential cross section obtained with a thin target may well show distinct fore-aft asymmetries.

Ericson Fluctuations

A second approach to the compound nucleus is that taken by Ericson. Instead of ignoring the fluctuations in the cross section, he found that they could be exploited to yield information difficult to obtain in other ways (Er 63). Consider a yield curve made up of overlapping resonances of width Γ. A particular resonance will make its influence felt over an energy range of order Γ. Thus if we compare the cross section at two energies, say E and E + ε where $\varepsilon << \Gamma$, then at both energies the same resonances will predominate, and the cross sections will be quite similar or correlated. On the other hand, if $\varepsilon >> \Gamma$, entirely different resonances

will contribute at the two energies, and the cross sections will be uncorrelated. Measurement of the correlation as a function of ε thus enables us to measure the width of the resonances. In fluctuation theory, the width is usually referred to as the coherence energy. Since the uncertainty principle relates the width of the resonances to the compound nucleus lifetime, the results of the experimental determination of the coherence energy may be compared with the compound nucleus lifetime as obtained from a Hauser-Feshbach calculation.

If a direct interaction is also present, it will contribute a "background" on which the fluctuations due to the presence of the compound nucleus reactions are built. Ericson also exploited this fact to obtain a measure of the portion of a reaction that is proceeding via the direct interaction.

The measurement of both the coherence energy and the portion of direct interaction are made using the autocorrelation function defined as:

$$C(\varepsilon) = \frac{\langle [\sigma(E)-\bar{\sigma}][\sigma(E+\varepsilon)-\bar{\sigma}] \rangle}{(\bar{\sigma})^2} \qquad 2.3$$

In this expression, $\langle \cdots \rangle$ represents the average taken with respect to the energy E, and $\bar{\sigma}$ is the average cross section. It can be seen that the essence of the correlation function is the comparison of the cross section to the average cross section at two neighbouring energies. Ericson obtained a useful expression for the autocorrelation function in the form:

$$C(\varepsilon) = \frac{1}{N} (1-\gamma_D{}^2) \frac{\Gamma^2}{\varepsilon^2 + \Gamma^2} \qquad 2.4$$

In this expression,

Γ is the coherence energy;

N is the fluctuation damping coefficient, and

γ_D is the ratio of the direct interaction cross section to the total cross section.

In an experiment using an unpolarized beam, contributions due to different spin projections are incoherent. If there are N equivalent incoherent contributions, the fluctuations in the experimental cross sections are reduced by a factor of $1/\sqrt{N}$. An approximate value for N is given by

$$N = \frac{1}{2}[(2I+1)(2i+1)(2I'+1)(2i'+1)] ,$$

where

i is the spin of the incident particle;

I is the spin of the target nucleus;

i' is the spin of the outgoing particle;

I' is the spin of the residual nucleus.

The value of N calculated using this expression is correct to within about 20% for yield curves measured at 90°. However, at far forward and backward angles it may be in error by as much as a factor of 3. In these cases, a much more involved expression must be used to calculate N (Wi 66).

As with most compound nucleus theories, Ericson's work is based on the assumption of random matrix elements. Essentially, this means that the compound nucleus states are so complicated that the matrix elements connecting a group of them to any other given state will be random complex numbers. In the derivation of expression 2.4 from 2.3 (Er 63), a great number of products of matrix elements appear. In many cases, a matrix element is multiplied by its complex conjugate. Since this product is then positive, the sum of all the matrix element products is not zero.

This accounts for the obvious fact that the autocorrelation function as given in expression 2.4 is nonzero in many cases.

On the other hand, if we consider the group cross correlation function $G(\sigma_1,\sigma_2,\varepsilon)$ a different situation arises. In this case, the expression used is:

$$G(\sigma_1,\sigma_2,\varepsilon) = \frac{1}{2}\left\{\frac{\langle[\sigma_1(E)-\bar{\sigma}_1][\sigma_2(E+\varepsilon)-\bar{\sigma}_2]\rangle}{\bar{\sigma}_1\bar{\sigma}_2} + \frac{\langle[\sigma_2(E)-\bar{\sigma}_2][\sigma_1(E+\varepsilon)-\bar{\sigma}_1]\rangle}{\bar{\sigma}_1\bar{\sigma}_2}\right\} \qquad 2.5$$

Here σ_1 and σ_2 are the cross sections for the population of different final states, and the other symbols have the same significance as in expression 2.3. When expression 2.5 is evaluated, no terms appear in which a matrix element is multiplied by its complex conjugate. Consequently, $G(\sigma_1,\sigma_2,\varepsilon)$ should approach zero for all ε as the energy range over which averages are taken is increased. In other words, the assumption of random matrix elements predicts that no correlation should exist between yield curves associated with the population of different final states.

The principle source of error in a fluctuation analysis usually arises from the fact that data are collected over only a finite energy range. Thus only a finite number of resonances appears, and the size of the sample of random matrix elements limits the accuracy of results. These finite range of data errors have been studied, and expressions given which estimate their size (Da 65). Since the measurement of the average cross section is also affected by resonances in the yield curves, the expressions of (Da 65) are also useful in estimating the accuracy of a

measurement of the absolute cross section. It is given in (Da 65) that the relative error in the compound nucleus component of the average cross section is $\sqrt{\pi/nN}$ where $1/n$ is the ratio of Γ to the energy range over which data are studied, and N is the fluctuation damping coefficient defined above. Similarly, the relative error in the autocorrelation function for

$$\varepsilon = 0 \quad \text{is} \quad \sqrt{\pi(N+1)/nN} \ .$$

Interference

In most work, the direct and compound nucleus reactions are treated as being incoherent. This greatly simplifies the analysis because the two reaction mechanisms can be treated independently. However, such a separation is not really valid unless the experimental cross sections are averaged over a wide energy range in order to remove the random variations in the cross section. As such extensive averaging is seldom used in practice, great care must be exercised when it is desired to obtain accurate absolute cross sections.

In spite of the great complexity in treating interference in the general case, some attempts have been made to study the phenomenon in cases where special simplifications arise. For instance, a study has been made of the reaction $^{12}C(d,n)^{13}C$ near the resonance at 4.0 MeV deuteron energy (Fu 67). It was concluded that the observations fit the model of combined direct interactions, compound nucleus interactions and interference terms.

It is pointed out in chapter 4 of this work that interference effects

may produce variations of yield with energy much larger than the calculated compound nucleus cross section. In such cases, a small calculated compound nucleus cross section gives little assurance that only small fluctuations will occur in the yield curve.

2.4 Previous Studies of ^{17}O and ^{17}F

The reactions of interest in this work are $^{16}O(d,d)^{16}O$, $^{16}O(d,p)^{17}O$ and $^{16}O(d,n)^{17}F$. The low lying levels of ^{17}O and ^{17}F are shown in figure 2.1 (He 61, Se 63). Not all the levels shown in figure 2.1 were extensively studied in this work. The 3.01 MeV level of ^{17}F is unbound to proton emission, and was too weak to be observed in the present experiment. The levels in ^{17}O above 4.5 MeV and the level at 3.058 MeV were not studied because the associated proton groups were obscured by other proton groups at too many angles to make an extensive analysis possible. Two levels in ^{17}F (the ground and 0.500 MeV levels) and 3 levels in ^{17}O (the ground, 0.871 and 3.846 MeV levels) were studied in this work.

The nucleus ^{16}O is usually considered to approximate closed shells for both protons and neutrons. In the approximation of ^{16}O constituting an inert core in ^{17}O and ^{17}F, the states available to the extra nucleon should correspond to the $1d_{\frac{5}{2}}$, $2s_{\frac{1}{2}}$ and $1d_{\frac{3}{2}}$ shell model orbitals. In reality, ^{16}O is not inert, but causes some spreading of the single particle strength to other states. The majority of the single particle strength can still be said to reside in a single level, however, and to that extent table 2.1 identifies the single particle levels in ^{17}O and ^{17}F. The levels in table 2.1 each carry about 90% of the single particle strength according to the model of Brown (Br 63). In ^{17}F, the $1d_{\frac{3}{2}}$ level is well

TABLE 2.1

Predominantly Single Particle States of ^{17}O and ^{17}F

Excitation Energy		Dominant Single Particle State	ℓ-value in deuteron stripping
^{17}F	^{17}O		
0.0	0.0	$1d_{\frac{5}{2}}$	2
0.500	0.871	$2s_{\frac{1}{2}}$	0
(5.1)	5.08	$1d_{\frac{3}{2}}$	2

Figure 2.1 Level diagram of ^{17}O and ^{17}F. The arrows indicate the excitation energies at which the nuclei become unbound to particle emission.

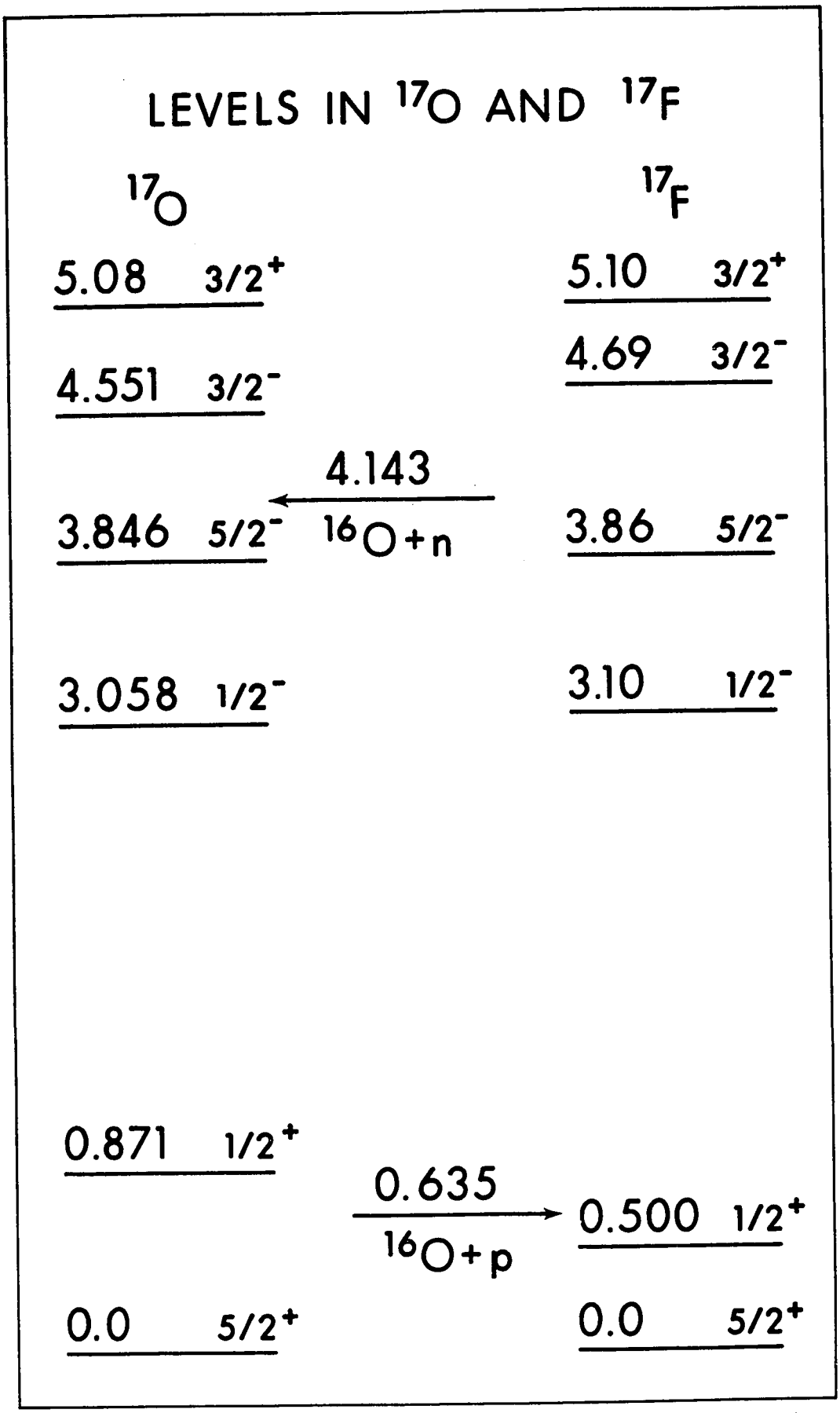
LEVELS IN ^{17}O AND ^{17}F
^{17}O
^{17}F
5.08 3/2+
5.10 3/2+
4.69 3/2-
4.551 3/2-
4.143
$^{16}O+n$
3.846 5/2-
3.86 5/2-
3.058 1/2-
3.10 1/2-
0.871 1/2+
0.635
$^{16}O+p$
0.500 1/2+
0.0 5/2+
0.0 5/2+

above the excitation energy at which ^{17}F becomes unbound to proton emission. As a result, the identification of the $1d_{\frac{3}{2}}$ orbital with a specific level is considerably less meaningful. However, the ^{17}F level at 5.1 MeV is the mirror level of the 5.08 MeV level of ^{17}O which carries most of the single particle strength of the $1d_{\frac{3}{2}}$ shell model orbital (Al 67).

The ground and first excited states of ^{17}F and ^{17}O were studied quite early in the history of deuteron reactions, and their approximately single particle nature was recognized (Ya 61, Ba 57). The calculations by Brown mentioned above (Br 63), have indicated that the levels should carry about 90% of the single particle strength. The remaining 10% is spread out to other levels by coupling of the single particle states to odd parity vibrations in the core. Unfortunately, experiment has not yet been able to confirm or reject Brown's model (Ol 69).

Several experiments over a wide range of energies have been carried out in an attempt to obtain the spectroscopic factors of the ground and first excited states of ^{17}O and ^{17}F. See for example references Ga 66, Al 67, Di 68, Na 68 and Ol 69. The results of Ol 69 are interesting because they discuss the measurement of the spectroscopic factors for the ground and first excited states of both ^{17}O and ^{17}F over a wide range of deuteron energies. It was found that all 4 states have spectroscopic factors in the vicinity of 1.0. The spread of the spectroscopic factors is about 20%. Conversely, Alty (Al 67), in a somewhat similar measurement on ^{17}O found quite different values for the spectroscopic factors. In this case, they were found to be of the order of 0.50 with roughly the same uncertainty as in Ol 69. One of the purposes of the present work

was to shed some light on the reason for the discrepancies between earlier results.

So far little mention has been made of the negative parity states. They can be described by coupling a single particle state to an octupole vibration in the ^{16}O core. However, it is quite interesting to note that the levels with spin-parity $1/2^-$ and $3/2^-$ could also have components with two particles in the 2s-1d shell and one hole in the 1p-shell (Ma 66). For brevity of notation, we designate such a level as a 2p-1h level. Stripping reactions could populate these levels via the 2p-2h or 4p-4h components of the ^{16}O ground state. The determination of the spectroscopic factor of the 3.058 MeV level could thus produce some very useful nuclear structure information (Wo 68). In the present work, it was not possible to study the 3.058 MeV level because of contaminants. However, previous workers have measured the angular distributions of protons associated with populating this level by using higher deuteron energies (Sc 64, Ke 61). Calculations are compared with these earlier experimental results in order to obtain an estimate of the spectroscopic factors.

In the case of the 3.846 MeV level with spin-parity $J^\pi = 5/2^-$, there may be some $1f_{\frac{5}{2}}$ strength (Br 63). A measurement of the spectroscopic factor would again be useful for comparison with the results of Brown's work. Both the present and previous measurements were used in estimating the spectroscopic factor for this level.

Finally something should be said about previous compound nucleus work as applied to the ^{16}O + d reactions. Most estimates of the compound nucleus cross sections have not been based on a Hauser-Feshbach calculation.

The intent has been only to subtract an isotropic cross section such as to improve an much as possible the DWBA fits to the experimental angular distributions. It is found that the compound nucleus cross sections are appreciable only at lower energies, but since the negative parity levels have not been studied at such energies, it has not yet been possible to make any sort of comparison between theory and experiment. In the work of Dietzsch (Di 68) where the bombarding energies were below 3.5 MeV, Hauser-Feshbach calculations were carried out, but the negative parity levels were not studied.

The only study of the lifetime of the compound nucleus levels was made in the work of Dietzsch (Di 68), but the Hauser-Feshbach calculations did not include a calculation of the lifetimes. The value obtained for the coherence energy in (Di 68) exceeds that obtained in the present work by over a factor of 2. As discussed in chapter 4, the difference probably lies in the methods of analysis.

CHAPTER 3

EXPERIMENTAL RESULTS

The techniques of obtaining raw data and of carrying out the preliminary analysis can be divided into 3 sections:

(1) the reaction $^{16}O(d,n)^{17}F$

(2) the reactions $^{16}O(d,p)^{17}O$ and $^{16}O(d,d)^{16}O$

(3) absolute cross sections for the charged particle reactions.

3.1 The Reaction $^{16}O(d,n)^{17}F$

The neutron time-of-flight system used in this work has been extensively described elsewhere (Mc 67). However, several remarks should be made in order that the following discussion may be somewhat clearer.

The electronics contained a system for discriminating between pulses arising from the detection of neutrons and γ-rays. Counts identified as arising from γ-rays were stored in channels 0 to 2047 of the kicksorter region of the computer memory. Neutron counts were stored in channels 2048 to 4095. For small pulse heights, however, the neutron-gamma discrimination may be in error. Consequently, it is usually necessary to examine the γ-ray spectrum for peaks arising from misidentified neutrons. Due to minute electronic drifts, the fraction of neutrons misidentified

varied with time, and a correction had to be applied to each run on an individual basis.

The neutron detector efficiency depends on several quantities among which are the type of scintillator and minimum pulse height accepted for further analysis. In the energy range of this experiment, the efficiency varied between approximately 8% and 12%. The efficiency was calculated using a computer program written at the University of Alberta (Gr 67). The results have been compared with experimental data, and are believed to be accurate to within about 5% in the energy range of interest (Bu 67).

The targets consisted of a layer of metal oxide on a thick backing approximately 0.01 cm thick. The target was clamped to a layer of gold 0.08 cm thick so as to improve heat dissipation. The whole assembly was supported in an air-cooled holder. Since the target backing stopped the beam, a bias of +300 volts was applied to the target to reduce the number of secondary electrons escaping from the target.

Scattering of neutrons in the target backing and in the gold heat conductor can be serious at some angles. A correction was made for single scattering of neutrons out of the solid angle intersecting the detector (out-scattering). Scattering of neutrons into the detector that otherwise would not have passed through the detector was estimated to be less than 1/5 of the out-scattering. The in-scattering was thus considered to be unimportant.

Although the majority of the data for the (d,n) reaction was obtained using thick target techniques described below, it was felt that a limited amount of data should be taken with a thin target in order to provide a

check on the thick target procedures. A target of tantalum oxide (Ta_2O_5) was deposited on a backing of 0.013 cm thick tantalum foil. The yield curves for the reactions populating the ground and first excited states of ^{17}F were measured in 20 keV steps over the energy range 5.80 MeV to 6.00 MeV at detector angles of 30° and 140°. The results are compared in figure 3.2 with similar regions of the yield curves derived from the thick target analysis.

Thick targets of oxygen were prepared by heating a molybdenum foil in air to between 500 and 600°C for between 10 and 20 minutes depending on the desired thickness. Care had to be taken that excess heating did not cause sublimation of the molybdenum oxide (MoO_2) and thereby cause subsequent growth of long needle-like crystals of monoclinic MoO_2. Although the monoclinic crystals were quite lovely, they were not at all suitable for a target.

Because some sublimation could not be avoided, it was impossible to determine the thickness of the target by such direct methods as weighing. Several targets of differing thicknesses were made and tested for suitability under actual experimental conditions. The target subsequently used in the main body of the experiment had a uniform concentration of oxygen to a depth corresponding to a deuteron energy loss of about 230 keV for 5.00 MeV deuterons. At greater depths, the concentration decreased approximately linearly with depth into the target. The determination of the oxygen concentration as a function of depth is discussed in more detail in the description of the computer analysis.

Data for the population of the ground and first excited states of

^{17}F were measured at deuteron energies from 4.75 MeV to 6.00 MeV in steps of 250 keV. At 5.00, 5.50 and 6.00 MeV, measurements were taken in 5° steps in the range 0° to 140° in the laboratory system. At 4.75 and 5.25 MeV, measurements were taken over the same angular range, but in 10° steps. The measurements at 5.75 MeV were carried out as in the cases at 4.75 and 5.25 MeV except that measurements were not taken at 110° and at 130°.

No contaminant peaks were observed. The only elements other than oxygen expected to be in the target were carbon and molybdenum. If carbon were present on the target in significant amounts, 2 additional peaks would be present in the spectrum due to population of levels of ^{13}N in the reaction $^{12}C(d,n)^{13}N$. No such peaks were observed.

Because of the fairly large charge on the molybdenum nucleus (Z = 42), the cross sections for reactions producing neutrons were expected to be small. No evidence was found for any reactions involving molybdenum.

The targets were found to be stable when the power deposited by the incident beam was 6 watts. When the power was increased to approximately 10 watts, a slow deterioration was observed. The experiment itself was carried out with a power level of 5 to 6 watts.

A typical neutron time-of-flight spectrum is shown in figure 3.1. Even in the raw data, structure due to the variation of yield with deuteron energy can be seen. Subsequent analysis with the computer program THICK allowed the extraction of both the angular distributions and the yield curves (Da 69a).

In the following, the steps carried out by the computer are summarized, and then certain features of the extraction of the yield curves are discussed

Figure 3.1 Thick target neutron time-of-flight spectrum for the reaction $^{16}O(d,n)^{17}F$. A thick molybdenum oxide (MoO_2) target was used.

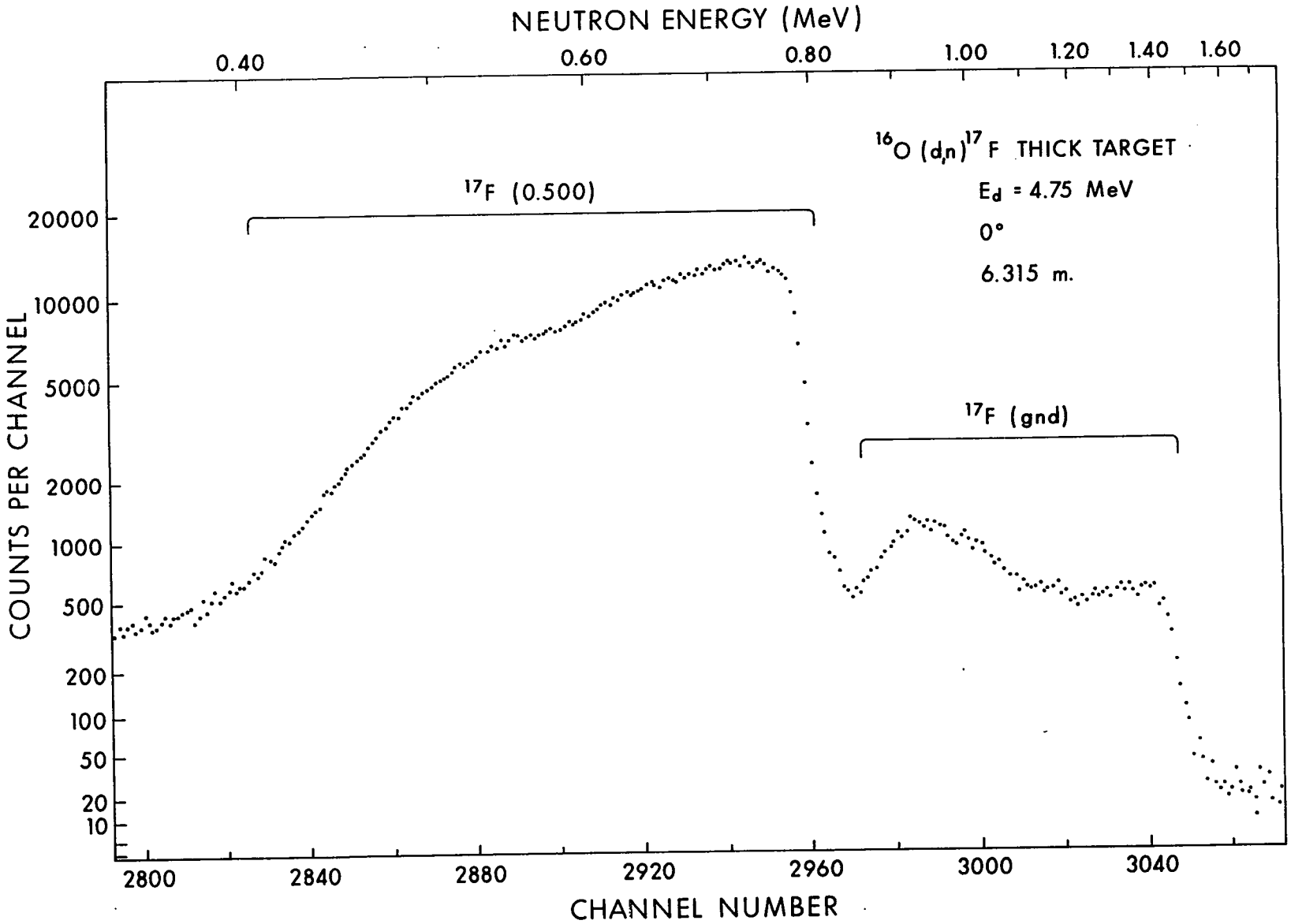
NEUTRON ENERGY (MeV)
0.40
0.60
0.80
1.00
1.20
1.40
1.60
$^{16}O(d,n)^{17}F$ THICK TARGET
E_d = 4.75 MeV
0°
6.315 m.
^{17}F (0.500)
^{17}F (gnd)
COUNTS PER CHANNEL
20000
10000
5000
2000
1000
500
200
100
50
20
10
2800
2840
2880
2920
2960
3000
3040
CHANNEL NUMBER

in more detail. Analysis was carried out in 11 steps.

(1) Input of raw data, program controls and other information necessary for the analysis.

(2) Background subtraction. This was accomplished by sampling the background above and below the neutron groups of interest, and then assuming that the background varied linearly with channel number between these points. An additional correction was applied when the two peaks overlapped slightly.

(3) The neutrons incorrectly identified as being γ-rays were added to the neutron spectrum.

(4) A correction for the variation of neutron detector efficiency with energy was applied.

(5) A correction for neutron scattering in the target backing was made.

(6) Corrections were applied for dead time in the main neutron detection system and in the monitor system.

(7) The spectrum was normalized using the monitor count.

(8) The two peaks of interest were summed. If it was not desired to extract the yield curves, the program returned to step 1. Otherwise it proceeded to step 9.

See below for a detailed discussion of steps 9, 10 and 11.

(9) The effect of the variation of the stopping power dE/dx with energy was calculated, and suitable corrections were applied.

(10) The spectrum was slightly smoothed so that the unfolding of the instrumental resolution from the

thick target spectrum would not be unduly affected by statistical errors on the data points.

(11) The finite resolution of the time-of-flight system was extracted leaving the "true" yield curve.

To a first approximation which will be removed later, we can assume that a monoenergetic neutron group will fall entirely within one channel of the kicksorter. In this case, a single channel represents only neutrons of a given energy range say E_n to $E_n + dE_n$. For brevity of notation, we will represent this energy interval by (E_n, dE_n). Knowing the detector angle, the particle masses etc., we can determine that the neutrons in the range (E_n, dE_n) arose from interactions initiated by deuterons in the energy range (E_d, dE_d). The effect of straggling can be shown to be unimportant in this experiment. Therefore, knowledge of the stopping power of the constituents of the target allows us to determine that the reactions produced by deuterons having energies in the range (E_d, dE_d) must have occurred at a depth into the target in the range (x, dx). It is important to note that the quantity dx is not constant because the stopping power is a function of energy.

The approximation mentioned above, that the total resolution is much narrower than the slices of neutron energy dE_n, can be removed without great difficulty. Define the following symbols:

T(E): the true yield curve as measured at a deuteron energy E

W(E): the yield curve as observed with a thick target at a deuteron energy E. In this

case, E is not the energy of the incident deuteron beam, but the energy of the deuteron when it undergoes a reaction.

R(e,E): the instrumental resolution. It is the yield observed at an apparent energy E (as defined by the kicksorter calibration) for a monoenergetic neutron group of energy e.

Using these symbols, we can express the spectrum observed with a thick target as:

$$W(E) = \int T(e)\ R(e,E)\,de \qquad 3.1$$

Obtaining the "true" yield curve then involves solving the integral equation for T(e). This is the purpose of step 11 in the program description given above. The solution procedure is usually referred to as "unfolding" in the discussion given below.

Solution of the Integral Equation

The function R(e,E) was taken from an experimental spectrum obtained with a thin target. The change in R(e,E) as a function of e was approximated by assuming the time resolution was made up of two parts: a constant due to beam pulse width, electronics etc., and a variable portion arising from the transit time of the neutron through the scintillator. The sensitivity of the final results to the expected errors in R(e,E) was found to be much less than the sensitivity to other errors in the solution of equation 3.1. The algorithm used in solving for T(e) was as follows.

(1) A function U(E) was calculated for each value of E.

$$U(E) = \int R(e,E)\, W(e)\, de$$

(2) An initial guess for T(e) was made by setting

$$T_1(e) = W(e) \left[\frac{W(e)}{U(e)}\right]^a$$

where a was input. A value of a = 1.5 was found to be best.

(3) An iterative procedure was set up in which on the "i"th iteration

$$U_i(E) = \int R(e,E)\, T_i(e)\, de \ ,$$

and

$$T_{i+1}(e) = T_i(e) \left[\frac{W(e)}{U_i(e)}\right]^{b_i(e)} \ .$$

$b_i(e)$ was calculated by the computer so as to emphasize improving the fit at those points where it was poorest on the previous iteration. A total of up to 7 iterations was allowed. After 7 iterations, the program spent most of its time in meaningless attempts to find fits to statistical errors on the data points. It was found in tests where T(e) and R(e,E) were known that the program was capable of solving the integral equation to an accuracy of about 3% to 4% except where there were sudden changes in the slope of W(E). Consequently, it is believed that the unfolding procedure gives results with errors in the above range except at the high energy edge of the experimental peak where a sudden drop-off occurs. At the high energy edge, errors are believed to be less than $\pm$ 8%.

Smoothing

It is frequently difficult to remove subjective considerations from

an investigation of data smoothing. Therefore, much of the testing of the smoothing routines was done using an artificial yield curve. To a smooth curve resembling the thick target data was added a series of random numbers of such a size as to simulate statistical fluctuations with a standard deviation of 5%. Since it was desired to study the structure in the yield curves, such smoothing techniques as averaging neighbouring points were deemed to be unsatisfactory because they tend to smear out details. The algorithm used consisted of the following steps.

(1) Select n points from the spectrum at channel numbers $x_i \ldots x_{i+n-1}$, and fit a polynomial of order m to the n points.

(2) Solve the resulting polynomial at each of the n points, and store the solutions $y_i \ldots y_{i+n-1}$ and their corresponding uncertainties $\delta_i \ldots \delta_{i+n-1}$ for further use.

(3) Move j points further along the spectrum, and repeat steps 1 and 2.

(4) When all the points in the spectrum have been treated in the above manner, the smoothed value of the yield in channel x_i is obtained by calculating the weighted average of all the polynomial solutions y_i corresponding to the same channel x_i. The weights are inversely proportional to the variances (δ_i^2) of the polynomial solutions.

The numbers n, m and j were read into the program. It was found that the most satisfactory smoothing was obtained using n = 9, m = 4 and j = 1. The method was finally tested on actual data to see if the resulting smoothed spectrum was "satisfying" to the eye. Again the most satisfactory smoothing

was obtained using the above parameters. This procedure does not appreciably affect structure in the yield curve with a width greater than 5 channels. Since 5 channels correspond roughly to the width of a thin target peak, or alternately to R(e,E), the smoothing routine removes little information from a thick target spectrum. On the other hand, the procedure is quite effective in reducing random errors.

Oxygen Concentration in the Target

The concentration of oxygen, C(x), as a function of depth into the target could not be determined to better than about $\pm$ 5% on the basis of its effect on the final results of the thick target calculation. To within this limitation, it was determined that C(x) was essentially constant as far as the point where the deuteron energy had been reduced by 230 keV. Beyond this point, (call it x_o), C(x) decreased. On the basis of aesthetics, therefore, C(x) was made constant as far as x_o. It was then smoothly connected to a segment in which C(x) decreased linearly with depth into the target. The slope of the decreasing portion of C(x) was adjusted so that the yield at a deuteron energy of 5.75 MeV was the same when measured with an incident energy of either 6.00 MeV or 5.75 MeV. In other words, the two segments of the yield curve were required to match up at 5.75 MeV. The value of the slope determined in this way was found to cause all segments of the yield curve to match up satisfactorily. The yield curve was still measurable well beyond the point where the deuteron energy had been decreased by 250 keV, but the difficulty in obtaining these extra data was too great to justify

calculating C(x) significantly beyond the depth x_o . In addition, as C(x) decreases, the number of counts per channel does too, and the statistical errors quickly become unmanageable.

Figure 3.2 compares sections of the yield curves obtained using both thick and thin targets. The data points shown are for the thin target. Since the thick target results have had most of the statistical errors smoothed out, the results are nearly a smooth line. In order to avoid confusing the diagram, the range of values commensurate with the results of the thick target analysis is shown as a band lying between the two dashed lines. The main features of the spectrum are accurately reproduced by the thick target results. It might be possible to build some case that the combined smoothing routine and solution of the integral equation have affected structures with widths slightly in excess of the 5 channels estimated for the smoothing routine. However, the accuracy with which the sharp rise in the yield curve for the ground state at 30° is reproduced shows that loss of structure is not a major worry.

The yield curves obtained for the reactions populating the ground and 0.500 MeV states of ^{17}F are shown in figures 4.15 and 4.16. The representative error bars shown include the following errors:

(1) statistical errors on the raw data points

(2) statistical error in the monitor count

(3) uncertainty in removing the background

(4) uncertainty in the correction for neutron scattering in the target backing

(5) uncertainty in the correction for neutrons misidentified as gamma rays

Figure 3.2 Comparison of results obtained using thick and thin targets. The discrete points were obtained by analyzing data taken with a thin Ta_2O_5 target. The ranges of cross sections compatible with the results of the thick target analysis are shown as bands lying between the dotted lines.
(a) ^{17}F (0.500 MeV 30°, (b) ^{17}F (0.500 MeV) 140°,
(c) ^{17}F (ground state) 30°, (d) ^{17}F (ground state) 140°.

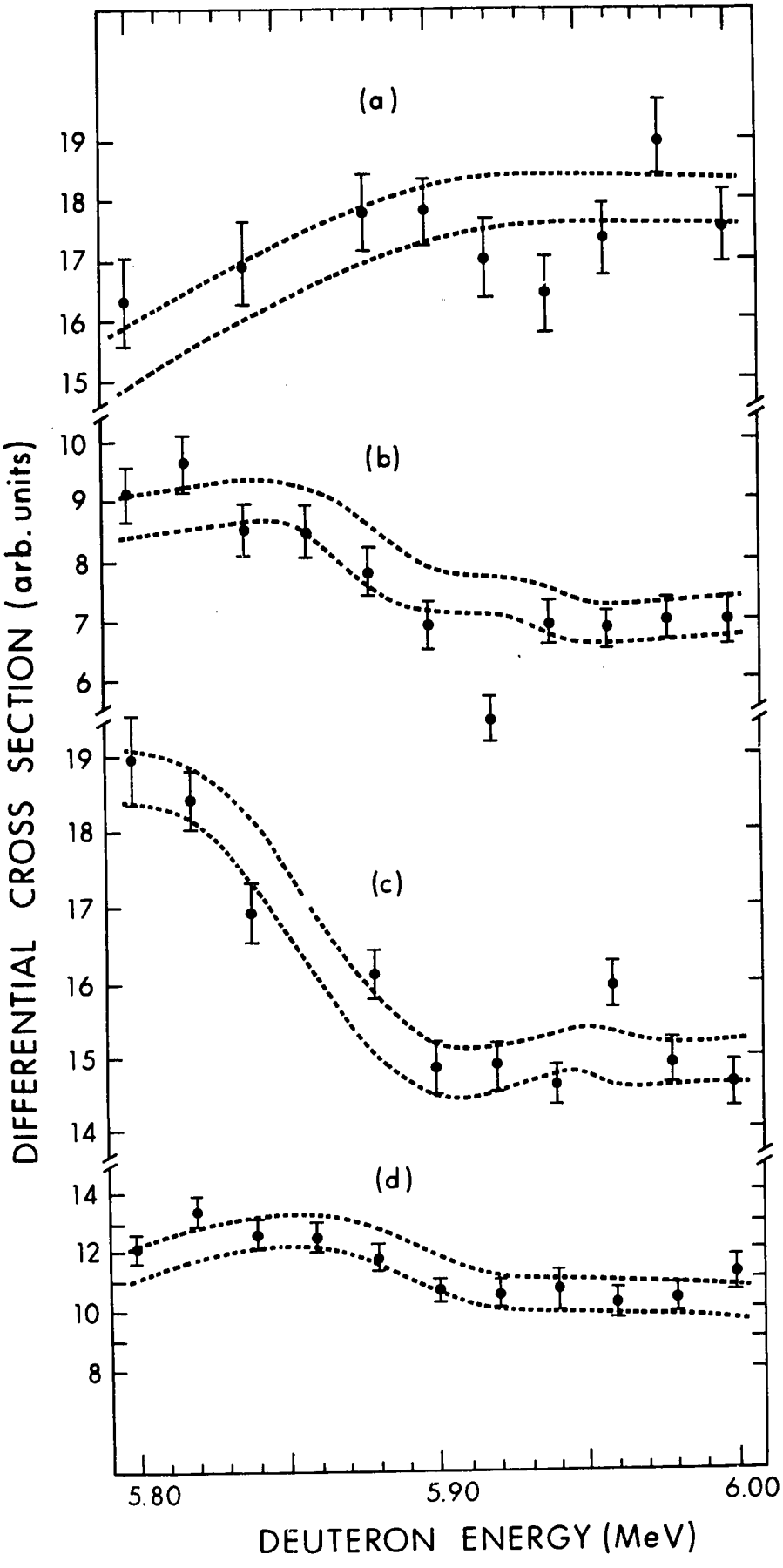
(a)
(b)
(c)
(d)
DIFFERENTIAL CROSS SECTION (arb. units)
DEUTERON ENERGY (MeV)
5.80
5.90
6.00

(6) uncertainty in the neutron detector efficiency

(7) uncertainty in the values of the stopping powers of oxygen and molybdenum

An attempt was also made to include the errors from 3 other sources:

(8) smoothing

(9) inaccuracies in the solution of the integral equation

(10) uncertainties in the thin target peak shape R(e,E)

Concerning points 8 and 9, the errors are somewhat difficult to estimate directly, but it is believed on the basis of tests using artificial yield curves that they do not exceed 4%. Uncertainty in the function R(e,E) is believed to contribute only a small error to the total uncertainty. In figure 3.2, it will be noted that errors on the thick target results are estimated to be only slightly smaller than those on the thin target results. Although the thick target results are averaged over several data points by the smoothing and unfolding routine, the increase in accuracy from this source is largely balanced by errors introduced by the unfolding.

The angular distributions are shown in chapter 4 where the DWBA analysis is discussed. These experimental data are subject to only very small statistical errors which are of the order of 1%. A somewhat more important source of error lies in the correction for neutron scattering in the target backing. In the worst case (around 85°), this source is believed to contribute no more than 3%. The most important errors probably arise from background subtraction and the correction for

neutrons misidentified as γ-rays. Together, these sources probably contribute between 3 and 4%. Except for one or two points, the angular distribution data seem to conform to this estimate of the uncertainties.

Absolute cross sections for the reactions populating the ground and first excited states of ^{17}F were estimated from the work of Yaramis (Ya 61). He reported that the absolute cross section for the population of the 0.500 MeV state at 0° using an incident energy of 5.02 MeV and a target 150 keV thick was 138 ± 21 mb/sr.

The absolute cross sections for the $^{16}O(d,n)^{17}F$ reactions could also be calculated from the data measured in the present work. The total amount of oxygen could be obtained from the known concentration of oxygen as a function of depth into the target. In this way, it was calculated that the absolute cross section for the population of the 0.500 MeV state of ^{17}F at 0° using a deuteron energy of 5.00 MeV and the target described above was 148 ± 17 mb/sr. The most important sources of error were due to uncertainties in:

(1) the total amount of oxygen in the target - 10%

(2) the stopping power of molybdenum and oxygen - 5%

(3) the neutron detector efficiency - 5%

(4) subtraction of background and correction for neutrons misidentified as γ-rays - 3%

(5) counting statistics - 1%

(6) charge collection - 1%

The total uncertainty was thus determined to be of the order of 13%. The

absolute cross section obtained in this work is not directly comparable with that of Yaramis because the thicknesses of the targets were significantly different. When this effect is taken into account, it is found that the two values differ by about 10%. The weighted average of the absolute cross sections obtained in this work and by Yaramis is 142 $\pm$ 13 mb/sr.

3.2 Charged Particle Reactions

The data collection system used in the study of the charged particle reactions has been described in Hu 69. Four detectors suspended from a movable support allowed data to be collected simultaneously at 4 angles. A fifth detector was held fixed at 90° to the beam direction. It was used as a monitor during measurement of the angular distributions, and as a fifth detector during the measurement of the yield curves. Charge was collected in a Faraday cup mounted some distance behind the target. A secondary electron suppressor biased to -1000 volts was mounted in front of the Faraday cup. Data were collected, and stored in the kick-sorter region of the computer memory.

Most of the angular distributions and all the yield curves were obtained as part of a joint experiment with Mr. J.J.W. Bogaards who was studying the reactions $^{48}Ca(d,p)^{49}Ca$ and $^{48}Ca(d,d)^{48}Ca$. The target was prepared by Mr. Bogaards by evaporating calcium metal onto a thin backing consisting of a thin layer of carbon on formvar. The carbon layer was necessary to provide sufficient heat conductivity to avoid target breakage.

However, it was not possible to evaporate the calcium directly onto the carbon, as it rapidly disintegrated. Possibly this was due to the formation of calcium carbide (CaC_2). When great care was exercised, it was found possible to evaporate calcium metal onto the formvar side of the backing. Oxidation and subsequent formation of calcium hydroxide gave a target which was uniform and quite stable under beam.

Three points should be made in connection with the nature and stability of the targets. Firstly, as will be pointed out later, it is quite important in the determination of the absolute cross section that the chemical composition of the targets be known. A total of 3 targets were used in the course of the experiment, and all targets showed the same ratio of oxygen to calcium to within approximately 5%. As the targets were exposed to air for differing lengths of time, this indicates that the targets probably consisted entirely of calcium hydroxide ($Ca(OH)_2$), as calcium oxide (CaO) will be converted to $Ca(OH)_2$ in the presence of air-borne moisture. Comparison of the absolute values of the cross section for the $^{16}O(d,d)^{16}O$ reaction with previous results (Ba 57) confirm this expectation.

Secondly, it was found that the targets were quite stable under beam. During the measurement of the yield curve, numerous check runs were taken. In most cases, repeat runs at the same bombarding energy were separated by about 10 hours, but in some cases the separation exceeded 30 hours. In no case did the deviation between the cross sections measured in repeated runs significantly exceed statistical errors. In all, the yield curve measurement required approximately 200 hours of beam on target.

If the target were deteriorating, the sum of all the deviations between the cross sections measured in repeated runs would differ significantly from zero. The sum of all the deviations was approximately 0.5% indicating negligible target deterioration. The r.m.s. deviation between repeated runs was between 3% and 4% depending on which yield curve was being considered. This error, of course, includes inaccuracies in the current integration and non-uniformities in the target which would not appear in cases where a monitor detector was being used for normalization. When the statistical errors due to counting are removed from the r.m.s. deviations, the residual error of only 2% to 2.5% gives an indication of the excellent quality of the targets.

Thirdly, the targets were highly enriched in ^{48}Ca. The angular distributions were measured with targets in which the ^{48}Ca enrichment was 87%.† When the yield curves were measured, better targets, enriched to 97% ^{48}Ca were available.† In both cases, the high proportion of ^{48}Ca, had the important effect that the numerous peaks arising from the reaction $^{40}Ca(d,p)^{41}Ca$ were not prominent. As can be seen from figure 3.3, the only important contaminant was carbon. It was hoped that the 3.058 MeV level in ^{17}O could be studied, but large peaks arising from (d,p) reactions on carbon obscured the peak at nearly all angles forward at 90°. Fortunately the peaks arising from the population of the 3.846 MeV level in ^{17}O were visible at all energies above 5.00 MeV. An attempt was made to study the 3.058 MeV level using a self-supporting target of silicon monoxide.

---

†The targets were prepared using ^{48}Ca obtained as the carbonate from Oak Ridge National Laboratory, Oak Ridge, Tenn.

Figure 3.3 Charged particle spectrum. A target of $Ca(OH)_2$ enriched to 97% ^{48}Ca was used. The target was deposited on a self-supporting carbon backing.

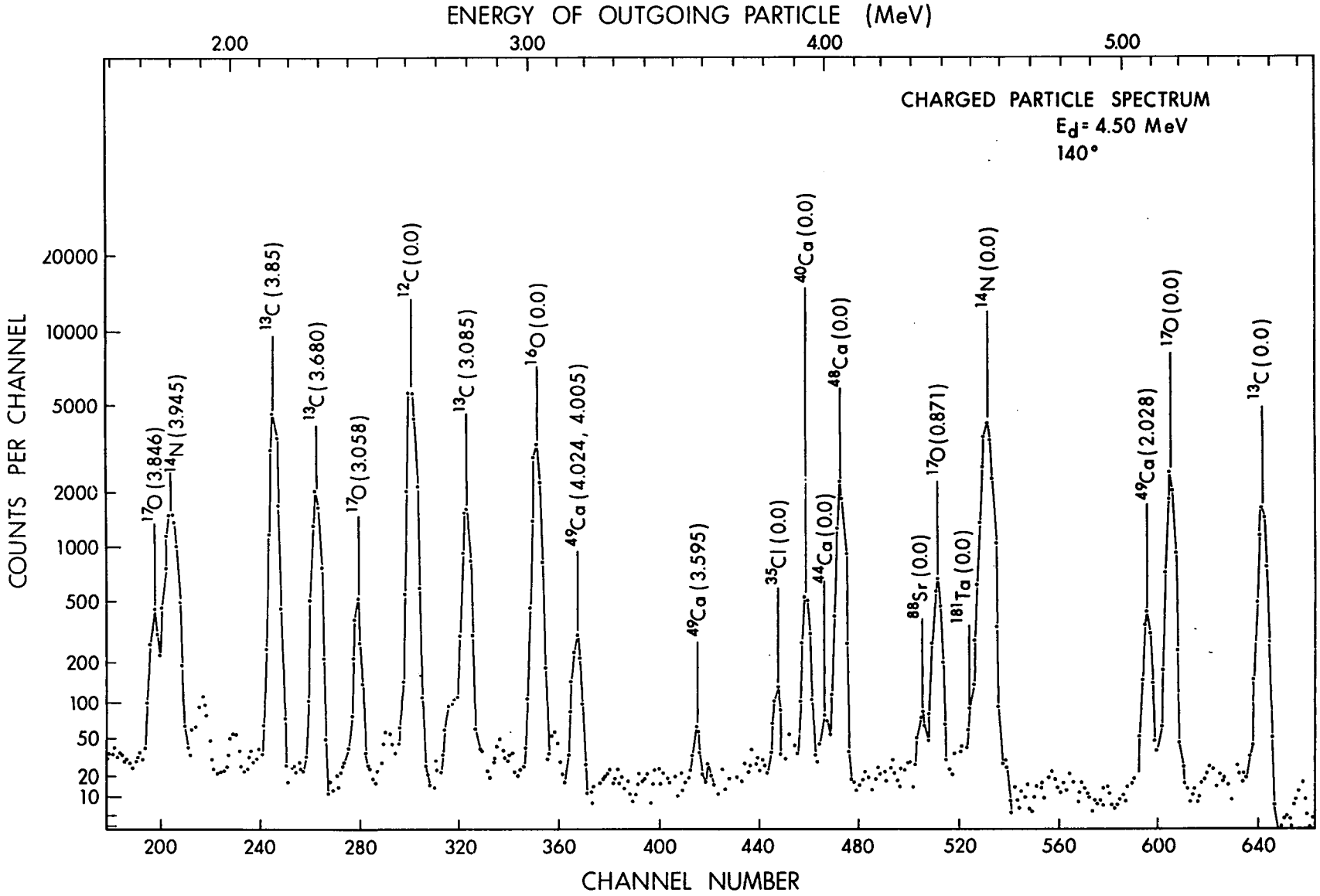
ENERGY OF OUTGOING PARTICLE (MeV)
2.00
3.00
4.00
5.00
CHARGED PARTICLE SPECTRUM
E_d = 4.50 MeV
140°
COUNTS PER CHANNEL
20000
10000
5000
2000
1000
500
200
100
50
20
10
^{17}O (3.846)
^{14}N (3.945)
^{13}C (3.85)
^{13}C (3.680)
^{17}O (3.058)
^{12}C (0.0)
^{13}C (3.085)
^{16}O (0.0)
^{49}Ca (4.024, 4.005)
^{49}Ca (3.595)
^{35}Cl (0.0)
^{40}Ca (0.0)
^{44}Ca (0.0)
^{48}Ca (0.0)
^{88}Sr (0.0)
^{17}O (0.871)
^{181}Ta (0.0)
^{14}N (0.0)
^{49}Ca (2.028)
^{17}O (0.0)
^{13}C (0.0)
200
240
280
320
360
400
440
480
520
560
600
640
CHANNEL NUMBER

However, the build-up of carbon on the target made analysis impossible.

Yield Curves

The yield curves were measured in 10 keV steps between 4.00 MeV and 6.00 MeV at 65°, 90°, 115°, 145° and 165°. The average beam current was held at approximately 0.3 μamps. The $Ca(OH)_2$ portion of the target was estimated to be between 3 and 5 keV thick for 5.0 MeV deuterons. Since the energy spread of the beam is believed to be less than 3 keV, the total energy spread was significantly less than the energy separation of the data points.

In the preliminary analysis of the yield curves, the large quantity of data (approximately 3000 data points) made impossible the use of such techniques as automatic selection and subtraction of background. Although automatic background routines are frequently more accurate than a human with a lightpen, the output per man-hour invested is much lower. Sufficient accuracy for the study of the yield curve was obtained by sampling background near the peak of interest and subtracting the appropriate quantity from the sum of the peak and background counts. In fact, the error introduced by this method is included in the 3% to 4% r.m.s. error quoted above. The yield curves for the charged particle reactions are shown in figures 4.11, 4.12, 4.13 and 4.14. The analysis is discussed in the next chapter.

Angular Distributions

Angular distributions were measured at 4.00, 4.50, 5.00, 5.25, 5.50 and 6.00 MeV bombarding energy. In most cases, the measurements were

taken in 5° steps between 15° and 170°. The exceptions were:

(1) the 6.00 MeV angular distribution in which a very thin layer of gold was used in place of the carbon film. The gold layer was used in a relatively simple method of obtaining the absolute cross section as described below. Unfortunately, the very large cross section for elastic scattering from gold made it impossible to carry the measurements forward of 20°.

(2) the angular distribution at 5.25 MeV. This run was not part of the joint experiment, and was intended primarily to extend the range of energies at which angular distributions for the population of the 3.846 MeV level of ^{17}O were available. The target used was prepared in a way similar to that described above except that barium was used in place of calcium. Due to the large elastic scattering cross section from barium, the measurements were not carried forward of 30°.

In the preliminary analysis of the angular distributions, accuracy was of prime importance so that automatic subtraction of background was used. The approximately 600 peaks to be summed made this procedure tedious but possible over a period a graduate student could consider finite.

The angular distributions were normalized to the count in the monitor detector and corrections were made for the dead time of the detectors. The angular distributions are shown in figures 4.1, 4.4, 4.5 and 4.8 in the next chapter.

3.3 Absolute Cross Sections

In order to obtain the absolute normalization, the elastic scattering of 2.0 MeV protons was studied using the same target as was used in the measurement of the angular distribution at 6.00 MeV. Unfortunately, it cannot be assumed that the cross section for the elastic scattering of 2.0 MeV protons from oxygen is entirely due to Coulomb forces. However, the presence of both calcium and gold on the target makes the determination of the absolute cross section fairly straightforward. The essential features are that the elastic scattering of protons from calcium at 2.0 MeV is due entirely to Coulomb forces while the elastic scattering of protons from gold is due to Coulomb forces at both 2.0 MeV and at 6.0 MeV.

The method can be expressed as follows. Let us use a subscript R to designate a Rutherford cross section. The quantity r is the ratio of the number of oxygen atoms in the target to the number of calcium atoms. Similarly c is the ratio of the number of calcium atoms to the number of gold atoms. The notation $\sigma(Ca,6.0)$ is used to designate the cross section for elastic scattering of protons (or equivalently of deuterons to within 0.1%) from calcium at 6.0 MeV. Then recalling that the Rutherford cross section is proportional to the square of the charge of the target nucleus, we obtain

$$\frac{\sigma_R(Ca,6.0)}{\sigma_R(Au,6.0)} = \frac{\sigma_R(Ca,2.0)}{\sigma_R(Au,2.0)} = \left[\frac{20}{79}\right]^2 .$$

The value of c is obtained from the expression

$$\frac{\text{peak area (Ca,2.0)}}{\text{peak area (Au,2.0)}} = \left[\frac{20}{79}\right]^2 c$$

The absolute cross section for the elastic scattering of deuterons from calcium is then given by

$$\sigma(\text{Ca},6.0) = \sigma_R(\text{Au},6.0)\,\frac{1}{c}\,\frac{\text{Peak area (Ca,6.0)}}{\text{Peak area (Au,6.0)}}$$

Using this expression, we obtain the elastic scattering cross section from oxygen as

$$\sigma(0,6.0) = \sigma_R(\text{Au},6.0)\,\frac{1}{rc}\,\frac{\text{peak area (0,6.0)}}{\text{peak area (Au,6.0)}}$$

Use of the yield curves then allows the normalization to be extended to angular distributions obtained at other bombarding energies. At least four peaks must be summed in order to obtain the absolute normalization, and it is doubtful whether this could be carried out with less than 6% or 7% error. Since data for the determination of the absolute normalization were available at several angles, some use could be made of averaging. The spread of values found for the absolute normalization was between 4% and 5%, in agreement with this estimate. However, there are several other sources of systematic error, and the size of their effect is difficult to estimate. Firstly, if the target were slightly non-uniform and the focussing conditions of the 2.0 MeV proton beam and the 6.0 MeV deuteron beam were significantly different, an error might be introduced. Secondly, although it seems virtually assured that the target was in the form $Ca(OH)_2$, it would be difficult to maintain that this may not be slightly in error.

Taking these points into consideration, it would be overly optimistic to ascribe an uncertainty of less than 10% to the determination of the absolute cross sections for the charged particle reactions. A comparison of the results obtained here for the absolute normalization with the results obtained by Baumgartner et al. (Ba 57) shows a discrepancy of 14%. Since their work was judged to have a 15% uncertainty, the agreement is satisfactory.

Total Cross Sections

Using the absolute cross sections calculated as described above, it was possible to estimate the total cross sections for populating given final states. It is necessary to know this quantity for all reactions in which there is a significant direct interaction component so that a correction to the calculated compound nucleus cross sections may be obtained. The results are shown in table 4.1 of the next chapter. Note that an error of $\pm$ 15% has been assumed for all integrated cross sections. The error is larger than that estimated above because there is some uncertainty in extrapolating the angular distributions to far forward and backward angles.

CHAPTER 4

ANALYSIS

The analysis of the experimental results was carried out in three sections:

(1) analysis of the elastic scattering of deuterons

(2) analysis of the angular distributions obtained from the reactions $^{16}O(d,p)^{17}O$ and $^{16}O(d,n)^{17}F$.

(3) analysis of the yield curves

4.1 Compound Nucleus Calculations

Although the calculation of compound nucleus properties involves optical model parameters not yet discussed, the results of the calculations are used in nearly all parts of the analysis. Therefore several of the methods used will be discussed here before beginning the main body of the section on analysis.

The calculations concerning the compound nucleus were carried out using the program HAUSER (Sm 65, Da 69b) and potentials D3, P3, N3 and A1 of table 4.3. Since the spins and parities of nearly all necessary levels in the residual nuclei were known, it was not necessary to use statistical techniques to predict the density and properties of the levels in the residual nuclei.

Calculation of meaningful cross sections was greatly complicated by

the large direct interaction cross sections. Many previous workers have suggested that the compound nucleus cross sections must be reduced before comparison with experiment (Vo 68). The justification for this reduction is that the absorption in the compound nucleus calculations should not include the effect of deuterons disappearing because of direct interactions. Since the optical model parameters obtained from the analysis of elastic scattering include the effects of both direct and compound nucleus absorption, the compound nucleus cross sections must be reduced.

The usual correction is calculated in the following way:

$$\sigma_{CN} = \left[\frac{\sigma_{tot} - \sigma_D}{\sigma_{tot}}\right] \sigma_{CN}'$$

Here σ_{CN}' is the cross section given by the compound nucleus program; σ_{CN} is the corrected value to be compared with experiment; σ_{tot} is the total reaction cross section, and σ_D is the total direct interaction cross section. At a deuteron energy of 5.0 MeV, the total reaction cross section as calculated by the optical model program SNOOPY2 (See section 4.2) and by the compound nucleus program HAUSER was approximately 1030 mb in both cases. However, of this total, 700 $\pm$ 90 mb were estimated to come from direct interactions, as shown in table 4.1. It was thus necessary to reduce the magnitude of the calculated compound nucleus cross sections by a large amount.

The large direct interaction cross sections also introduce more subtle uncertainties which have to be considered when the correction to the calculated compound nucleus cross sections is large. Since the decay

TABLE 4.1

Total Cross Sections at E_d = 5.00 MeV

Reaction	σ_{exp} (mb)	σ_{CN} (mb) (±60%)	σ_D (mb)
$^{16}O(d,d)^{16}O$		30.*	
$^{16}O(d,p)^{17}O$			
gnd	180 ± 30	70.	110 ± 40
0.871	240 ± 40	20.	220 ± 40
3.058		10.	
3.846		20.	
4.555		9.	
5.08		5.	
5.38		3.	
5.70		1.	
$^{16}O(d,n)^{17}F$			
gnd	180 ± 30	40.	140 ± 40
0.500	190 ± 30	20.	170 ± 30
$^{16}O(d,\alpha)^{14}N$			
gnd	120 ± 20	60.	60 ± 40
2.312		10.	
3.945		10.	
4.90		0.2	
Totals	910 ± 70	300 ± 180	700 ± 90

*The error in the compound elastic scattering is $^{+90\%}_{-70\%}$.

of the compound nucleus via emission of a deuteron involves the same transmission coefficients as does the formation, the cross section for compound elastic scattering should be further reduced, and the cross sections in other channels appropriately increased so as to leave the total cross section unaltered. If there were no corrections for direct interactions in other channels, the appropriate factor would be the same as the reduction of the total cross section. It is difficult to estimate the direct interaction corrections in other channels because the range of energies of the outgoing particles is large. However, it would seem that a factor slightly larger than the correction factor to the total compound nucleus cross section would by proper.

In the present case, the correction factor to the total cross section was 0.31 ± 0.15, and a further correction of 0.4 was applied to the compound elastic cross section. When the additional reduction to the compound elastic scattering was varied over the range 0.3 to 1.0, the range of the reduction in the total cross section was found to be 0.37 to 0.28. The above quoted values of 0.31 ± 0.15 and 0.40 seem to be a reasonable compromise between the extremes listed. In this manner the total compound nucleus cross section was found to be 300 ± 180 mb. The large error bars are primarily due to uncertainty in the correction factor which is in turn due to the estimated 15% error in the experimental integrated cross sections.

There will also be an effect on the calculated lifetimes of the compound nucleus, but in this case, it is quite difficult to estimate the size of the correction. However, it will likely be small ($< 10\%$) because the calculation of lifetimes does not seem to be greatly affected by moderate redistributions

of the flux between various decay channels.

4.2 Optical Model Analysis

Previous studies of elastic scattering of deuterons from ^{16}O have raised several questions. Alty (Al 67) found a significant improvement in the fits to deuteron elastic scattering data taken at 12 MeV when a spin-orbit term was added to the potential. The necessity of such a term has not been investigated at lower energies. Secondly, previous workers have tended to fix r_R, and adjust the depth of the well V to obtain the best fit to the data. Two sets of potentials have been favoured by previous workers. One set uses V ≈ 85 MeV and r_R = 1.25 fm; the other uses V ≈ 110 MeV and r_R = 1.0 fm. This raises the question of whether it is possible to use any value of r_R between 1.0 and 1.25 fm, and still obtain a good fit. Finally, there seems to be a wide range of values of W_S and r_W used. Any light that can be shed on these parameters would be useful.

Two computer codes were used in the analysis. The first, written by Perey (Pe 63, Ob 66) will be referred to here as the code PEREY. This code did not allow the use of a spin-orbit potential for the deuteron, but did include a correction for nonlocality. The second code, SNOOPY2,† allowed a spin-orbit potential for deuterons, but did not include non-locality corrections. The effect of nonlocality corrections on the elastic scattering calculations seems to be small in the case of $^{16}O(d,d)^{16}O$.

---

†Obtained from W. Haeberli, University of Wisconsin, Madison, Wis.

The angular distributions of deuterons elastically scattered from ^{16}O are shown in figure 4.1, and the corresponding plots of σ/σ_R in figures 4.2 and 4.3. In figure 4.1, the lines labelled HF give the cross section for compound elastic scattering. In the plots of σ/σ_R, σ was obtained by subtracting the calculated average compound nucleus cross section from experimental data. Initial calculations were performed using a deuteron potential proposed by Alty (Al 67). After approximate optical model parameters had been calculated for the energy range of interest in this work, the compound elastic cross section and σ/σ_R were recalculated. This iterative procedure to improve the calculation of σ/σ_R was repeated until no further significant improvement was obtained.

Even the most cursory examination of figures 4.2 and 4.3 points out the most serious problem in this investigation; fluctuations in the compound nucleus cross sections seriously affect σ/σ_R. Not only does the magnitude at back angles fluctuate greatly, but the position of the minimum near 100° varies by as much as 10°. Since there seemed to be little way of deciding which of the angular distributions was least affected by fluctuations, it was decided to obtain optical model parameters at all 6 energies and then calculate an averaged set of parameters. In calculating the averaged parameter set, the potentials obtained at each energy were given a weight inversely proportional to the χ^2 of the fit obtained.

As part of the effort to determine if a spin-orbit term is necessary in the analysis of deuteron scattering, attempts were made to find fits without use of the spin-orbit term. The best fits to the plots of σ/σ_R

Figure 4.1 Cross sections for the reaction $^{16}O(d,d)^{16}O$. The solid lines labelled HF give the calculated compound nucleus cross sections as calculated by the program HAUSER and the methods of section 4.1.

Figure 4.2 Plots of σ/σ_R for the reaction $^{16}O(d,d)^{16}O$; $V_{SO} = 0$. Calculations were carried out using potential D2 of table 4.3. The spin-orbit potential was set equal to zero. Note the dip that developes near 150° in the theoretical curve as the deuteron energy increases.

Figure 4.3 Plots of σ/σ_R for the reaction $^{16}O(d,d)^{16}O$; $V_{SO} \neq 0$. Calculations were carried out using potential D3 of table 4.3. Note the absence of the dip in the theoretical curve near 150°.

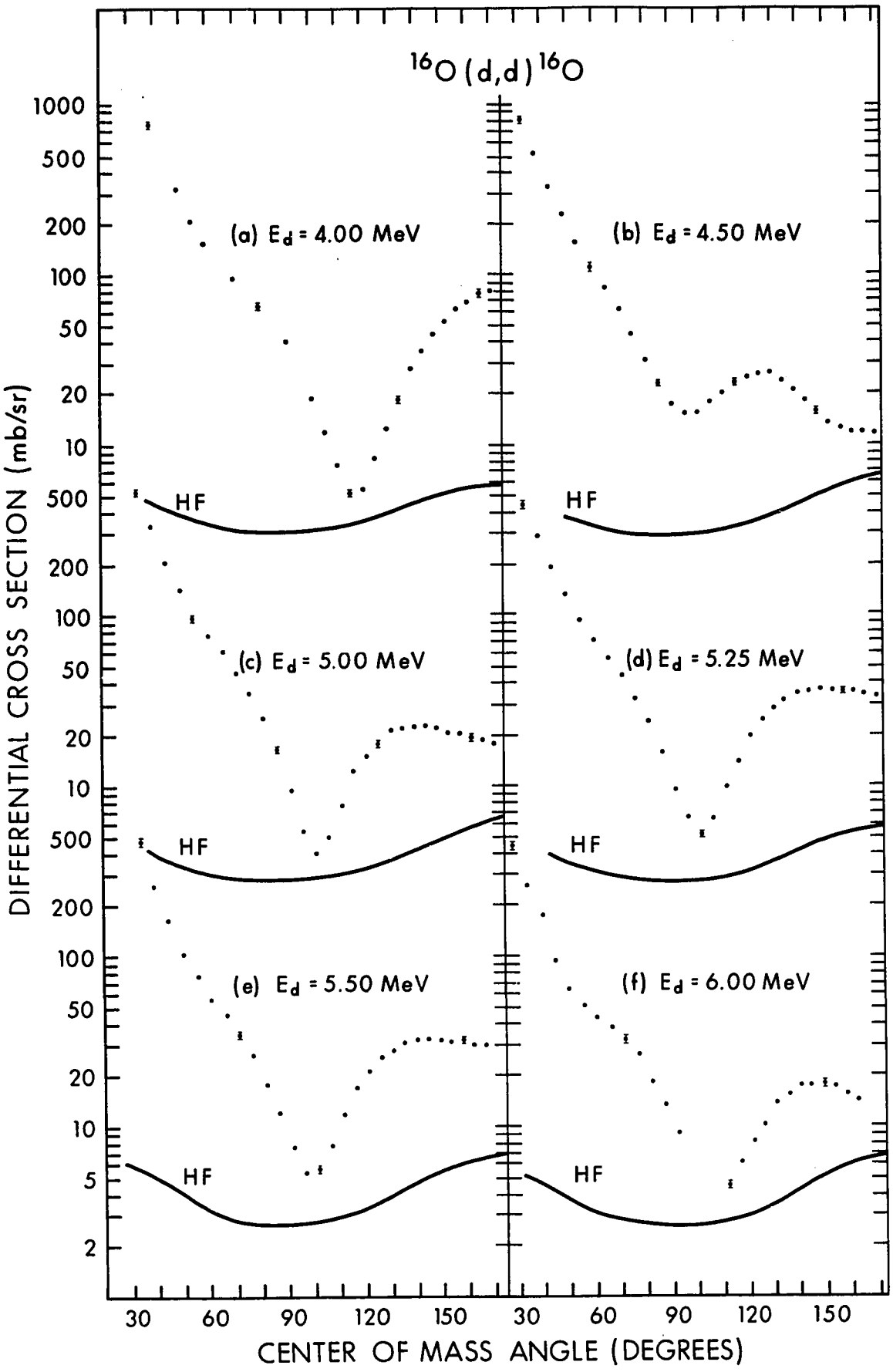
$^{16}O(d,d)^{16}O$
DIFFERENTIAL CROSS SECTION (mb/sr)
CENTER OF MASS ANGLE (DEGREES)
(a) E_d = 4.00 MeV
(b) E_d = 4.50 MeV
(c) E_d = 5.00 MeV
(d) E_d = 5.25 MeV
(e) E_d = 5.50 MeV
(f) E_d = 6.00 MeV
HF
1000
500
200
100
50
20
10
5
2
30
60
90
120
150

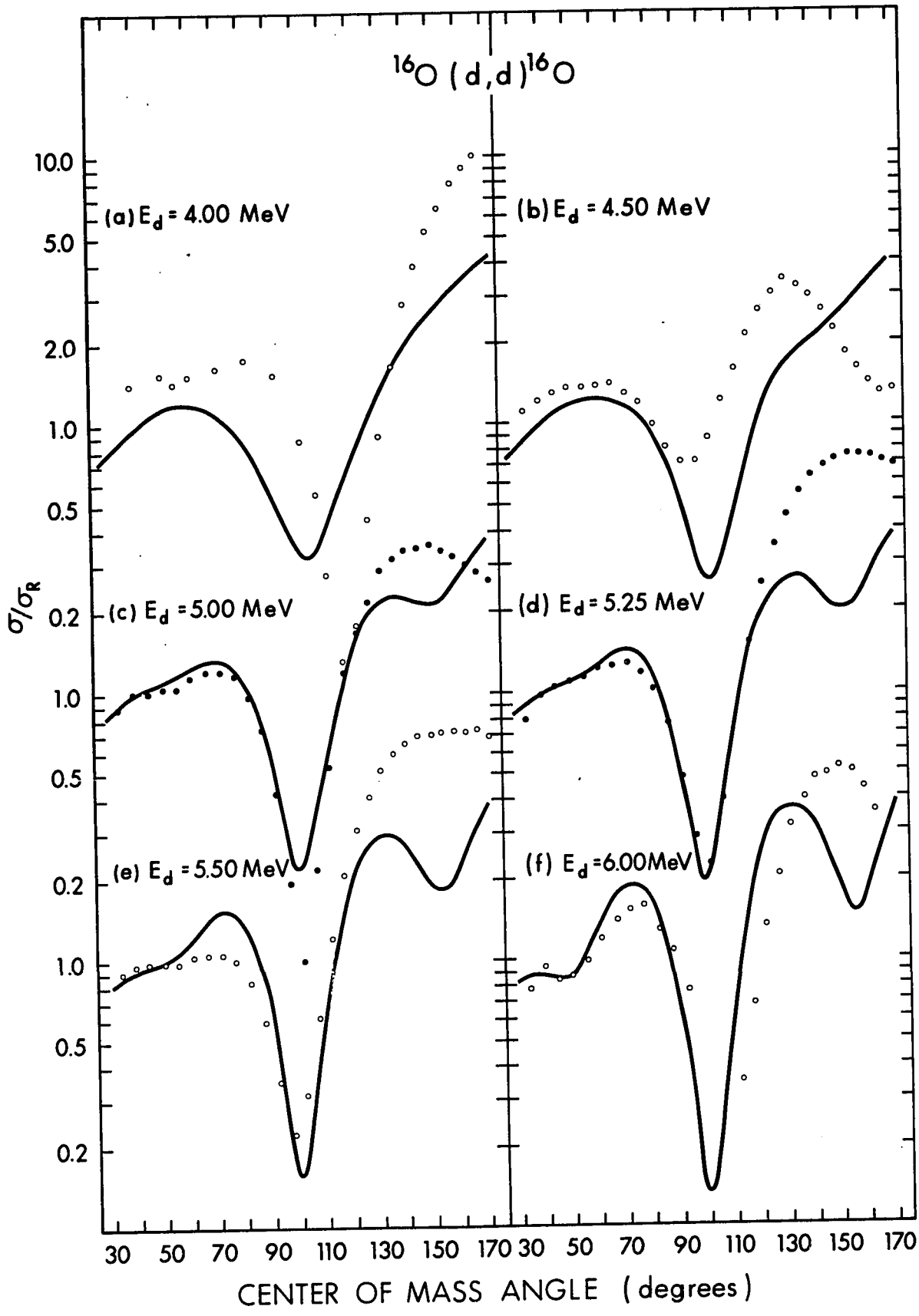
$^{16}O(d,d)^{16}O$
(a) E_d = 4.00 MeV
(b) E_d = 4.50 MeV
(c) E_d = 5.00 MeV
(d) E_d = 5.25 MeV
(e) E_d = 5.50 MeV
(f) E_d = 6.00 MeV
σ/σ_R
10.0
5.0
2.0
1.0
0.5
0.2
30 50 70 90 110 130 150 170
CENTER OF MASS ANGLE (degrees)

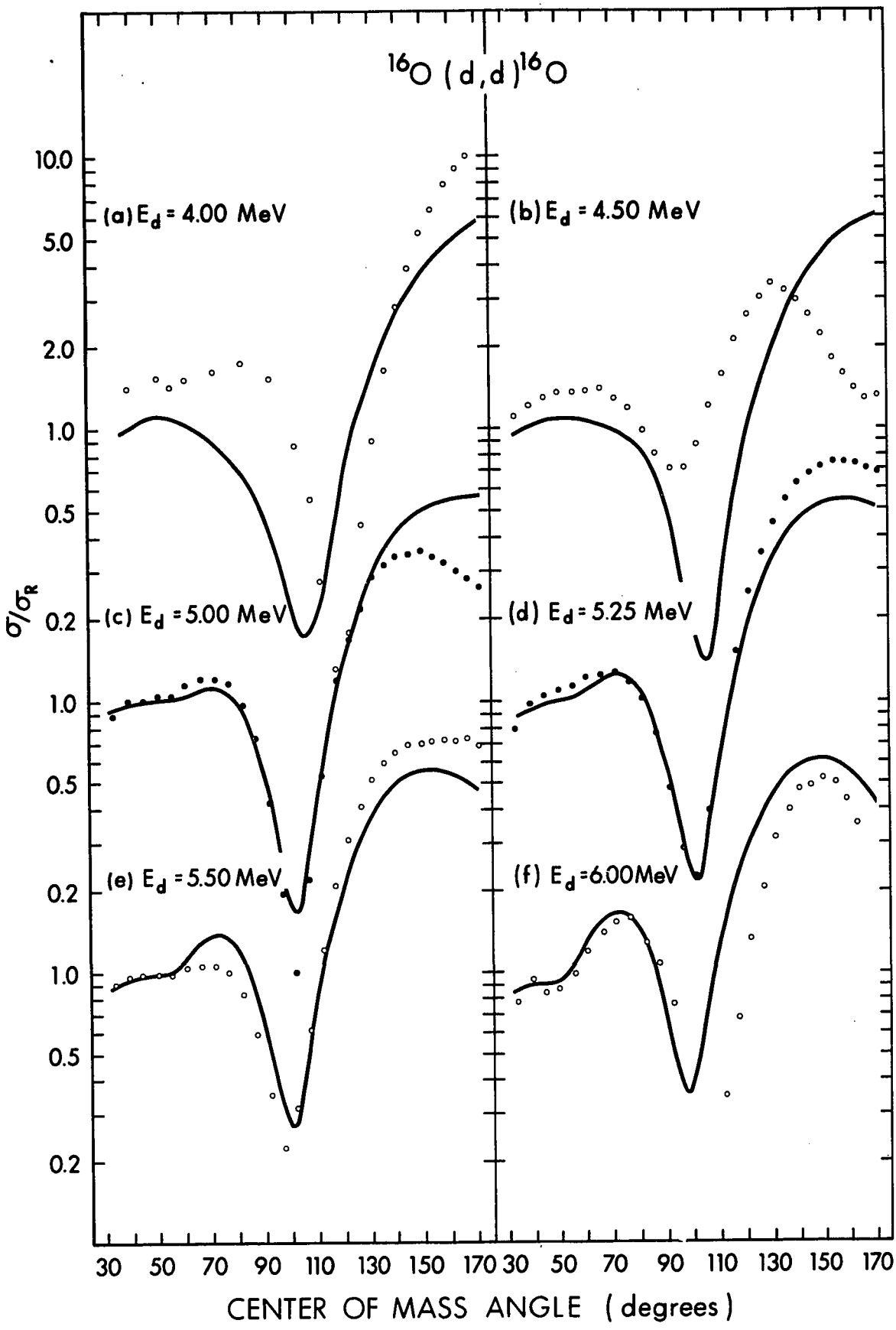
$^{16}O(d,d)^{16}O$
(a) E_d = 4.00 MeV
(b) E_d = 4.50 MeV
(c) E_d = 5.00 MeV
(d) E_d = 5.25 MeV
(e) E_d = 5.50 MeV
(f) E_d = 6.00 MeV
σ/σ_R
10.0
5.0
2.0
1.0
0.5
0.2
30 50 70 90 110 130 150 170
CENTER OF MASS ANGLE (degrees)

are shown in figure 4.2, and the potential is that labelled D2 in table 4.3. A prominent feature is the dip in the theoretical distribution that developes near 150° as the bombarding energy is increased. No combination of parameters could be found that would significantly reduce the magnitude of the dip without seriously impairing the fit elsewhere. Thus, it was concluded that this dip was a necessary feature of the analysis without spin-orbit potentials.

Using the code SNOOPY2, optical model fits using a nonzero spin-orbit term were investigated. In most cases r_{SO} and a_{SO}, the radius and diffuseness a parameters of the spin-orbit well, were set equal to 1.0 fm and 0.8 fm respectively. In some cases, these parameters were modified, but it was felt that the slight improvement in the fits did not justify the introduction of more parameters. The depth of the real well was varied over the range 80 to 110 MeV to determine if a particular value of V gave noticeably better fits than did neighbouring values. It was found that the value of χ^2 for the best fits did not change more than 30% over the entire range of well depths between 80 and 110 MeV. A detailed search was carried out to find the best optical model parameters with V in the vicinity of 80, 90 and 100 MeV. The parameters obtained in this analysis are shown in table 4.2, and the averaged potentials are those labelled D3, D4 and D5 in table 4.3. The potential with V ≈ 100 MeV (D3 in table 4.3) was used in obtaining the theoretical curves shown in figure 4.3 because when all the fits were compared by eye, D3 was judged to give marginally better fits to the data.

Several conclusions can be drawn. Firstly, the fact that the quality of fits obtained using a large range of real well depths differed only slightly, means that one can obtain satisfactory fits with V fixed anywhere

TABLE 4.2

Deuteron Optical Model Parameters Obtained in this Work

E_d (MeV)	V (MeV)	r_R (fm)	a_R (fm)	V_S (MeV)	r_I (fm)	a_I (fm)	V_{SO} (MeV)	χ^2
4.00	101.	1.04	0.83	4.7	1.58	0.42	4.8	1640
4.50	101.	1.07	0.82	5.4	2.39	0.53	6.7	514
5.00	101.	1.04	0.86	5.5	2.04	0.50	8.1	531
5.25	102.	1.04	0.89	5.4	2.06	0.35	8.3	190
5.50	104.	1.04	0.89	5.9	1.96	0.36	8.9	285
6.00	100.	1.01	0.85	6.1	1.72	0.54	12.3	3930
Averaged	102.	1.04	0.87	5.5	2.05	0.41	8.1	
4.00	91.	1.15	0.84	4.3	1.82	0.42	5.2	1599
4.50	90.	1.17	0.80	4.6	2.40	0.55	4.1	337
5.00	90.	1.13	0.86	5.4	2.07	0.50	8.3	423
5.25	91.	1.13	0.90	6.0	2.07	0.33	8.5	207
5.50	90.	1.17	0.86	4.5	1.93	0.50	8.2	386
6.00	88.	1.12	0.85	6.3	1.75	0.54	11.3	3851
Averaged	90.	1.14	0.86	5.2	2.09	0.45	7.7	
4.00	81.	1.21	0.84	4.6	1.83	0.41	5.2	1757
4.50	82.	1.23	0.85	5.2	2.36	0.50	4.4	369
5.00	80.	1.23	0.86	5.9	2.04	0.49	8.2	539
5.25	81.	1.23	0.88	6.1	2.06	0.35	7.8	351
5.50	80.	1.27	0.84	4.9	1.89	0.48	7.8	491
6.00	80.	1.22	0.83	6.7	1.74	0.53	10.8	3641
Averaged	81.	1.24	0.86	5.5	2.08	0.45	6.9	

in the approximate range 85 to 105 MeV. As will be mentioned in section 4.3, the DWBA analysis does not provide a basis for further restricting the range of real well parameters.

Secondly, it will be noted from figure 4.3 that the dip in the theoretical curve of σ/σ_R near 150° has disappeared. The fact that fits are significantly better with a nonzero spin-orbit term in the potential confirms the suspicion that a spin-orbit potential is necessary to describe the deuteron elastic scattering from ^{16}O.

It will also be noted that several other parameters have changed noticeably upon the introduction of the spin-orbit term. In particular, a_R has increased from 0.58 to 0.86 fm, and W_S has decreased from 12.5 MeV to between 5.2 and 5.5 MeV. Attempts were made to find fits using a potential similar to D2 but including a spin-orbit term. No success was obtained. It can, therefore, be concluded that the addition of a spin-orbit term to a set of deuteron potentials obtained in the course of an analysis using $V_{SO} = 0$ is not valid.

Finally, a comparison of the potentials obtained here with those found by Schwandt and Haeberli (Sc 69) for scattering of polarized deuterons from ^{40}Ca (D6 in table 4.3) is interesting. When allowance is made for the Vr_R^2 ambiguity, the real well parameters of the ^{16}O and ^{40}Ca potentials are found to be nearly the same. The absorptive well parameters are also quite similar. One is thus tempted to speculate that the optical model parameters for ^{16}O may have nearly as much physical significance as do those for heavier nuclei.

4.3 Direct Interactions

Optical Model Parameters

In the DWBA description of direct interactions, it is necessary to calculate the wavefunctions of 3 systems consisting of a particle and a nucleus. A total of 17 parameters were used in this work to describe the 3 systems - 7 each for the systems involving the deuteron and outgoing particle, and 3 for the system involving the captured particle. Calculations were carried out using the DWBA computer code DWUCK[†]. All calculations used a finite range parameter $\beta = 0.60$ fm^{-1} and nonlocality ranges of 0.5 fm for the deuteron and 0.85 fm for the captured and outgoing particles. The DWBA calculations were carried out using a deuteron nonlocality even though the optical model parameters calculated using the code SNOOPY2 were obtained without this correction. As the program DWUCK also calculated the elastic scattering angular distributions, it was possible to estimate the inaccuracy introduced by this procedure. The cross sections calculated by SNOOPY2 and DWUCK were nearly identical except in the vicinity of 100° where the discrepancy increased to about 3% to 5%.

Because of the great complexity of the DWBA model, and the large number of parameters used, a thorough investigation of all aspects of the calculation is not possible. It is thus customary to restrict calculations to those involving optical model parameters obtained in previous elastic scattering experiments. This is, of course, in accord with the picture of direct interactions being a perturbation to be added to the elastic scattering.

Calculations indicated that there was little reason to prefer one set of

---

[†]Obtained from P.D. Kunz, University of Colorado, Boulder, Col.

TABLE 4.3

Optical Model Parameters Used in this Work

Particle	Name	V (MeV)	r_R (fm)	a_R (fm)	V_S (MeV)	r_I (fm)	a_I (fm)	V_{SO} (MeV)	Source
Deuteron	D1	106.	1.0	0.68	4.6	1.8	0.76	8.2	01 69 (a_{SO}=0.6 fm)
	D2	85.5	1.27	0.58	12.5	1.7	0.47	--	this work
	D3	102.	1.04	0.87	5.5	2.05	0.41	8.1	this work
	D4	90.	1.14	0.86	5.2	2.09	0.45	7.7	this work
	D5	81.	1.24	0.86	5.5	2.08	0.45	6.9	this work
	D6*	112.	1.05	0.85	8.5	1.66	0.53	9.0	Sc 69
Proton	P1**	57.32	1.25	0.425	7.694	1.207	0.254	10.5	Al 67
	P2	54.6-0.55E	1.25	0.65	13.5	1.25	0.47	7.5	Ro 66
	P3	52.6-0.28E	1.25	0.65	10.6	1.25	0.47	8.0	Ro 66
	P4	44.7	1.25	0.65	3.42	1.25	0.47	12.0	Na 68
	P5	48.0	1.25	0.65	6.55	1.25	0.47	12.0	Na 68
Neutron	N1	48.0	1.25	0.65	5.75	1.25	0.7	5.5	Ro 66
	N2	48.46	1.20	0.71	7.07	1.20	0.47	4.0	Lu 63
	N3†	47.2	1.25	0.52	5.7	1.25	0.47	3.0	Mc 64
	N4†	49.4	1.20	0.58	5.2	1.20	0.56	3.2	Mc 64
	N5	47.0	1.25	0.65	6.0	1.25	0.47	12.0	Va 65
α-particle	A1††	185.	1.4	0.6	9.0	1.4	0.6	--	

*Obtained in analysis of the reaction $^{40}Ca(d,d)^{40}Ca$ using polarized deuterons. r_{SO} = 0.9 fm; a_{SO} = 0.6 fm.

**A volume absorptive well is used.

†In McDonald's work, a gaussian absorptive well was used. Potentials N3 and N4 are the closest approximations to McDonald's potentials possible using a derivative Woods-Saxon form for the absorptive term.

††Potential A1 was constructed artifically in the absence of suitable experimental data.

optical model potentials over another, as the shapes of the resulting angular distributions were quite similar. In the calculation of the results shown in figures 4.4, 4.5, 4.6 and 4.7, and in table 4.5 deuteron potential D3 was used. This potential was chosen primarily because it had seemed to give slightly better fits to the elastic scattering data. It does lead to spectroscopic factors about 10% lower than do potentials D4 and D5, but this is not a disturbing observation. Since the choice of optical model potentials for the outgoing particles exerted little influence on the shape of the stripping distributions, the choice of proton potential P3 and neutron potential N3 for use in the DWBA calculations was made quite arbitrarily.

Uncertainties in Spectroscopic Factors

As it was desired to see what range of spectroscopic factors would be produced by using a variety of deuteron, proton and neutron potentials, calculations were carried out using a bombarding energy of 5.0 MeV for the (d,p) reaction and 5.125 MeV for the (d,n) reactions and the potentials implicit in table 4.4. It is apparent that the variation of the spectroscopic factors obtained is approximately $\pm$ 10% about the mean. This is probably a reasonable estimate of the uncertainty introduced through use of different parameters sets obtained by analysing the same data but with different starting values in the parameter searches.

Many of the parameters used in the study of stripping reactions on ^{16}O have become fairly standard in recent studies. For instance, the captured particle was considered to be bound by the potential proposed

TABLE 4.4

Spectroscopic Factors Using Various Optical Model Parameters*

^{17}O						
	Ground State			0.871 MeV State		
	D3	D4	D5	D3	D4	D5
P1	0.80	0.94	0.98	0.70	0.75	0.72
P2	0.94	1.06	1.09	0.69	0.75	0.71
P3	0.89	0.99	1.04	0.67	0.71	0.68
P4	0.90	1.00	1.03	0.67	0.71	0.68
P5	0.91	1.02	1.04	0.68	0.72	0.69
^{17}F						
	Ground State			0.500 MeV State		
N1	0.82	0.90	0.90	0.70	0.78	0.76
N2	0.84	0.92	0.91	0.71	0.78	0.76
N3	0.80	0.88	0.88	0.75	0.82	0.81
N4	0.83	0.91	0.90	0.75	0.82	0.80
N5	0.84	0.96	0.96	0.71	0.79	0.77

*See table 4.3 for the optical model parameters.

TABLE 4.5

Spectroscopic Factors for Levels in ^{17}O and ^{17}F

Incident Energy (MeV)	^{17}O				^{17}F	
	gnd	0.871	3.058	3.846	gnd	0.500
4.00	0.97	0.97				
4.50	0.58	0.61				
4.75					0.86	0.77
5.00	0.89	0.67			0.82	0.80
5.25	0.83	--		<0.1	0.80	0.75
5.50	0.90	0.66		<0.1	0.74	0.79
5.75					0.73	0.83
6.00	0.68	0.61		<0.1	0.75	0.83
11.8[b]			0.025[a]	0.020[a]		
15.0[c]			0.038[a]	0.036[a]		
Average	0.81	0.71	0.032	0.028	0.78	0.80

(a) Deuteron potential D1 was used in these analyses.

(b) Data taken from ref. Sc 64.

(c) Data taken from ref. Ke 61.

Figure 4.4 Angular distributions of protons leading to the ground state of ^{17}O. See below.

Figure 4.5 Angular distributions of protons leading to the 0.871 MeV state of ^{17}O. See below.

Figure 4.6 Angular distributions of neutrons leading to the ground state of ^{17}F. See below.

Figure 4.7 Angular distributions of neutrons leading to the 0.500 MeV state of ^{17}F. See below.

In figures 4.4 through 4.7, the lines labelled HF give the compound nucleus cross sections as calculated by the program HAUSER and the methods of section 4.1. Refer to table 4.5 for the spectroscopic factors.

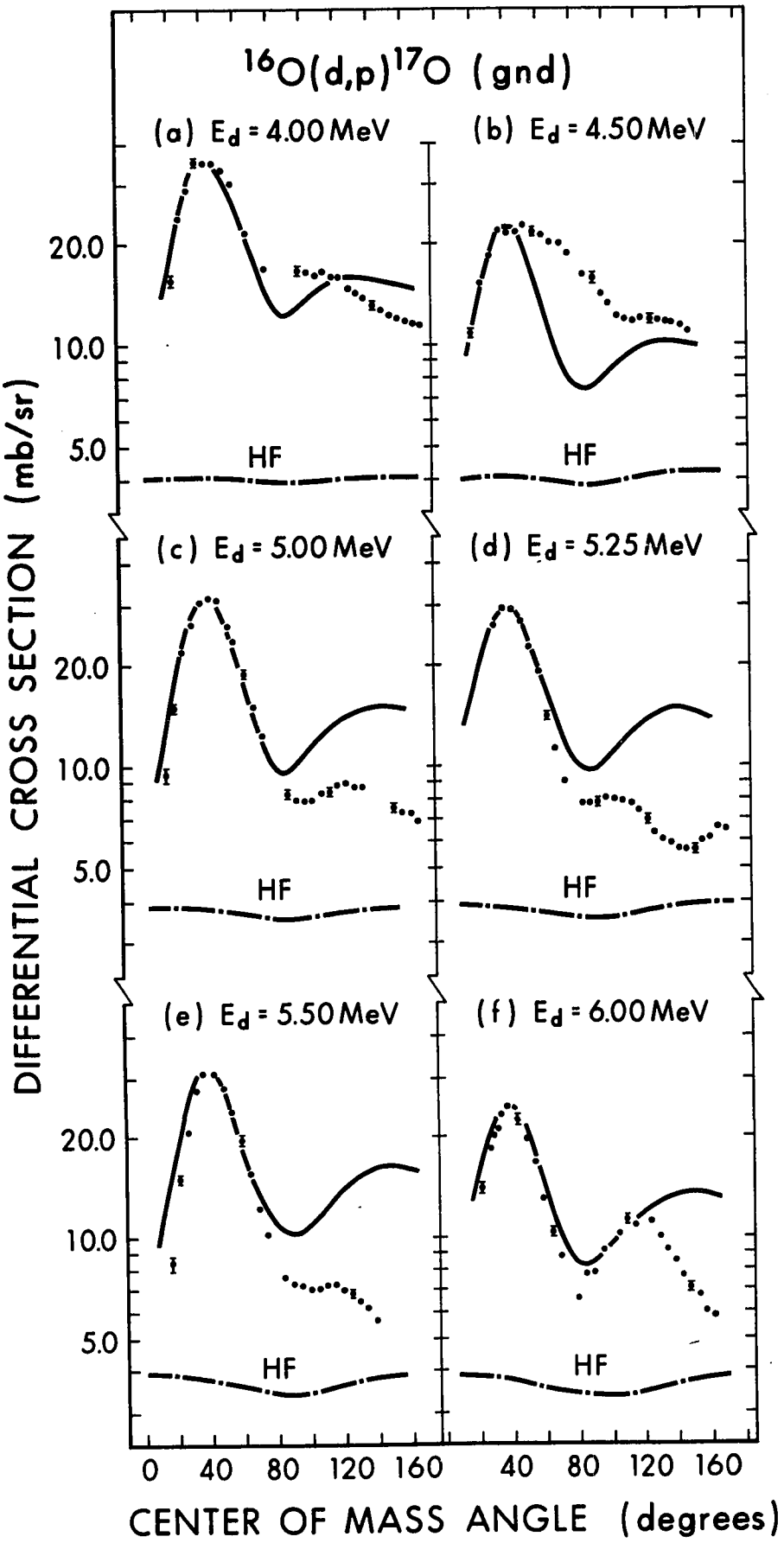
$^{16}O(d,p)^{17}O$ (gnd)
(a) E_d = 4.00 MeV
(b) E_d = 4.50 MeV
(c) E_d = 5.00 MeV
(d) E_d = 5.25 MeV
(e) E_d = 5.50 MeV
(f) E_d = 6.00 MeV
HF
20.0
10.0
5.0
DIFFERENTIAL CROSS SECTION (mb/sr)
0
40
80
120
160
CENTER OF MASS ANGLE (degrees)

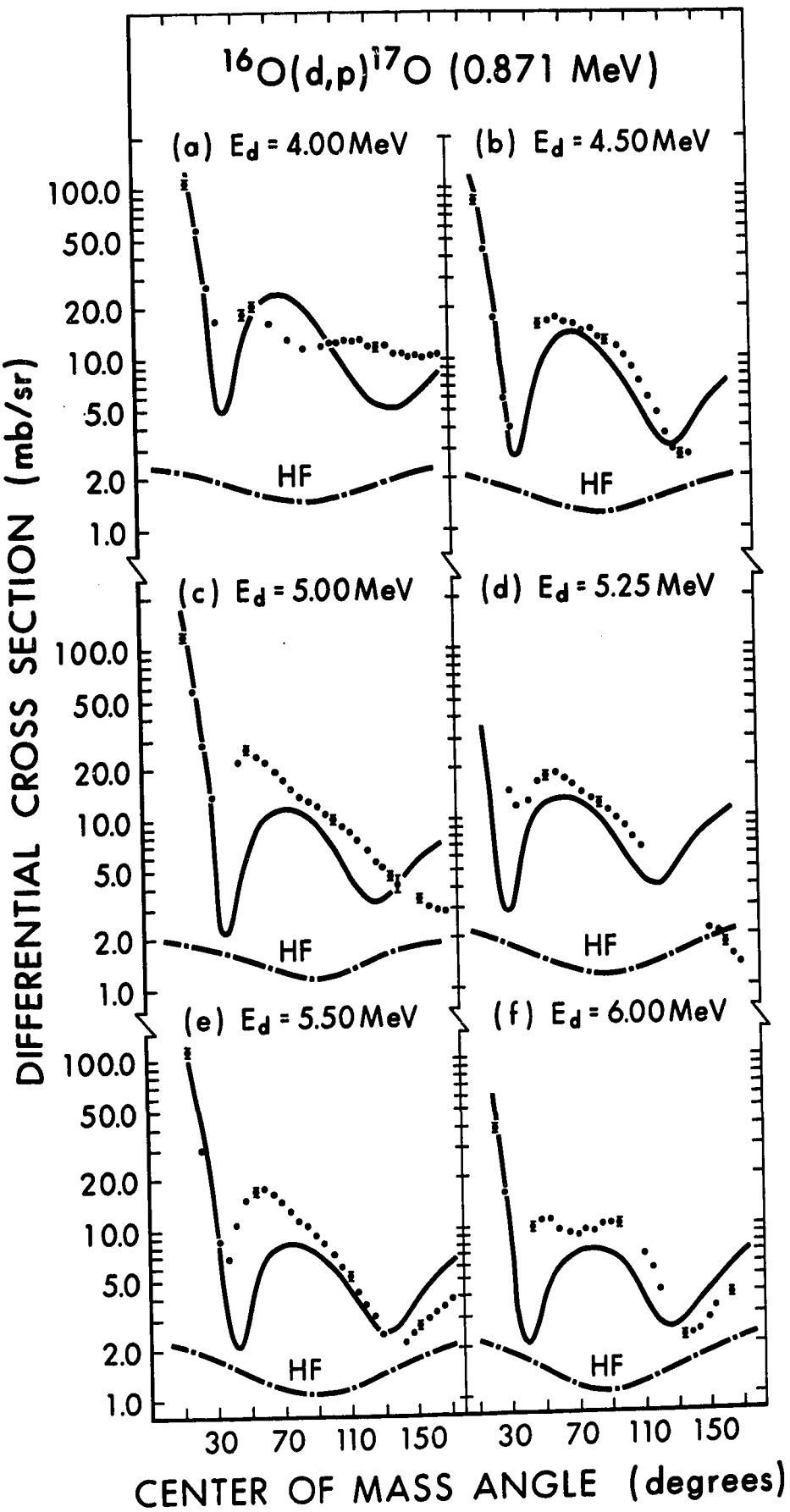
$^{16}O(d,p)^{17}O$ (0.871 MeV)
(a) E_d = 4.00 MeV
(b) E_d = 4.50 MeV
(c) E_d = 5.00 MeV
(d) E_d = 5.25 MeV
(e) E_d = 5.50 MeV
(f) E_d = 6.00 MeV
HF
100.0
50.0
20.0
10.0
5.0
2.0
1.0
DIFFERENTIAL CROSS SECTION (mb/sr)
30
70
110
150
CENTER OF MASS ANGLE (degrees)

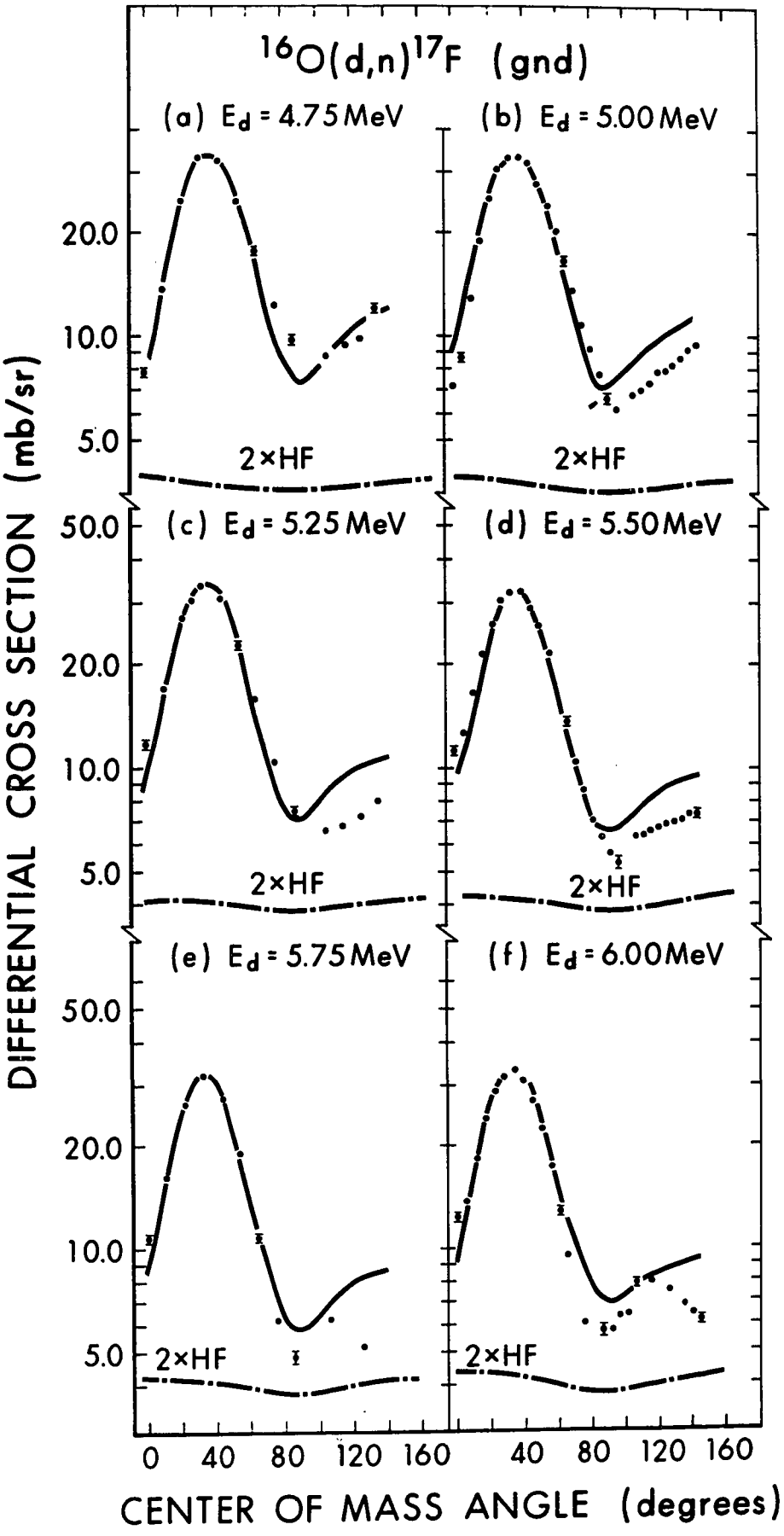
$^{16}O(d,n)^{17}F$ (gnd)
(a) E_d = 4.75 MeV
(b) E_d = 5.00 MeV
(c) E_d = 5.25 MeV
(d) E_d = 5.50 MeV
(e) E_d = 5.75 MeV
(f) E_d = 6.00 MeV
2×HF
DIFFERENTIAL CROSS SECTION (mb/sr)
CENTER OF MASS ANGLE (degrees)
0
40
80
120
160
5.0
10.0
20.0
50.0

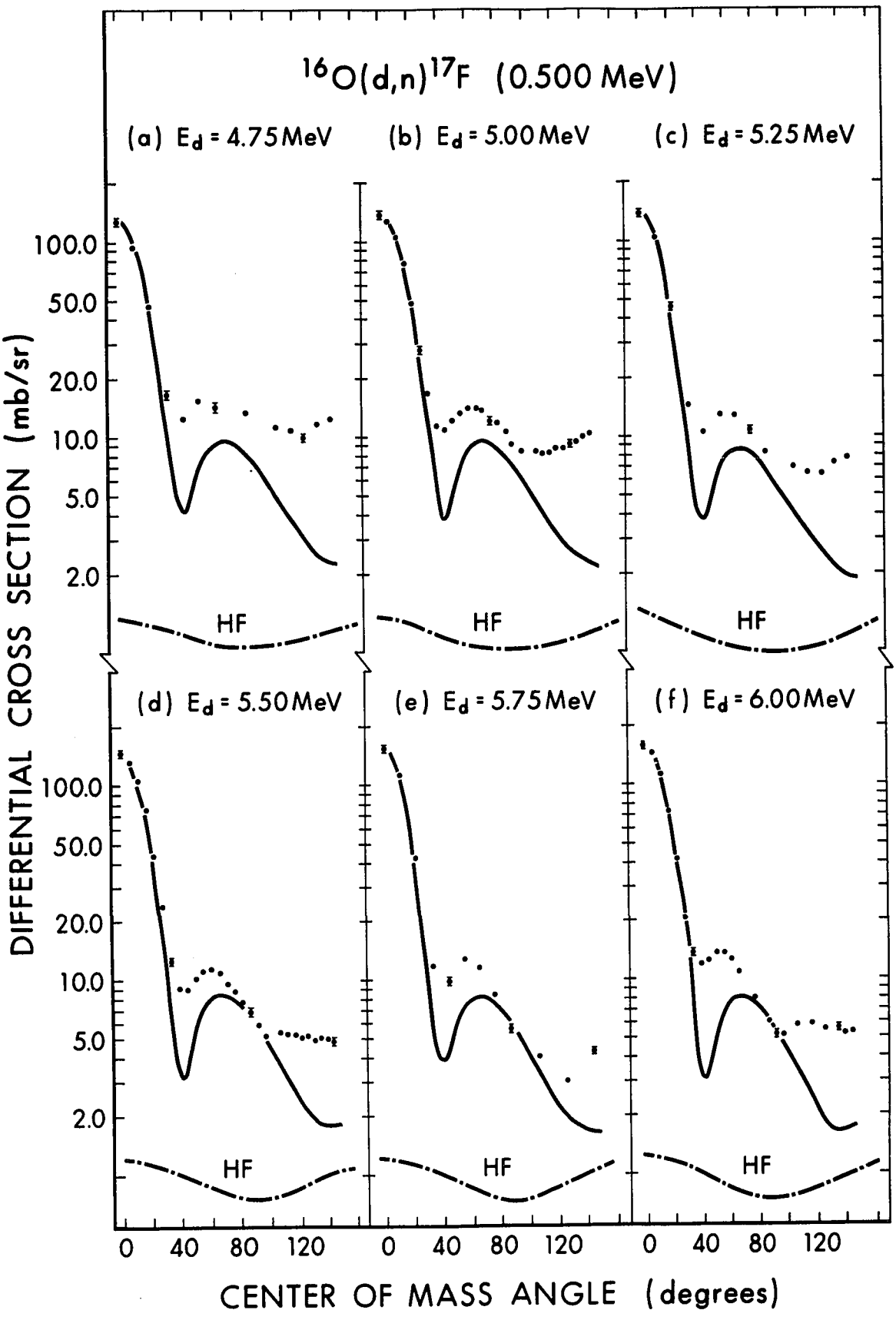
$^{16}O(d,n)^{17}F$ (0.500 MeV)
(a) E_d = 4.75 MeV
(b) E_d = 5.00 MeV
(c) E_d = 5.25 MeV
(d) E_d = 5.50 MeV
(e) E_d = 5.75 MeV
(f) E_d = 6.00 MeV
HF
100.0
50.0
20.0
10.0
5.0
2.0
DIFFERENTIAL CROSS SECTION (mb/sr)
0
40
80
120
CENTER OF MASS ANGLE (degrees)

by Fowler (Fo 60) in Al 67, Na 68, and Ol 69, as well as in the present work. The slight differences which do exist in such parameters as those governing the finite range and nonlocality corrections are expected to produce only minor discrepancies. In spite of the fact that most parameters have become fairly standard, there are still considerable uncertainties as to whether these values are the proper ones to use in a stripping calculation. The errors due to inaccuracies in our knowledge of the nonlocality, finite range and potential binding the captured particle are likely of the order of 20% (Al 67, Ol 69, Ph 68).

One source of error whose effect is difficult to estimate is the use of different computer programs in the analysis. This is particularly important in the case of ^{17}F where the binding energy is quite low (about 600 keV for the ground state and 100 keV for the first excited state). The program used in Ol 69 was that developed by Hutton and Jones at the University of Liverpool. It had been specially modified to better handle the low binding energies. However, since the quality of the fits and the values of the spectroscopic factors obtained in the present study of the 0.500 MeV level of ^{17}F do not differ significantly from those obtained using the code of Hutton and Jones, there seems to be little reason to suspect that the program used here is in any way inferior.

In summary, the probable errors influencing the calculation of spectroscopic factors are:

(1) choice of the optical model parameters 10%

(2) uncertainty in the nonlocality, finite range and potential binding the captured particle 20%

(3) absolute cross section measurements 10%

(4) compound nucleus cross sections 2% - 5%

Inspection of table 4.5 indicates that fluctuations in the cross sections due to compound nucleus components introduce a considerable uncertainty into the estimation of spectroscopic factors. The uncertainty is approximately ± 13% for the levels in ^{17}O and ± 7% for the levels in ^{17}F. It can thus be seen that there is at least a 25% to 30% uncertainty in the spectroscopic factors calculated in this work. The results are thus in agreement with the spectroscopic factors of 0.9 estimated by Brown (Br 63).

Negative Parity Levels

Before leaving the discussion of direct interactions, some mention should be made of the 3.058 and 3.846 MeV states of ^{17}O. Shape variations as a function of energy in the angular distributions of protons associated with the 3.846 MeV state made it difficult to calculate the spectroscopic factor using data obtained in this work. As can been seen from figure 4.8, no stripping pattern is visible, and the Hauser-Feshbach calculations give a fair description of the absolute cross sections. It was estimated on the basis of DWBA calculations performed using deuteron potential D3 of table 4.3 that the absence of a stripping pattern would require the spectroscopic factor to be less than 0.1.

The cross sections for populating the 3.058 and 3.846 MeV levels of ^{17}O have also been measured at deuteron energies of 11.8 (Sc 64) and 15.0 MeV (Ke 61). In these cases, stripping peaks were observed, and the compound nucleus cross sections may be assumed to be small. The data measured with

a bombarding energy of 11.8 MeV show only a small portion of the stripping peak so that it is difficult to estimate the spectroscopic factor. However, data taken at 15.0 MeV show much of the stripping peak. DWBA calculations were carried out using deuteron potential D1 as this potential was determined from elastic scattering of 12.0 MeV deuterons (O1 69). The spectroscopic factors calculated for the 3.058 and 3.846 MeV levels are given in table 4.5. Although there is a considerable discrepancy between the spectroscopic factors obtained using the data of Sc 64 and Ke 61, it is still possible to conclude that neither level carries more than a few percent of the single particle strength.

Brown's model (Br 63) predicted that there should be an $\ell = 3$ level at the approximate position of the 3.846 MeV state carrying about 5% of the 1f strength. The observed spectroscopic factor of about 0.03 is in fair agreement with Brown's prediction. Brown's model also predicted that an $\ell = 1$ level near the position of the 3.058 MeV level should carry about 5% of the 2p strength. Unfortunately, the model did not consider the possibility of a 1p component in this level. The spectroscopic factor of about 0.03 obtained here is in approximate agreement with the results of Brown's model.

Wong calculated centroids and stripping sums for the $1p_{\frac{1}{2}}$ strength in ^{17}O using a variety of 2-body interactions (Wo 68). Of the four interactions used, the Rosenfeld and Soper potentials were referred to as "central" potentials, whereas the Brueckner-Gammel-Thaler and Hamada-Johnston potentials were referred to as "realistic" potentials. Wong showed that the stripping sum for the $1p_{\frac{1}{2}}$ orbital is 0.1 or slightly larger. Since

only one level with $J^{\pi} = 1/2^{-}$ has been studied in the present work (the 3.058 MeV level), Wong's prediction is not directly comparable with the results of this work.

On the other hand, Wong also showed that whereas the central forces placed the $1p_{\frac{1}{2}}$ centroid at a sufficiently low excitation energy that some stripping strength might be observable in the 3.058 MeV level, the realistic forces placed the centroid so high as to preclude the observation of a stripping pattern. It thus becomes quite important to know whether the stripping strength observed is due to $1p_{\frac{1}{2}}$, $2p_{\frac{1}{2}}$ or both orbitals as this might lead to a choice between "central" and "realistic" potentials for calculations in the ^{16}O region. Unfortunately, the position of the $2p_{\frac{1}{2}}$ centroid is not at all well known, and there seems to be little way of drawing a conclusion as to the origin of the stripping strength.

Calculations of the polarization of protons and neutrons produced by the reactions $^{16}O(d,p)^{17}O$ and $^{16}O(d,n)^{17}F$ are not in agreement with experiment (Ev 63, Ge 67). However, the polarization phenomena are a rather sensitive test of the DWBA theory, and it may be too much to expect agreement considering the uncertainties discussed above. In addition, the effects of the compound nucleus reactions on polarization are not well known for these reactions. More polarization data will be needed before it can be ascertained whether the proton and neutron polarization data should be interpreted solely in terms of direct interactions.

Figure 4.8 Angular distributions of protons leading to the 3.846 MeV state of ^{17}O. E_d = 5.25, 5.50 and 6.00 MeV. The line labelled HF gives the compound nucleus cross sections as calculated by the program HAUSER and the methods of section 4.1.

Figure 4.9 Angular distributions of protons leading to the 3.846 MeV state of ^{17}O. E_d = 11.8 and 15.0 MeV. See below.

Figure 4.10 Angular distributions of protons leading to the 3.058 MeV state of ^{17}O. E_d = 11.8 and 15.0 MeV.

In figures 4.9 and 4.10, the experimental data are those of Ke 61 and Sc 64. Refer to table 4.5 for spectroscopic factors.

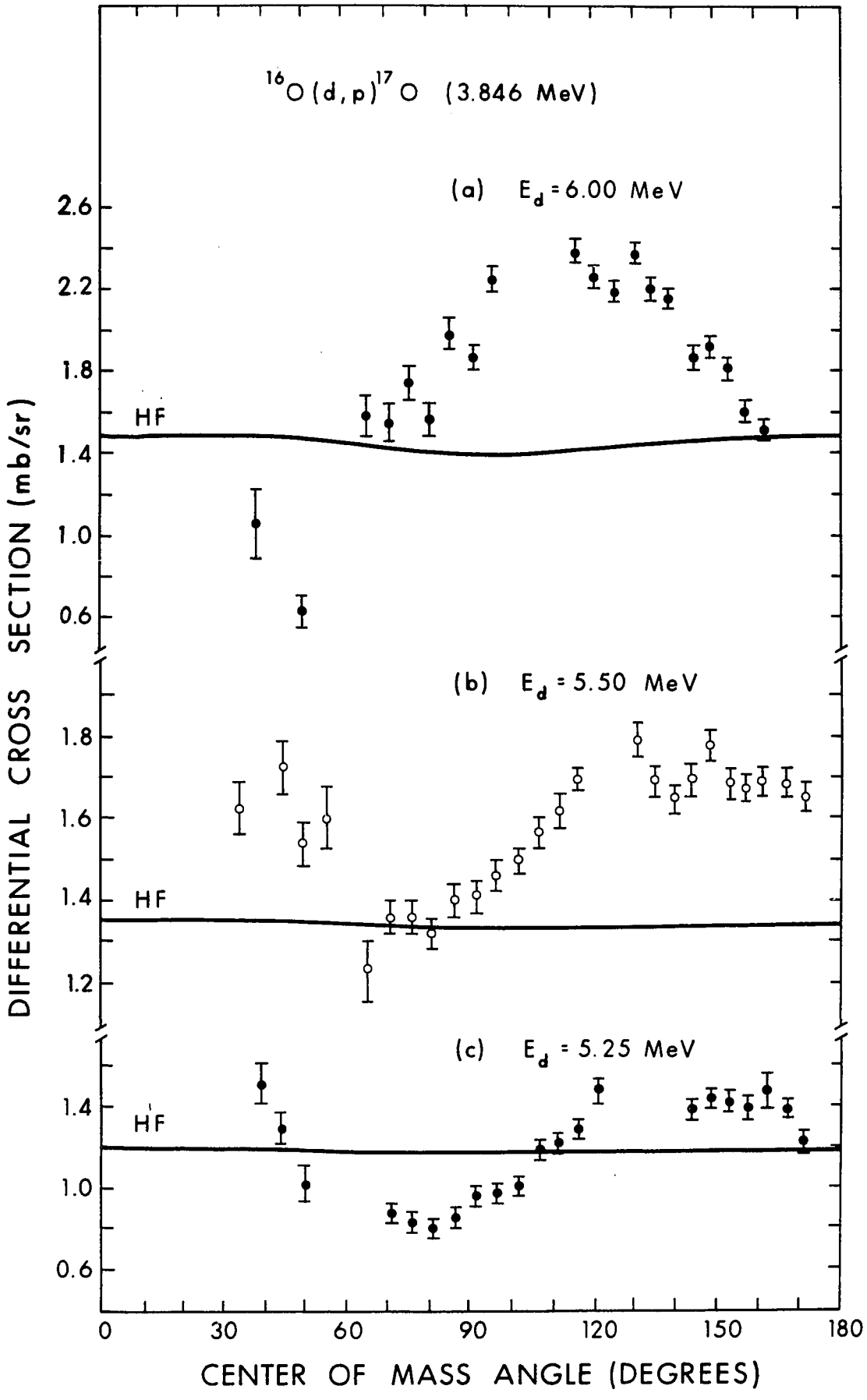
$^{16}O(d,p)^{17}O$ (3.846 MeV)
(a) E_d = 6.00 MeV
(b) E_d = 5.50 MeV
(c) E_d = 5.25 MeV
HF
HF
HF
DIFFERENTIAL CROSS SECTION (mb/sr)
CENTER OF MASS ANGLE (DEGREES)
2.6
2.2
1.8
1.4
1.0
0.6
1.8
1.6
1.4
1.2
1.4
1.0
0.6
0
30
60
90
120
150
180

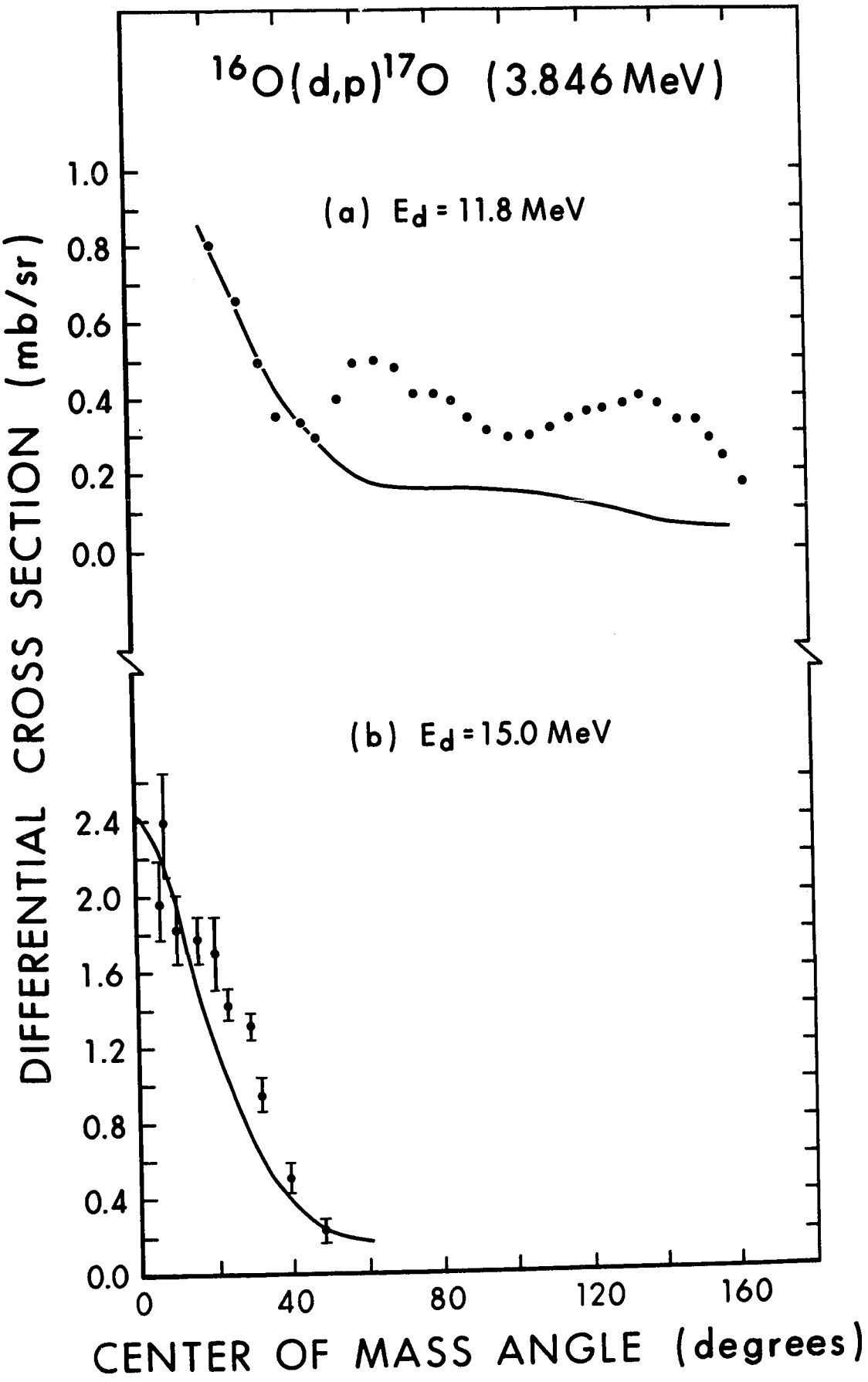
$^{16}O(d,p)^{17}O$ (3.846 MeV)
(a) E_d = 11.8 MeV
(b) E_d = 15.0 MeV
DIFFERENTIAL CROSS SECTION (mb/sr)
CENTER OF MASS ANGLE (degrees)
1.0
0.8
0.6
0.4
0.2
0.0
2.4
2.0
1.6
1.2
0.8
0.4
0.0
0
40
80
120
160

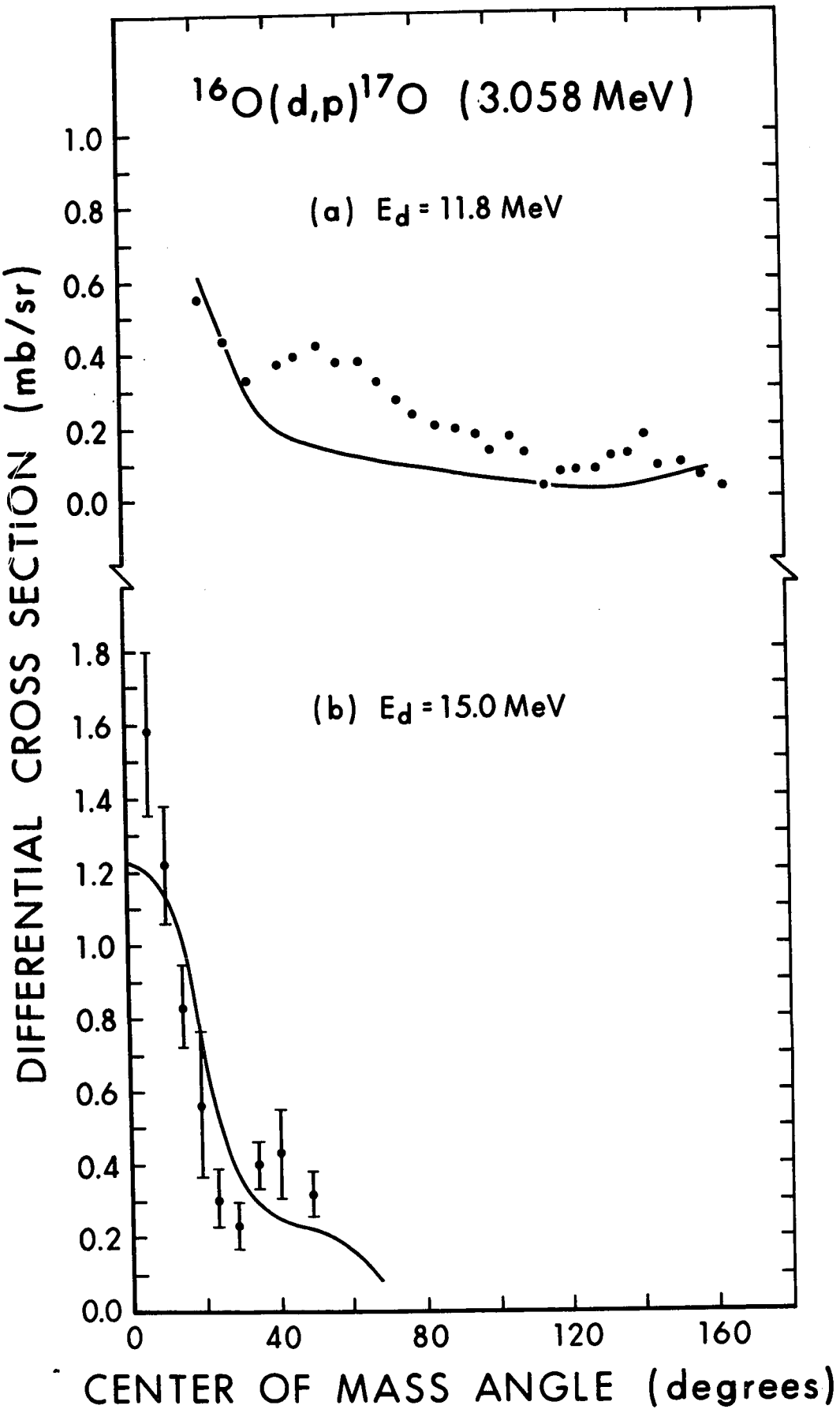
$^{16}O(d,p)^{17}O$ (3.058 MeV)
(a) E_d = 11.8 MeV
(b) E_d = 15.0 MeV
DIFFERENTIAL CROSS SECTION (mb/sr)
CENTER OF MASS ANGLE (degrees)
1.0
0.8
0.6
0.4
0.2
0.0
1.8
1.6
1.4
1.2
1.0
0.8
0.6
0.4
0.2
0.0
0
40
80
120
160

4.4 Analysis of the Yield Curves

Compound Nucleus Lifetimes

The quantity most easily obtained from an analysis of yield curves is the coherence energy Γ. As outlined in chapter 2, the coherence energy is closely related to the average width of the levels in the compound nucleus. In an Ericson fluctuation analysis, (Er 63), the assumption is usually made that the width of the compound nucleus levels is independent of spin. Theoretical values of Γ were calculated using the program HAUSER. In this theory, Γ is not independent of the spin J of the compound nucleus levels. As is shown in 4.6, the J-dependence is actually rather strong. Before comparing theory and experiment, however, two additional effects must be considered. Firstly, only a few levels in the compound nucleus have spin 5 or higher. Values of Γ associated with such large spins will not contribute appreciably to the experimental value. Secondly, resonances with widths less than about 15 keV will not be observable because of the resolution with which the yield curves were studied. As a result, the levels actually contributing to the experimental value of Γ (those with J = 1, 2, 3 and 4) show only a much smaller J-dependence. The theoretical value of Γ is thus estimated to be in the neighbourhood of 55 keV.

In the analysis of the experimental data, a problem arose in the interpretation of $\bar{\sigma}$ in the expression for the autocorrelation function:

$$C(\varepsilon) = \frac{\langle [\sigma(E) - \bar{\sigma}][\sigma(E+\varepsilon) - \bar{\sigma}] \rangle}{(\bar{\sigma})^2}$$

TABLE 4.6

Calculated Compound Nucleus Lifetimes and Resonance Widths

Spin	Lifetime ($\times 10^{-20}$ sec)	Γ (keV)
0	9.1	7.
1	1.2	54.
2	1.1	61.
3	1.3	51.
4	1.6	41.
5	3.7	18.
6	10.	6.

The usual interpretation is that $\overline{\sigma}$ is the average cross section calculated over the entire energy range for which data are available. The assumption that direct interaction cross sections and the average compound nucleus cross sections, in the sense of a Hauser-Feshbach calculation, are independent of energy is thus built into the analysis. In the energy range of this experiment, however, neither of these assumptions is correct. An alternate approach is to consider $\overline{\sigma}$ as a "smooth" cross section varying slowly with energy. $\overline{\sigma}$ is intended to represent all processes other than the rapid fluctuations in the compound nucleus cross section. One is then capable of allowing various amounts of structure in $\overline{\sigma}$ depending on the degree to which energy dependent intermediate structure and direct interactions contribute. The effect of allowing progressively narrower structure in $\overline{\sigma}$ is to reduce the value of Γ obtained.

In the present work, it was found that if $\overline{\sigma}$ was forced to be independent of energy, consistent values of Γ could not be obtained. On the other hand, satisfactory results were obtained when it was allowed to vary linearly with energy. The results shown in table 4.7 were calculated in this way. When structure as narrow as 400 keV was allowed in $\overline{\sigma}$, the value of Γ was reduced by about 40%. Exact agreement between experiment and theory could likely have been obtained by juggling the amount of structure in $\overline{\sigma}$, but no purpose would have been served by doing so.

The major source of error in the experimental determination of Γ is the result of the statistical methods used. Since data are measured over only a finite range of energies, only a finite number of resonances make their influence felt. Using the expressions of Da 65, it is found that

TABLE 4.7

Experimental Values of the Coherence Energy

Reaction	Γ (keV)
$^{16}O(d,n)^{17}F$ (gnd)	70
$^{16}O(d,n)^{17}F$ (0.500 MeV)	67
$^{16}O(d,p)^{17}O$ (gnd)	75
$^{16}O(d,p)^{17}O$ (0.871 MeV)	63
$^{16}O(d,p)^{17}O$ (3.846 MeV)	62
Mean Value	67

Figure 4.11 Yield curves for the reaction $^{16}O(d,d)^{16}O$.

Figure 4.12 Yield curves for the reaction $^{16}O(d,p)^{17}O$ populating the ground state of ^{17}O.

Figure 4.13 Yield curves for the reaction $^{16}O(d,p)^{17}O$ populating the 0.871 MeV state of ^{17}O.

Figure 4.14 Yield curves for the reaction $^{16}O(d,p)^{17}O$ populating the 3.846 MeV state of ^{17}O.

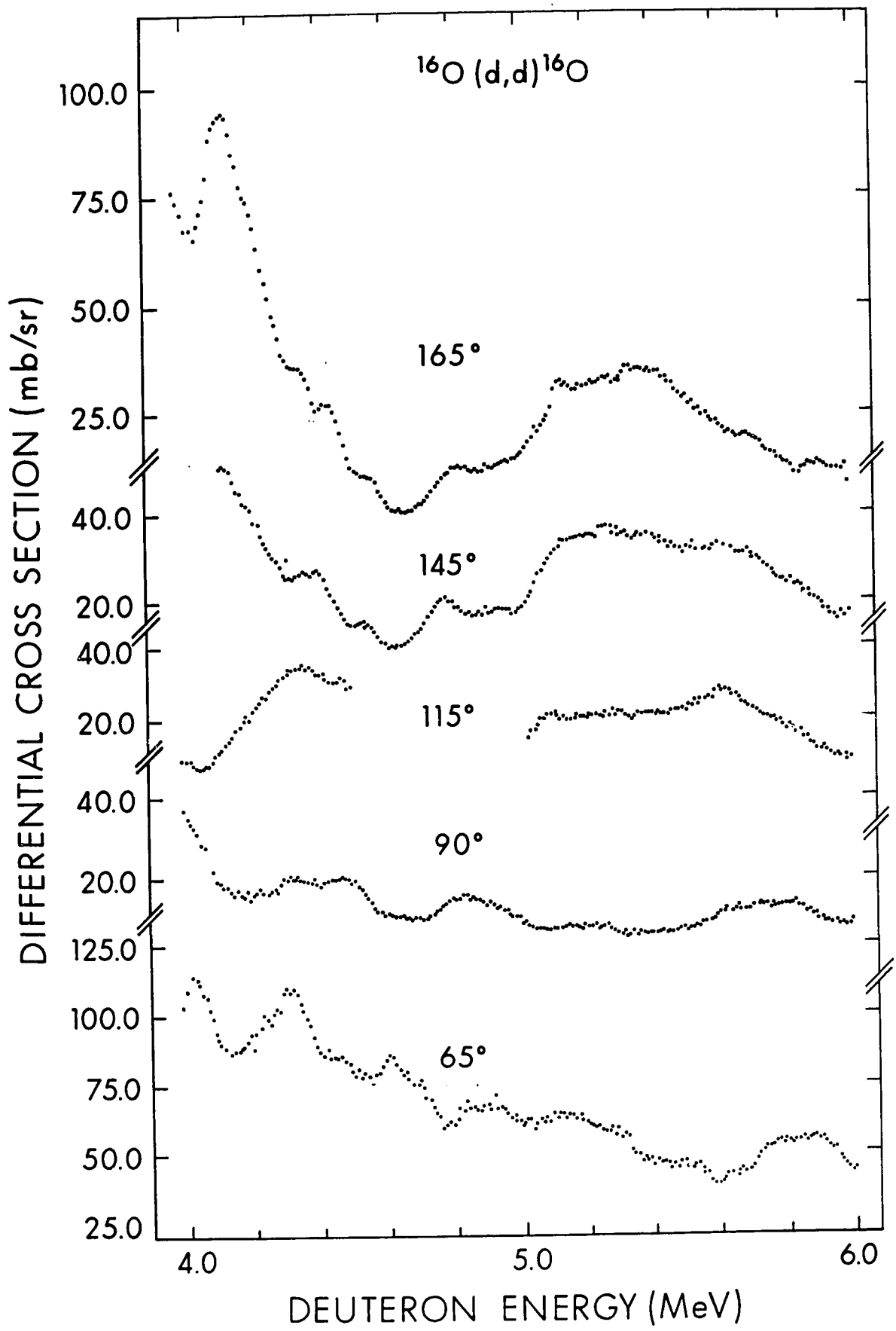
^{16}O (d,d)^{16}O
100.0
75.0
50.0
25.0
165°
40.0
20.0
145°
40.0
20.0
115°
40.0
20.0
90°
125.0
100.0
75.0
50.0
25.0
65°
DIFFERENTIAL CROSS SECTION (mb/sr)
4.0
5.0
6.0
DEUTERON ENERGY (MeV)

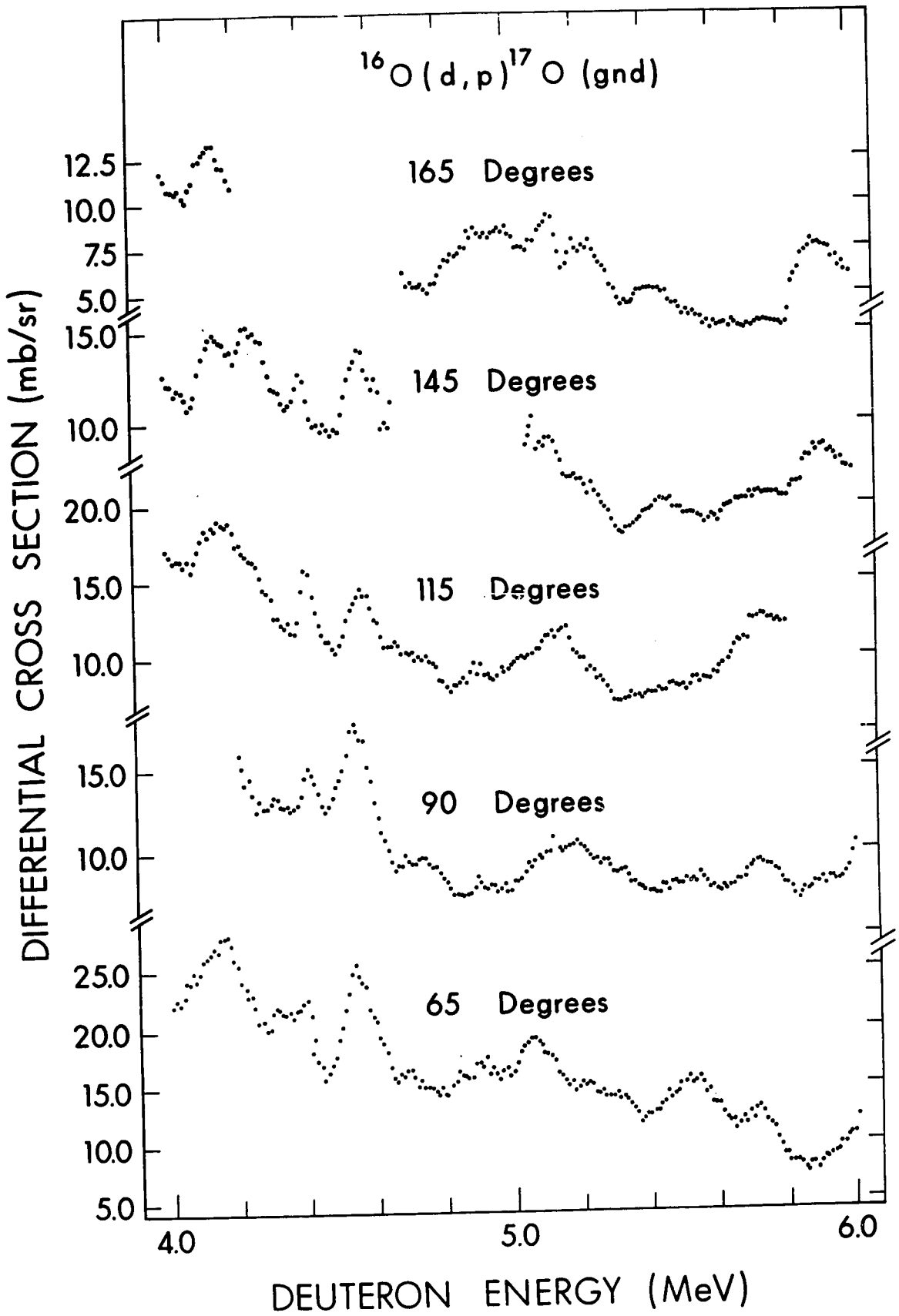
$^{16}O(d,p)^{17}O$ (gnd)
165 Degrees
145 Degrees
115 Degrees
90 Degrees
65 Degrees
12.5
10.0
7.5
5.0
15.0
10.0
20.0
15.0
10.0
15.0
10.0
25.0
20.0
15.0
10.0
5.0
4.0
5.0
6.0
DIFFERENTIAL CROSS SECTION (mb/sr)
DEUTERON ENERGY (MeV)

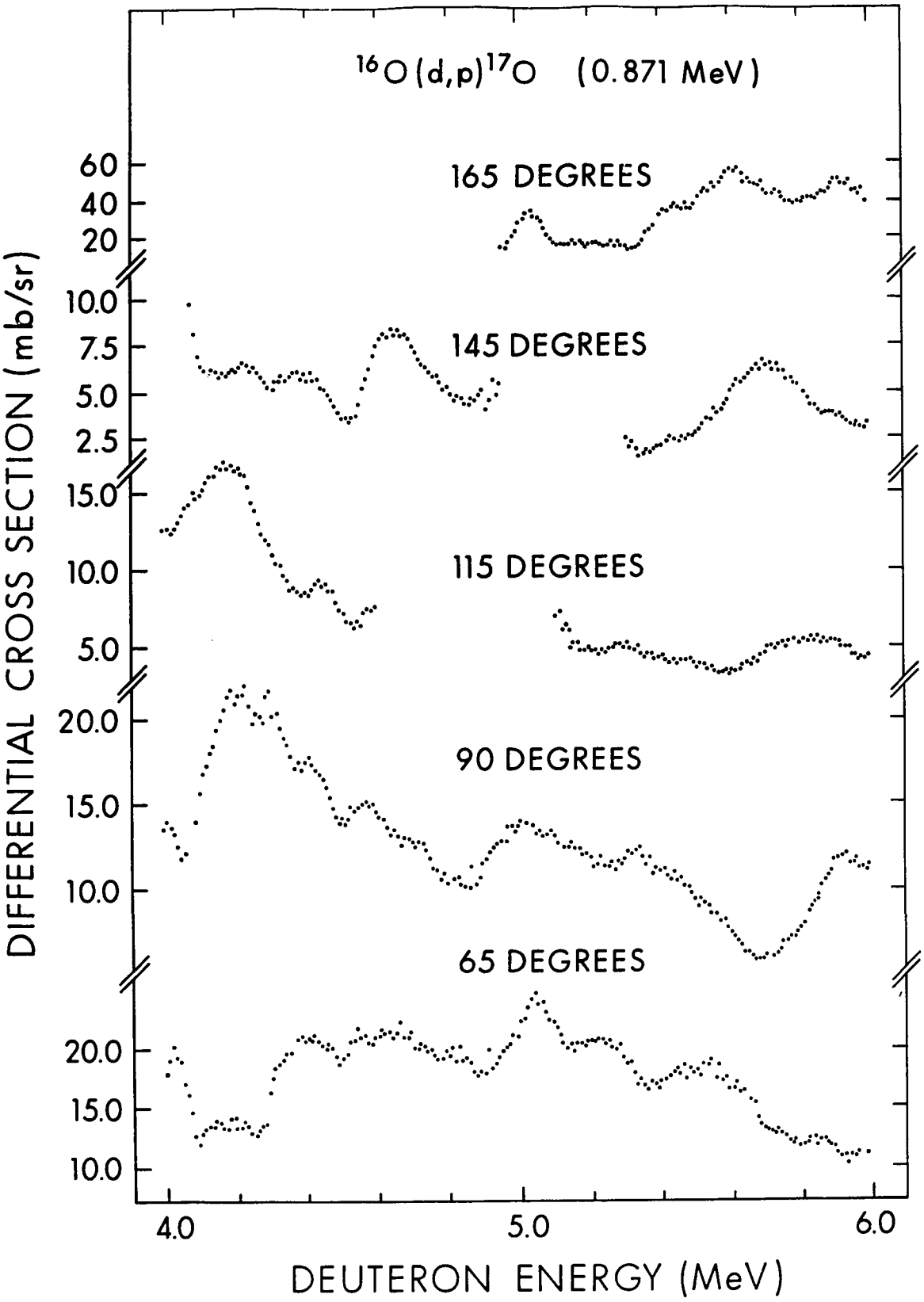
$^{16}O(d,p)^{17}O$ (0.871 MeV)
165 DEGREES
145 DEGREES
115 DEGREES
90 DEGREES
65 DEGREES
60
40
20
10.0
7.5
5.0
2.5
15.0
10.0
5.0
20.0
15.0
10.0
20.0
15.0
10.0
DIFFERENTIAL CROSS SECTION (mb/sr)
4.0
5.0
6.0
DEUTERON ENERGY (MeV)

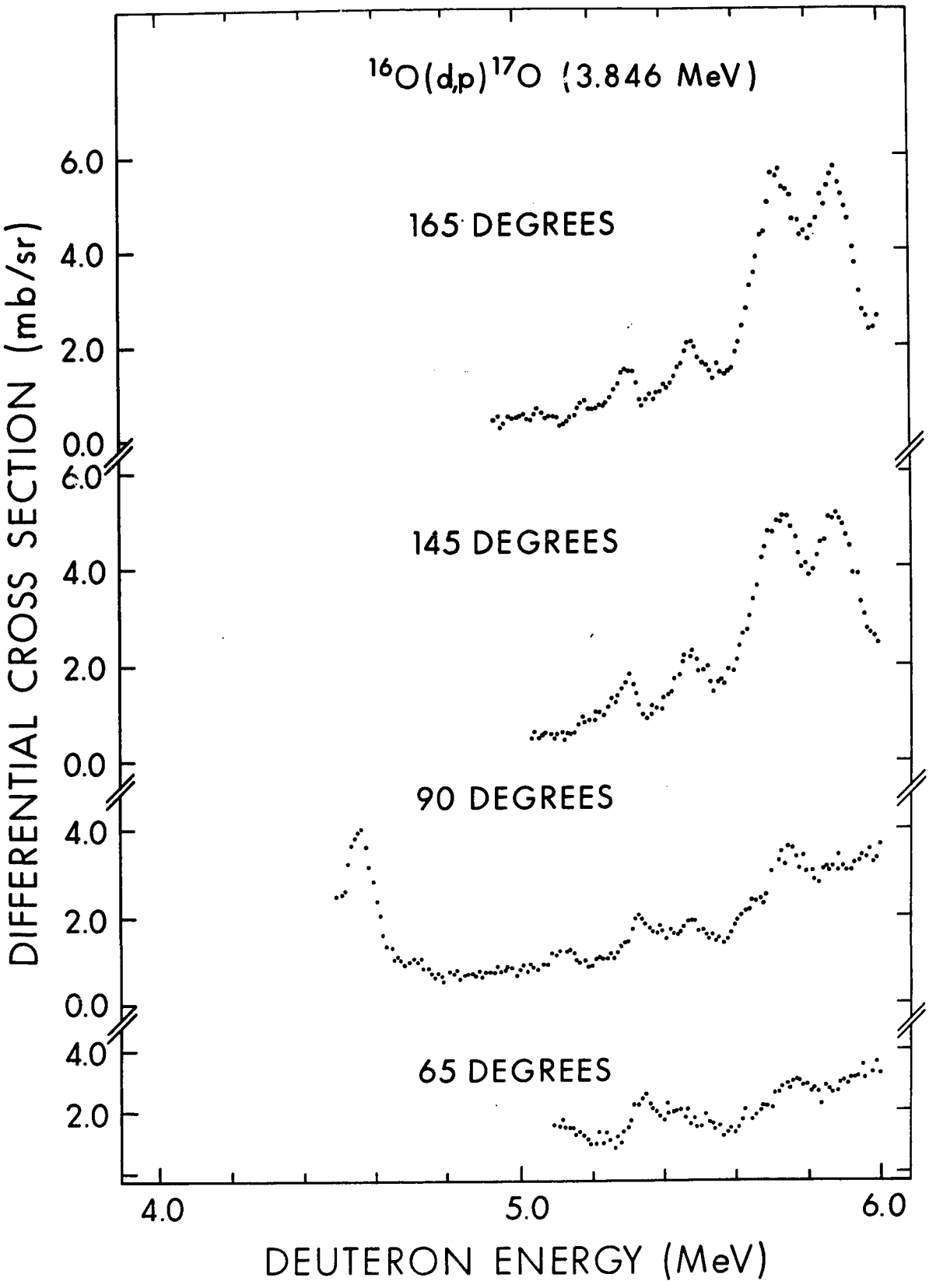
$^{16}O(d,p)^{17}O$ (3.846 MeV)
165 DEGREES
145 DEGREES
90 DEGREES
65 DEGREES
DIFFERENTIAL CROSS SECTION (mb/sr)
DEUTERON ENERGY (MeV)
6.0
4.0
2.0
0.0
4.0
5.0
6.0

Figure 4.15 Yield curves for the reaction $^{16}O(d,n)^{17}F$ populating the ground state of ^{17}F.

Figure 4.16 Yield curves for the reaction $^{16}O(d,n)^{17}F$ populating the 0.500 MeV state of ^{17}F.

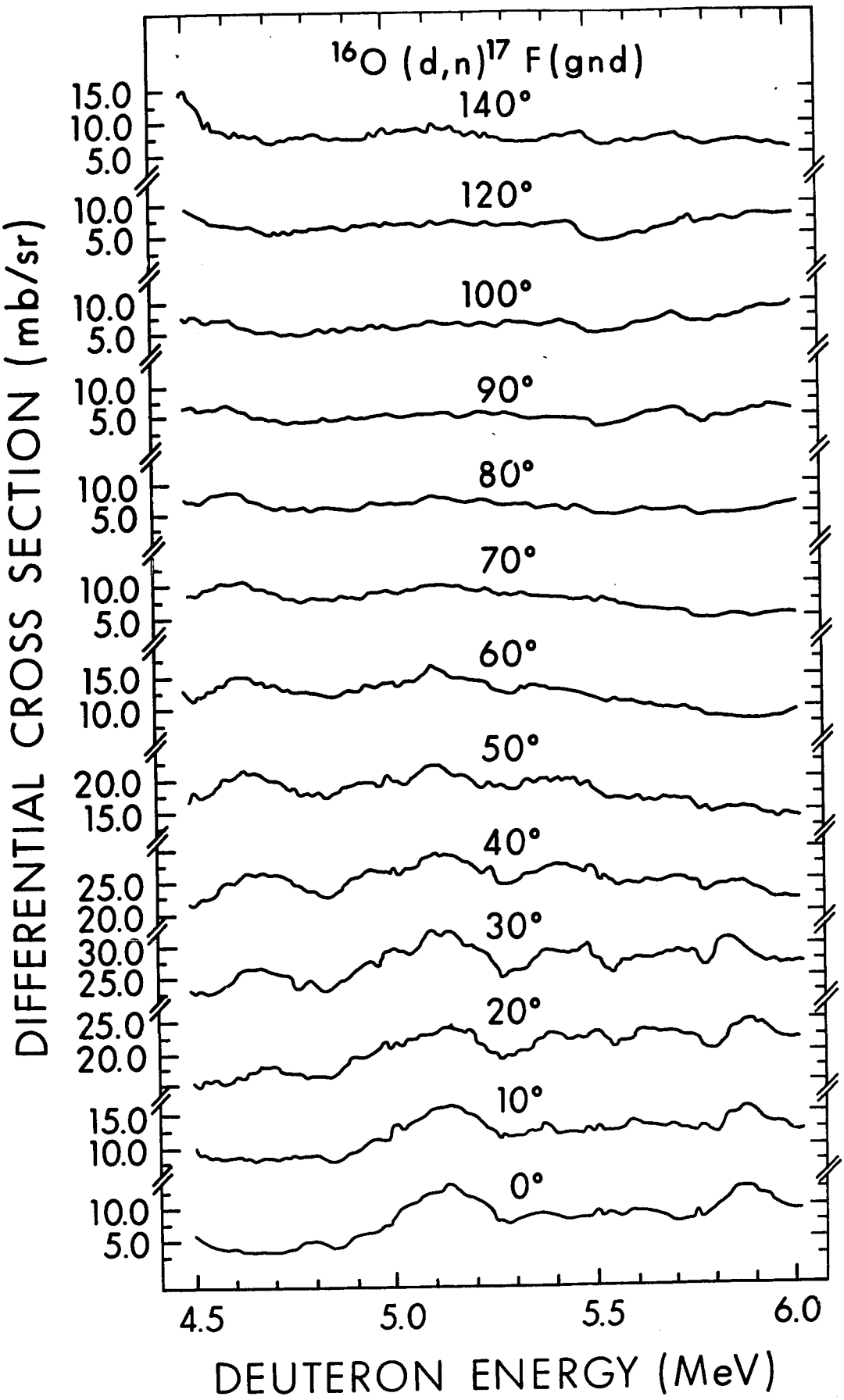
^{16}O (d,n)^{17} F(gnd)
140°
120°
100°
90°
80°
70°
60°
50°
40°
30°
20°
10°
0°
15.0
10.0
5.0
10.0
5.0
10.0
5.0
10.0
5.0
10.0
5.0
15.0
10.0
20.0
15.0
25.0
20.0
30.0
25.0
25.0
20.0
15.0
10.0
10.0
5.0
4.5
5.0
5.5
6.0
DIFFERENTIAL CROSS SECTION (mb/sr)
DEUTERON ENERGY (MeV)

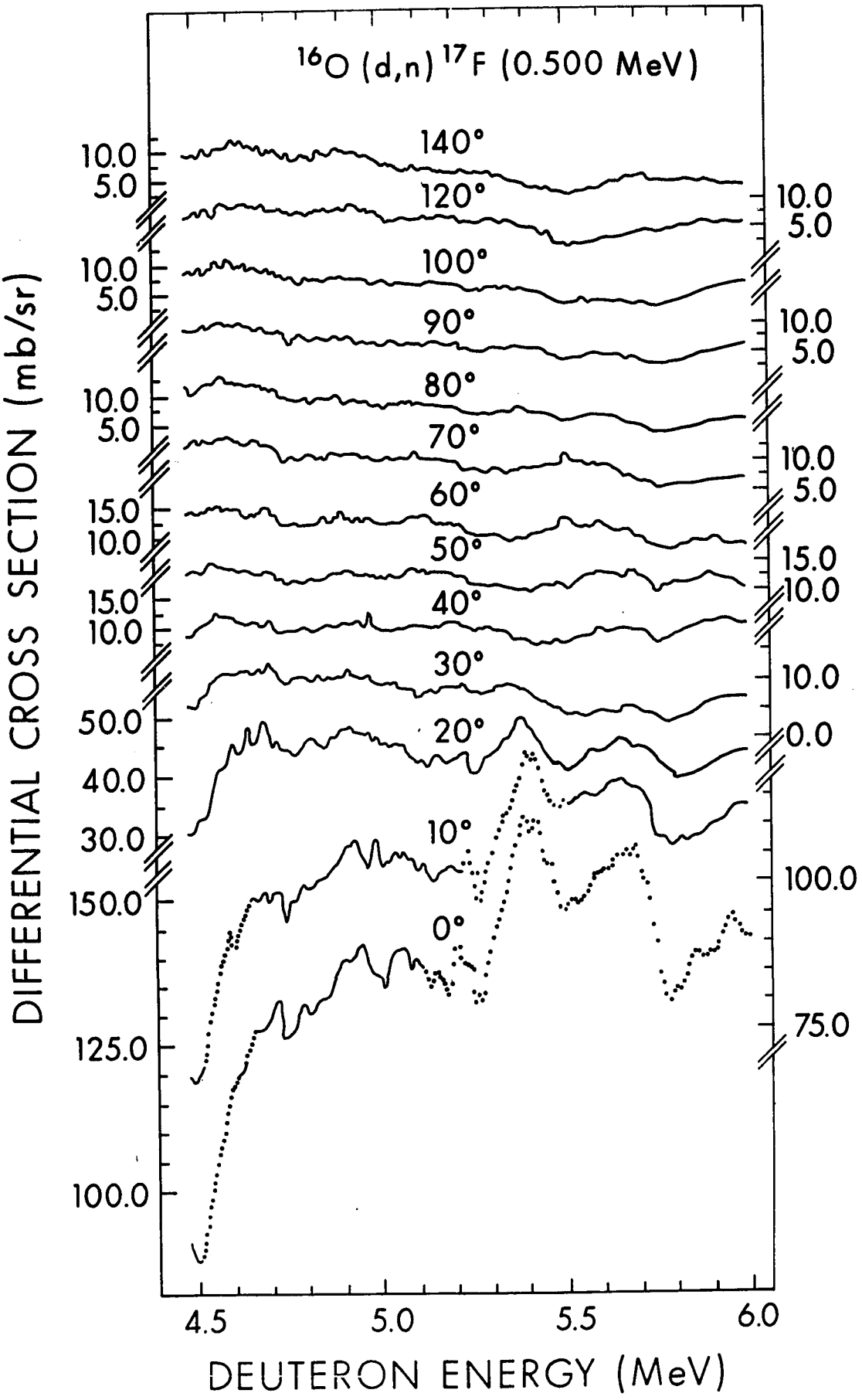
^{16}O (d,n) ^{17}F (0.500 MeV)
140°
120°
100°
90°
80°
70°
60°
50°
40°
30°
20°
10°
0°
10.0
5.0
10.0
5.0
10.0
5.0
10.0
5.0
15.0
10.0
15.0
10.0
50.0
40.0
30.0
150.0
125.0
100.0
10.0
5.0
10.0
5.0
10.0
5.0
15.0
10.0
10.0
0.0
100.0
75.0
DIFFERENTIAL CROSS SECTION (mb/sr)
4.5
5.0
5.5
6.0
DEUTERON ENERGY (MeV)

the "finite range of data" errors in calculating the magnitude of the autocorrelation function are about 30%. It is easily shown that there is also approximately 30% error in the determination of Γ.

Table 4.7 shows experimental values of Γ determined from the yield curves of several reactions. In most cases, the agreement with the theoretical value of 55 keV is quite satisfactory. The spread of values obtained likely arises from a combination of finite range of data errors and other uncertainties introduced by using a form of $\overline{\sigma}$ varying only linearly with energy.

Interference Effects

It is generally considered difficult to establish the presence of interference between the compound nucleus and direct interaction components of a reaction. This is primarily because of the difficulty of distinguishing interference effects from the more common fluctuations arising solely from the compound nucleus reactions. However, in the reaction $^{16}O(d,n)^{17}F$ populating the 0.500 MeV state (figure 4.16), there seems to be a chance of separating the two effects. At forward angles, the direct interaction is of the order of 100 times as strong as the compound nucleus cross section. On the other hand, at backward angles, the difference is only a factor of 4 or 5. At all angles back of 30°, the observed fluctuations are of the order of $\pm$ 3 mb/sr or approximately 20% of the total cross section. This is much as expected for a level of spin 1/2 (Er 60). At forward angles, however, the fluctuations are much larger. At 0°, the fluctuations are as large as 30 mb/sr, or some 20 times as large as the average compound

nucleus cross section as calculated by the Hauser-Feshbach program. It is also important to note that the size of these large fluctuations decreases as we move off the stripping peak, and the direct interaction component of the reaction decreases.

The maximum size expected for interference effects can be estimated. If we write the amplitude T for the combined direct and compound nucleus reactions as

$$T = T_{CN} + T_D \quad ,$$

where T_{CN} is the amplitude for the compound nucleus component of the reaction, and T_D is the direct reaction amplitude, then the total cross section is given by

$$\sigma = |T|^2 = |T_{CN}|^2 + |T_D|^2 + 2\ \mathrm{Re}(T_{CN}\ T_D^*)$$

$$= \sigma_{CN} + \sigma_D + 2\ \mathrm{Re}(T_{CN}\ T_D^*) \ .$$

The rather crude approximation that

$$T_{CN}\ T_D^* = \sqrt{\sigma_{CN}\ \sigma_D}$$

allows us to estimate the maximum size of the interference cross section:

$$\sigma_I^{max} = \max[2\ \mathrm{Re}(T_{CN}\ T_D^*)] \approx 2\sqrt{\sigma_{CN}\ \sigma_D}$$

Using values for the reaction $^{16}O(d,n)^{17}F$ populating the 0.500 MeV state as measured at 0°, ($\sigma_{CN} \approx 1.5$ mb/sr and $\sigma_D \approx 140$ mb/sr), we get

$$\sigma_I^{max} \approx 2\sqrt{1.5 \times 140} \approx 30 \text{ mb/sr}$$

Since the various spin projections contribute incoherently, this value should be reduced by a factor $1/\sqrt{N}$, where N is the fluctuation damping

coefficient of page 19. For a final state spin of 1/2, N = 6. The resulting value of $\sigma_I^{max} \approx 30/\sqrt{6} \approx 12$ mb/sr is somewhat smaller than the maximum of 30 mb/sr observed, but is not so small as to rule out interference as the source of the fluctuations. This is certainly not a conclusive test, but it does show that interference effects could indeed be as large as the largest resonances seen in this experiment.

An observation perhaps more difficult to explain is the fact that some large resonances seem to be significantly wider than the width Γ obtained previously. As the wide resonances seem to have some structure, they may be only the result of a random combination of resonances which add together to form what is apparently a single large resonance. On the other hand, the large width could result from intermediate structure. There seems to be little way of distinguishing the two possibilities within the context of this experiment.

In addition to the above considerations, at least one practical point of some importance to the experimenter should be made. From the standpoint of planning an experiment, it is interesting to note that a small calculated compound nucleus cross section gives little assurance that there will not be large resonances in the yield curve.

Group Cross Correlations

The measurement of correlations between yield curves associated with different final states has led to some unexpected observations. As outlined in chapter 2, the assumption of random matrix elements predicts that no correlation should exist between yield curves associated with the population of different final states. However, as can be seen from figure 4.17, there

Figure 4.17 Yield curves measured at 65° for the reaction $^{16}O(d,d)^{16}O$ and the $^{16}O(d,p)^{17}O$ reactions populating the ground, 0.871 and 3.846 MeV states of ^{17}O.

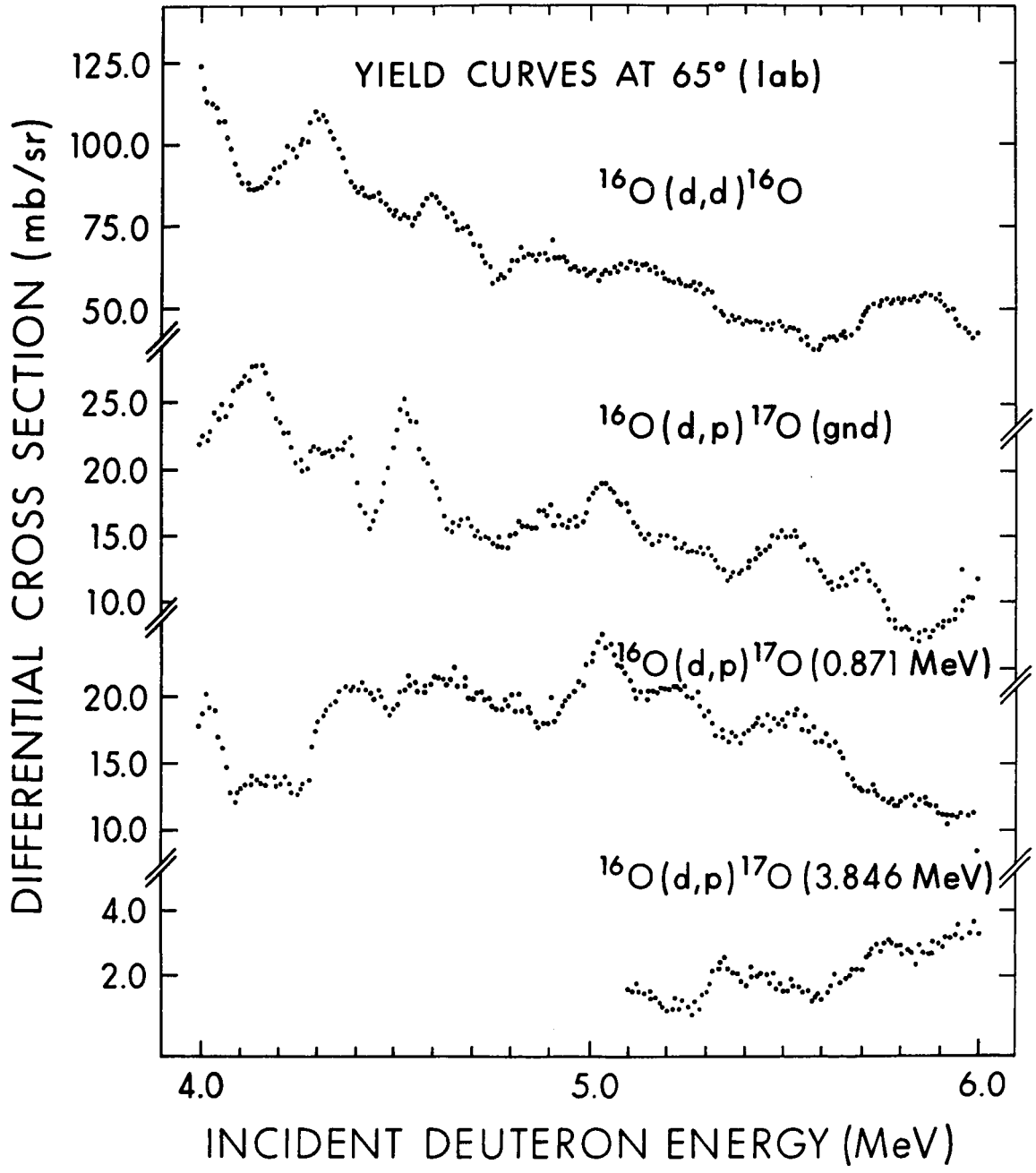
YIELD CURVES AT 65° (lab)
$^{16}O(d,d)^{16}O$
$^{16}O(d,p)^{17}O$ (gnd)
$^{16}O(d,p)^{17}O$ (0.871 MeV)
$^{16}O(d,p)^{17}O$ (3.846 MeV)
DIFFERENTIAL CROSS SECTION (mb/sr)
125.0
100.0
75.0
50.0
25.0
20.0
15.0
10.0
20.0
15.0
10.0
4.0
2.0
4.0
5.0
6.0
INCIDENT DEUTERON ENERGY (MeV)

is apparently a correlation between the charged particle yield curves taken at an angle of 65°. It can be seen that at bombarding energies above 4.8 MeV, the yield curves for the ground and first excited states are in phase except for one area near 5.8 MeV. Conversely, the yield curve for the 3.846 MeV level of ^{17}O is out of phase with the previously mentioned yield curves. The deuteron elastic scattering yield curve has features which suggest that the same correlation may be present but only weakly.

To test this observation on a more objective basis, the group cross correlation function $G(\sigma_1,\sigma_2,\varepsilon)$ was employed. Here, the group cross correlation G is calculated between yield curves denoted by σ_1 and σ_2. Correlations were calculated between sets of yield curves of two types.

(1) Type 1 consisted of yield curves which apparently showed an anomalous correlation.

(2) Type 2 yield curves showed no apparent correlation but were used as a control calculation.

It was felt that a control calculation was necessary because the effect of direct interactions on the size of group cross correlations is not easily estimated. The following comments should be made concerning the results of this analysis.

(1) The value of $G(\sigma_1,\sigma_2,\varepsilon)$ calculated using type 1 yield curves was consistently 2 to 3 times as large as that calculated using the type 2 yield curves.

(2) For type 1 yield curves, the value of $G(\sigma_1,\sigma_2,\varepsilon)$ decreased as ε increased. On the other hand, there was no consistent behaviour in the calculations performed using type 2 yield curves.

(3) The magnitude of the correlation expressed by $G(\sigma_1,\sigma_2,\varepsilon)$ was only slightly larger than the uncertainty introduced by the finite range of data errors. The importance of this observation is difficult to assess, however, because of the difficulty in allowing for the effect of direct interactions.

(4) The correlations were observed only in the charged particle reactions and there only at an angle of 65°. They were not observed in the neutron work.

An estimate of the finite range of data errors is difficult to calculate in the presence of direct interactions. An estimate can be made, however, if the magnitude of the direct interaction cross section is similar in the two yield curves being compared. Under this assumption, the magnitude of $G(\sigma_1,\sigma_2,\varepsilon=0)$ is found to be equal to or slightly larger than the finite range of data errors. Although this result suggests that the observed correlations may only be random associations of levels, the inaccuracy of the finite range of data errors when the direct interaction cross sections are not equal greatly reduces its weight. If the finite range of data errors could be trusted, there could be no reasonable case made that the correlations observed here were anything other than statistical fluctuations. It is only because there is considerable uncertainty that any weight can be given to other arguments.

The fact that the behaviour of $G(\sigma_1,\sigma_2,\varepsilon)$ as a function of ε is greatly different for type 1 and type 2 yield curves must be given considerable weight in the absence of a good understanding of finite range of data errors. Calculation of $G(\sigma_1,\sigma_2,\varepsilon)$ between type 2 yield curves shows

no consistent dependence on ε. On the other hand, calculations with type 1 yield curves show a consistent decrease in $G(\sigma_1,\sigma_2,\varepsilon)$ as ε is increased from zero. This allows a measurement of Γ, and the result obtained (~40 keV) agrees with the value obtained from the analysis of the autocorrelation functions.

Finally, it must be pointed out that the anomalous correlations are only observed in a few restricted cases. They are observed only in the charged particle yield curves measured at 65°. No explanation can be offered as to why this should be so.

In attempting to explain the apparent presence of anomalous correlations, the most difficult point is the fact that the yield curve of the 3.846 MeV state is out of phase with those of the ground and first excited states. If an attempt is made to explain the correlations on the basis of changes in the deuteron penetrability, then it might be expected that an increase in compound nucleus decay via deuteron emission would entail a decrease in proton emission to other channels. However, an increase in decay via the 3.846 MeV level accompanies a decrease in decay via the ground and first excited states, in disagreement with the behaviour expected.

Ericson (Er 63) pointed out a type of reaction that might produce correlations between yield curves associated with different final states. In the approximation of random matrix elements used in most compound nucleus calculations, it is usually assumed that the mean value of the matrix elements is zero. However, this is not necessarily correct. If the mean value is nonzero, a compound nucleus contribution from distant resonances appears, and part of the compound nucleus cross section is

mediated by the non-random average value of the matrix elements.

In the process discussed by Ericson, the compound nucleus can either form or decay via the "distant resonance" mechanism. The most important form is that in which the formation is in the "distant resonance" mechanism, and the decay is mediated by the nearby resonances, or vice versa. These reactions are called "mixed" because the compound nucleus forms and decays via somewhat different processes. It will be recalled from chapter 2, that with the assumption of random matrix elements, the group cross correlation function was always zero to within statistical deviations because all matrix element products were random. In the "mixed" reactions, however, some matrix elements are no longer random, and nonzero correlations can appear.

Ericson also specified that the conditions for observing the "mixed" reactions required a large direct interaction component in at least one of the two reactions being compared and a large coherence energy in the part of the reactions proceeding via the nearby resonances. Both the conditions are met in this experiment. Unfortunately, Ericson did not pursue the subject further, so that it is not known if mixed reactions can account for the yield curve of the 3.846 MeV state being out of phase with those of the ground and 0.871 MeV states.

Whatever the cause of the anomalous correlations, they are not explained within the context of the approximations used in the Hauser-Feshbach theory. Consequently, they may indicate that a significant portion of the cross section is not accounted for by current theories. As this could affect the measurement of spectroscopic factors, the effect should be sought at higher energies and in neighbouring nuclei.

CHAPTER 5

5.1 Summary and Conclusions

As outlined in the introduction, the primary purpose of this work was to determine to what extent the currently used models of the direct and compound nucleus reactions can describe the reactions $^{16}O(d,d)^{16}O$, $^{16}O(d,p)^{17}O$ and $^{16}O(d,n)^{17}F$ in the energy range 4.0 to 6.0 MeV. The results of the experiment can be summarized as follows.

(1) Elastic scattering of deuterons from ^{16}O is strongly affected by fluctuations in the compound nucleus cross sections. Consequently, the averaged parameter sets produce satisfactory fits to the elastic scattering data at some energies, but at other energies the fits are poor. It was found that a spin-orbit term is a necessary part of the theoretical description of deuteron scattering from ^{16}O. Several parameters are observed to change significantly when the spin-orbit term is introduced. It is thus concluded that the addition of a spin-orbit term to a parameter set obtained in an analysis with $V_{SO} = 0$ is not valid. A good fit to the elastic scattering data could be obtained with V anywhere in the range 85 MeV to 105 MeV. Neither the elastic scattering data nor the DWBA calculations were capable of further restricting the parameters sets. When allowance is made for the Vr_R^2 ambiguity, the geometry of the real well is nearly the same as that found by Schwandt and Haeberli for ^{40}Ca. As the other parameters also differ only slightly from the ^{40}Ca results, one is tempted to speculate that the optical model parameters

obtained for ^{16}O have nearly as much physical significance as do parameters for considerably heavier nuclei. This is particularly important because it suggests that the parameters may be capable of generating wavefunctions able to describe a wide range of reactions.

(2) The predictions of the compound nucleus model are in satisfactory agreement with experiment for the most part. In order to correct for the effect of the large direct interaction cross section, a major reduction of the total cross section and of the elastic cross section in particular was necessary before theory and experiment could be compared. Nevertheless, the model satisfactorily predicted the absolute cross section for the $^{16}O(d,p)^{17}O$ reaction populating the 3.846 MeV state. The calculated values of the compound nucleus lifetimes are in excellent agreement with the values obtained from the analysis of the fluctuations in the yield curves.

(3) Satisfactory fits to the angular distributions resulting from the population of the ground and first excited states of ^{17}O and ^{17}F were obtained with a variety of optical model potentials. The spectroscopic factors in all cases were found to be in the vicinity of 0.8 to 0.9. This is in satisfactory agreement with the spectroscopic factors of about 1.0 found at higher energies by previous workers and with the value of 0.9 predicted by Brown.

(4) It was found that the negative parity levels at excitation energies of 3.058 and 3.846 MeV in ^{17}O both had spectroscopic factors in the vicinity of 0.03, indicating only very small single particle components in the wavefunctions. There was considerable discrepancy between the absolute cross sections measured by previous workers using

bombarding energies of 11.8 and 15.0 MeV, and additional measurements of the absolute cross sections for the population of these levels would be useful. However, the discrepancy does not change the conclusion that only very small single particle components are present in the wavefunctions of these levels.

The spectroscopic factor of 0.03 for the 3.846 MeV state is in agreement with the results of Brown's model. The spectroscopic factor of 0.03 for the 3.058 MeV level is also in agreement with Brown's prediction that about 5% of the 2p strength should lie in this vicinity. On the other hand, Wong's calculations show that the use of the Rosenfeld or Soper 2-body potentials in a shell model calculation for ^{17}O allows the 3.058 MeV level to carry some $1p_{\frac{1}{2}}$ strength whereas the Brueckner-Gammel-Thaler or Hamada-Johnston potentials do not allow any measureable stripping strength. Since the centroid of the $2p_{\frac{1}{2}}$ orbital is not known, it is not possible to decide on the probable origin of the small stripping strength observed for the 3.058 MeV level.

(5) It was not possible to obtain agreement between theory and experiment concerning the polarization of neutrons and protons produced in the reactions $^{16}O(d,p)^{17}O$ and $^{16}O(d,n)^{17}F$. However, it is not clear what the effect of the compound nucleus is on the polarization in these cases. Therefore more data are required before it can be ascertained whether or not the presently available data should be interpreted in terms of the DWBA theory alone.

(6) There is some evidence that interference effects between the direct interactions and compound nucleus components of the reaction play

some role in the ^{16}O + d reactions at the energies of this experiment.

(7) There is also some evidence that a part of the cross section may be produced by a reaction mechanism not contained in either the DWBA or compound nucleus descriptions as they are currently used. The latter evidence is certainly not conclusive. However, as the presence of an additional component in the total cross section could have serious effects on the measurement of small spectroscopic factors, an attempt should be made to extend the observations to higher energies and to neighbouring nuclei.

BIBLIOGRAPHY

Al 66 J.L. Alty, L.L. Green, G.D. Jones and J.F. Sharpey-Schafer, Nucl. Phys. 86 (1966) 65

Al 67 J.L. Alty, L.L. Green, R. Huby, G.D. Jones, J.R. Mines and J.F. Sharpey-Schafer, Nucl. Phys. A97 (1967) 541

Au 64 N. Austern, R.M. Drisko, E.C. Halbert and G.R. Satchler, Phys. Rev. 133 (1964) B3

Ba 57 E. Baumgartner and H.W. Fulbright, Phys. Rev. 107 (1957) 219

Ba 62 R.H. Bassel, R.M. Drisko and G.R. Satchler, Oak Ridge National Laboratory Report ORNL-3240 (UC-34-Physics) 1962 (unpublished)

Bl 52 J.M. Blatt and L.C. Biedenharn, Revs. Modern Phys. 24 (1952) 258

Bo 62 D. Bodansky, Ann. Rev. Nucl. Sci. 12 (1962) 79

Br 63 G.E. Brown, J.A. Evans and D.J. Thouless, Nucl. Phys. 45 (1963) 164

Bu 64 P.J.A. Buttle and L.J.B. Goldfarb, Proc. Phys. Soc. 83 (1964) 701

Bu 67 M.B. Burbank, M.Sc. Thesis, University of Alberta (1967) unpublished

Bu 68 M.B. Burbank, G.G. Frank, N.E. Davison, G.C. Neilson, S.S.M. Wong and W.J. McDonald, Nucl. Phys. A119 (1968) 184

Da 65 P.J. Dallimore and I. Hall, Phys. Lett. 18 (1965) 138

Da 69a N.E. Davison, University of Alberta, Nuclear Research Centre internal report. UAE-NPL-15 (1969) unpublished

Da 69b N.E. Davison, University of Alberta, Nuclear Research Centre internal report (1969) unpublished

Di 68 O. Dietzsch et al., Nucl. Phys. A114 (1968) 330

Er 60 T. Ericson, Annals of Physics 9 (1960) 425

Er 63 T. Ericson, Annals of Physics 23 (1963) 390

Ev 63 J.E. Evans, Phys. Rev. 131 (1963) 1642

Fo 60 J.L. Fowler, E.G. Corman and E.C. Campbell, Proc. Int. Conf. Nuclear Structure, Kingston, 1960, (North-Holland Publ. Co., Amsterdam, 1960) p. 474

Fu 67 H.W. Fulbright, J.A. Robbins, R. West, D.P. Saylor and J.W. Verba, Nucl. Phys. A94 (1967) 214

Ga 66 A. Gallmann, P. Fintz and P.E. Hodgson, Nucl. Phys. 82 (1966) 161

Ge 67 D.A. Gedcke, Ph.D. Thesis, University of Alberta (1967) unpublished

Gr 67 T.B. Grandy, Ph.D. Thesis, University of Alberta (1967) unpublished

He 61 Numerical Data and Functional Relationships in Science and Technology, Volume 1, ed. K.H. Hellwege, (Springer Verlag, Berlin 1961)

Hj 65 S.A. Hjorth, J.X. Saladin and G.R. Satchler, Phys. Rev. 138 (1965) B1425

Hu 69 R.G. Humphries, M.Sc. Thesis, University of Alberta (1969) unpublished

Ke 61 E.L. Keller, Phys. Rev. 121 (1961) 820

Le 64 L.L. Lee et al., Phys. Rev. 136 (1964) B971

Lu 63 H.F. Lutz, J.B. Mason and M.D. Karvelis, Nucl. Phys. 47 (1963) 521

Ma 66 B. Margolis and N. de Takacsy, Can. J. Phys. 44 (1966) 1431

Mc 64 W.J. McDonald, Ph.D. Thesis, University of Ottawa (1964) unpublished

Mc 67 W.J. McDonald and D.A. Gedcke, University of Alberta, Nuclear Research Centre internal report (1967) unpublished

Na 68 I.M. Naqib and L.L. Green, Nucl. Phys. A112 (1968) 76

Ni 55 S.G. Nilsson, Mat. Fys. Medd. Dan. Vid. Selsk, 29 No. 16 (1955)

Ob 66 A.W. Bost, M.Sc. Thesis, University of Alberta (1967) unpublished

Ol 69 C.J. Oliver, P.D. Forsyth, J.L. Hutton, G. Kaye and J.R. Mines, Nucl. Phys. A127 (1969) 567

Pe 63 F.G. Perey, Phys. Rev. 131 (1963) 745

Pe 64 F.G. Perey and D.S. Saxon, Phys. Lett. 10 (1964) 107

Pe 67 F.G. Perey and G.R. Satchler, Nucl. Phys. A97 (1967) 515

Ph 68 R.J. Philpott, W.T. Pinkston and G.R. Satchler, Nucl. Phys. A119 (1968) 241

Pr 62a M.A. Preston, Physics of the Nucleus, (Addison-Wesley Publ. Co., Reading 1962) p. 544

Pr 62b M.A. Preston, Physics of the Nucleus, (Addison-Wesley Publ. Co., Reading 1962) p. 147

Ro 66 L. Rosen, Proc. 2nd Int. Symp. on polarization phenomena of nucleons, Karlsruhe, September 1965, ed. by P. Huber and H. Schopper, (Birkhäuser Verlag, Basel 1966) p. 253

Sa 58 G.R. Satchler, Ann. of Phys. 3 (1958) 275

Sa 64 G.R. Satchler, Nucl. Phys. 55 (1964) 1

Sc 64 U. Schmidt-Rohr, R. Stock and P. Turek, Nucl. Phys. 53 (1964) 77

Sc 69 P. Schwandt and W. Haeberli, Nucl. Phys. A123 (1969) 401

Se 63 R.E. Segel, P.P. Singh, R.G. Allas and S.S. Hanna, Phys. Rev. Lett. 10 (1963) 345

Sh 63 A. de-Shalit and I. Talmi, Nuclear Shell Theory, (Academic Press, New York, 1963) p. 268

Sm 65 W.R. Smith, Oak Ridge National Laboratory Report ORNL-TM-1117 (1965) unpublished

Va 65 V. Valković et al., Phys. Rev. 139 (1965) B331

Vo 62 E. Vogt, Revs. Modern Phys. 34 (1962) 723

Vo 68 E. Vogt, Advances in Nuclear Physics 1 (1968) 261

Wi 66 W. von Witsch, P. von Brentano, T. Mayer-Kuckuk and A. Richter, Nucl. Phys. 80 (1966) 394

Wo 68 S.S.M. Wong, Nucl. Phys. A120 (1968) 625

Ya 61 B. Yaramis, Phys. Rev. 124 (1961) 836

APPENDIX A

TABULATION OF DIFFERENTIAL CROSS SECTIONS

In this section, the absolute differential cross sections of all angular distributions measured in the course of this experiment are tabulated.

In the study of the $^{16}O(d,n)^{17}F$ reaction, no contaminants were observed so that errors arise mainly from background subtraction and the correction for neutrons misidentified as γ-rays. It is estimated that in most cases, the error is of the order of 3% to 4%. Where cross sections become large, the errors may drop slightly below 3%, but this is restricted to the vicinity of the stripping peaks. As a result of this uniformity, no errors are listed for the angular distributions obtained in the study of the $^{16}O(d,n)^{17}F$ reaction.

On the other hand, in the analysis of the charged particle reactions, contaminant peaks caused difficulty at some angles, and the estimated errors are seen to vary considerably with angle. The errors listed on the following pages as well the estimates given above for the neutron work apply only to the relative cross sections. To these errors should be added approximately 10% uncertainty in the absolute normalization of the cross sections of the neutron work and 10% uncertainty in the absolute normalization of the charged particle cross sections.

$^{16}O(d,n)^{17}F$ (ground state)*

Angle (lab.)	E_d = 4.75 MeV		E_d = 5.00 MeV		E_d = 5.25 MeV	
	Angle (C.M.)	$\frac{d\sigma}{d\Omega}$ (mb/sr)	Angle (C.M.)	$\frac{d\sigma}{d\Omega}$ (mb/sr)	Angle (C.M.)	$\frac{d\sigma}{d\Omega}$ (mb/sr)
0.0	0.0	7.80	0.0	7.19	0.0	11.7
5.0			5.6	8.63		
10.0	11.1	13.7	11.1	12.9	11.1	17.0
15.0			16.6	18.8		
20.0	22.2	24.9	22.2	25.0	22.1	27.1
25.0			27.7	30.2		
30.0	33.2	33.0	33.2	33.0	33.1	33.6
35.0			38.6	32.9		
40.0	44.2	32.3	44.1	32.0	44.0	30.9
45.0			49.5	27.8		
50.0	55.0	24.7	54.9	24.1	54.8	22.9
55.0			60.2	20.2		
60.0	65.6	17.7	65.5	16.4	65.4	15.9
65.0			70.7	13.5		
70.0	76.1	12.4	75.9	10.7	75.9	10.3
75.0			81.1	9.08		
80.0	86.4	9.77	86.3	7.65	86.2	7.55
85.0			91.3	6.54		
90.0	96.5	7.67	96.4	6.09	96.3	6.04
95.0			101.3	5.68		
100.0	106.4	8.83	106.3	6.74	106.2	6.63
105.0			111.1	6.93		
110.0	116.1	9.41	116.0	7.19	115.9	6.79
115.0			120.8	7.85		
120.0	125.6	9.75	125.5	7.88	125.4	7.26
125.0			130.2	8.15		
130.0	135.0	12.2	134.9	8.56	134.8	8.07
135.0			139.5	9.12		
140.0	144.2	13.5	144.1	9.32	144.0	8.64

*In all cases, the uncertainties in the differential cross sections measured in the neutron work are believed to be between 3% and 4%.

$^{16}O(d,n)^{17}F$ (ground state)*

Angle (lab.)	E_d = 5.50 MeV		E_d = 5.75 MeV		E_d = 6.00 MeV	
	Angle (C.M.)	$\frac{d\sigma}{d\Omega}$ (mb/sr)	Angle (C.M.)	$\frac{d\sigma}{d\Omega}$ (mb/sr)	Angle (C.M.)	$\frac{d\sigma}{d\Omega}$ (mb/sr)
0.0	0.0	11.3	0.0	10.8	0.0	12.5
5.0	5.5	12.5			5.5	13.8
10.0	11.1	16.5	11.1	16.2	11.0	18.3
15.0	16.6	21.4			16.6	24.1
20.0	22.1	25.8	22.1	27.0	22.1	28.7
25.0	27.6	30.3			27.5	32.1
30.0	33.1	31.7	33.0	32.0	33.0	33.0
35.0	38.5	32.0			38.5	31.3
40.0	44.0	29.0	43.9	27.8	43.9	27.4
45.0	49.4	25.8			49.3	22.3
50.0	54.7	21.4	54.7	19.2	54.6	17.4
55.0	60.0	17.5			59.9	13.0
60.0	65.3	13.6	65.3	10.9	65.2	9.58
65.0	70.6	10.4				
70.0	75.8	8.63	75.7	6.24	75.7	6.12
75.0	81.0	7.06				
80.0	86.1	6.31	86.0	4.86	85.9	5.78
85.0	91.1	5.64			91.0	5.81
90.0	96.2	5.31	96.1	4.81	96.0	6.40
95.0	101.1	5.24			101.0	6.40
100.0	106.1	6.34	106.0	6.22	105.9	7.97
105.0	111.0	6.37				
110.0	115.8	6.60			115.7	7.99
115.0	120.6	6.72				
120.0	125.3	6.89	125.3	5.21	125.2	7.60
125.0	130.1	6.98				
130.0	134.7	7.13			134.6	6.86
135.0	139.4	7.35			139.3	6.50
140.0	144.0	7.39	143.9	6.69	143.9	6.14

*In all cases, the uncertainties in the differential cross sections measured in the neutron work are believed to be between 3% and 4%.

$^{16}O(d,n)^{17}F$ (0.500 MeV)*

Angle (lab.)	E_d = 4.75 MeV		E_d = 5.00 MeV		E_d = 5.25 MeV	
	Angle (C.M.)	$\frac{d\sigma}{d\Omega}$ (mb/sr)	Angle (C.M.)	$\frac{d\sigma}{d\Omega}$ (mb/sr)	Angle (C.M.)	$\frac{d\sigma}{d\Omega}$ (mb/sr)
0.0	0.0	129.	0.0	142.	0.0	136.
5.0			5.6	130.		
10.0	11.3	96.6	11.2	104.	11.2	103.
15.0			16.9	77.2		
20.0	22.5	47.1	22.4	48.0	22.4	44.8
25.0			28.0	27.4		
30.0	33.7	17.0	33.5	16.4	33.4	14.3
35.0			39.1	11.2		
40.0	44.7	12.2	44.6	10.9	44.4	10.3
45.0			50.0	12.0		
50.0	55.6	15.4	55.4	13.1	55.3	12.5
55.0			60.8	13.8		
60.0	66.3	16.8	66.1	13.8	66.0	12.4
65.0			71.4	13.5		
70.0	76.9	15.9	76.7	12.0	76.5	10.4
75.0			81.9	11.7		
80.0	87.2	14.4	87.0	10.5	86.8	8.18
85.0			92.1	8.92		
90.0	97.3	11.0	97.1	8.31	96.9	6.44
95.0			102.1	7.37		
100.0	107.2	11.3	107.0	8.33	106.8	6.78
105.0			111.8	8.02		
110.0	116.9	10.8	116.7	8.20	116.5	6.32
115.0			121.4	8.58		
120.0	126.3	9.99	126.1	8.46	126.0	6.24
125.0			130.8	9.02		
130.0	135.6	11.7	135.4	9.19	135.3	7.13
135.0			140.0	9.80		
140.0	144.7	12.2	144.6	10.2	144.4	7.50

*In all cases, the uncertainties in the differential cross sections measured in the neutron work are believed to be between 3% and 4%.

$^{16}O(d,n)^{17}F$ (0.500 MeV)*

Angle (lab.)	E_d = 5.50 MeV		E_d = 5.75 MeV		E_d = 6.00 MeV	
	Angle (C.M.)	$\frac{d\sigma}{d\Omega}$ (mb/sr)	Angle (C.M.)	$\frac{d\sigma}{d\Omega}$ (mb/sr)	Angle (C.M.)	$\frac{d\sigma}{d\Omega}$ (mb/sr)
0.0	0.0	146.	0.0	156.	0.0	159.
5.0	5.6	134.			5.6	146.
10.0	11.2	107.	11.2	113.	11.1	113.
15.0	16.7	76.2			16.7	73.8
20.0	22.3	43.9	22.3	43.2	22.2	41.3
25.0	27.9	24.2			27.7	21.0
30.0	33.4	12.9	33.3	11.8	33.3	13.7
35.0	38.9	9.14			38.7	12.0
40.0	44.3	9.04	44.3	9.92	44.2	12.5
45.0	49.8	10.3			49.6	13.6
50.0	55.2	11.1	55.1	12.9	55.0	13.6
55.0	60.5	11.5			60.3	12.6
60.0	65.8	11.0	65.7	11.5	65.6	11.0
65.0	71.1	9.65				
70.0	76.3	8.92	76.2	8.44	76.1	7.94
75.0	81.5	7.81				
80.0	86.7	6.98	86.5	5.60	86.4	5.97
85.0	91.7	5.96			91.5	5.08
90.0	96.8	5.22	96.6	3.94	96.5	5.09
95.0	101.7	4.99			101.5	4.89
100.0	106.7	5.50	106.5	4.00	106.4	5.79
105.0	111.5	5.35				
110.0	116.3	5.31			116.1	5.81
115.0	121.1	5.05				
120.0	125.8	5.15	125.7	2.98	125.6	5.54
125.0	130.5	4.87				
130.0	135.2	5.08			135.0	5.50
135.0	139.8	5.01			139.6	5.20
140.0	144.3	4.95	144.3	4.27	144.2	5.26

*In all cases, the uncertainties in the differential cross sections measured in the neutron work are believed to be between 3% and 4%.

$^{16}O(d,d)^{16}O$

Angle (lab.)	E_d = 4.00 MeV		E_d = 4.50 MeV	
	Angle (C.M.)	$\frac{d\sigma}{d\Omega}$ (mb/sr)	Angle (C.M.)	$\frac{d\sigma}{d\Omega}$ (mb/sr)
30.0	33.6		33.6	806. ± 20.
35.0	39.1	748. ± 20.	39.2	501. ± 9.
40.0	44.7	285. ± 10.	44.7	327. ± 10.
45.0	50.1	320. ± 10.	50.1	221. ± 6.
50.0	55.5	206. ± 7.	55.5	154. ± 5.
55.0	60.9	156. ± 6.	60.9	111. ± 3.
60.0			66.3	83.7 ± 1.
65.0	71.6	95.6 ± 2.	71.6	60.6 ± 0.8
70.0			76.8	44.7 ± 0.5
75.0	82.0	66.0 ± 1.	82.0	30.5 ± 0.4
80.0			87.1	22.5 ± 0.3
85.0	92.2	40.5 ± 1.	92.2	17.0 ± 0.4
90.0			97.2	15.0 ± 0.2
95.0	102.2	19.0 ± 0.3	102.2	15.2 ± 0.2
100.0	107.1	12.0 ± 0.2	107.1	17.4 ± 0.2
105.0	112.0	7.30 ± 0.1	112.0	19.5 ± 0.2
110.0	116.8	5.14 ± 0.1	116.8	22.6 ± 0.2
115.0	121.6	5.59 ± 0.2	121.6	24.4 ± 0.4
120.0	126.3	8.40 ± 0.1	126.3	25.4 ± 0.3
125.0	130.9	12.6 ± 0.3	130.9	25.9 ± 0.4
130.0	135.5	18.9 ± 0.3	135.5	23.2 ± 0.4
135.0	140.1	28.0 ± 0.3	140.1	20.7 ± 0.2
140.0	144.6	35.6 ± 0.4	144.6	18.0 ± 0.2
145.0	149.1	45.0 ± 0.5	149.1	15.6 ± 0.2
150.0	153.6	51.5 ± 1.	153.6	13.6 ± 0.1
155.0	158.1	62.1 ± 1.	158.1	12.6 ± 0.2
160.0	162.5	68.9 ± 1.	162.5	12.0 ± 0.2
165.0	166.9	76.7 ± 1.	166.9	11.7 ± 0.2
170.0	171.3	79.5 ± 1.	171.3	11.9 ± 0.2

$^{16}O(d,d)^{16}O$

Angle (lab.)	E_d = 5.00 MeV		E_d = 5.25 MeV	
	Angle (C.M.)	$\frac{d\sigma}{d\Omega}$ (mb/sr)	Angle (C.M.)	$\frac{d\sigma}{d\Omega}$ (mb/sr)
30.0	33.6	538. ± 9.	33.7	424. ± 9.
35.0	39.2	340. ± 6.	39.2	291. ± 6.
40.0	44.7	207. ± 6.	44.7	193. ± 4.
45.0	50.1	142. ± 5.	50.1	133. ± 3.
50.0	55.5	97.1 ± 3.	55.5	93.7 ± 3.
55.0	60.9	76.2 ± 2.	60.9	72.3 ± 2.
60.0	66.3	60.4 ± 0.9	66.3	55.7 ± 2.
65.0	71.6	46.7 ± 0.6	71.6	44.5 ± 2.
70.0	76.8	35.7 ± 0.5	76.8	32.8 ± 0.5
75.0	82.0	25.0 ± 0.4	82.0	23.8 ± 0.4
80.0	87.1	16.7 ± 0.4	87.1	15.5 ± 0.4
85.0	92.2	9.51 ± 0.2	92.2	9.51 ± 0.2
90.0	97.2	5.47 ± 0.2	97.2	6.26 ± 0.2
95.0	102.2	4.05 ± 0.1	102.2	5.22 ± 0.1
100.0	107.1	5.14 ± 0.1	107.1	6.51 ± 0.1
105.0	112.0	7.77 ± 0.1	112.0	9.87 ± 0.2
110.0	116.8	12.7 ± 0.1	116.8	14.0 ± 0.2
115.0	121.6	15.5 ± 0.3	121.6	19.4 ± 0.4
120.0	126.3	18.0 ± 0.3	126.3	24.1 ± 0.5
125.0	130.9	21.2 ± 0.3	130.9	28.2 ± 0.6
130.0	135.5	22.0 ± 0.3	135.5	31.9 ± 0.6
135.0	140.1	22.6 ± 0.2	140.1	34.6 ± 0.4
140.0	144.7	22.3 ± 0.2	144.7	35.9 ± 0.5
145.0	149.1	22.1 ± 0.2	149.2	36.4 ± 0.5
150.0	153.6	20.9 ± 0.2	153.6	36.7 ± 0.5
155.0	158.1	20.4 ± 0.3	158.1	36.2 ± 0.7
160.0	162.5	19.4 ± 0.3	162.5	35.6 ± 0.7
165.0	166.9	18.7 ± 0.3	166.9	34.5 ± 0.6
170.0	171.3	18.0 ± 0.3	171.3	33.4 ± 0.6

$^{16}O(d,d)^{16}O$

Angle (lab.)	E_d = 5.50 MeV		E_d = 6.00 MeV	
	Angle (C.M.)	$\frac{d\sigma}{d\Omega}$ (mb/sr)	Angle (C.M.)	$\frac{d\sigma}{d\Omega}$ (mb/sr)
25.0			28.1	504. ± 20.
30.0	33.5	454. ± 10.	33.6	290. ± 9.
35.0	39.2	269. ± 5.	39.2	196. ± 5.
40.0	44.7	168. ± 5.	44.7	106. ± 2.
45.0	50.1	110. ± 3.	50.1	73.1 ± 2.
50.0	55.5	75.7 ± 2.	55.6	57.8 ± 1.
55.0	60.9	58.2 ± 2.	60.9	49.6 ± 1.
60.0	66.3	44.3 ± 0.7	66.3	43.5 ± 1.
65.0	71.6	34.6 ± 0.5	71.6	36.9 ± 0.8
70.0	76.8	26.2 ± 0.4	76.8	30.3 ± 0.5
75.0	82.0	18.5 ± 0.3	82.0	20.6 ± 0.4
80.0	87.1	11.8 ± 0.3	87.1	15.4 ± 0.3
85.0	92.2	7.27 ± 0.1	92.2	10.3 ± 0.2
90.0	97.3	5.23 ± 0.1	97.3	-- --
95.0	102.2	5.76 ± 0.1	102.2	-- --
100.0	107.1	7.90 ± 0.1	107.1	-- --
105.0	112.0	11.9 ± 0.2	112.0	5.08 ± 0.1
110.0	116.8	16.9 ± 0.2	116.8	6.93 ± 0.1
115.0	121.6	21.6 ± 0.4	121.6	9.31 ± 0.1
120.0	126.3	25.9 ± 0.4	126.3	11.7 ± 0.1
125.0	130.9	29.5 ± 0.5	130.9	15.6 ± 0.1
130.0	135.5	31.3 ± 0.5	135.5	17.7 ± 0.1
135.0	140.1	32.7 ± 0.3	140.1	19.7 ± 0.1
140.0	144.7	33.2 ± 0.3	144.7	20.0 ± 0.1
145.0	149.2	32.7 ± 0.3	149.2	20.4 ± 0.1
150.0	153.6	32.3 ± 0.3	153.6	19.7 ± 0.1
155.0	158.1	32.3 ± 0.5	158.1	18.1 ± 0.1
160.0	162.5	31.7 ± 0.5	162.5	16.3 ± 0.1
165.0	166.9	32.3 ± 0.5		
170.0	171.3	30.5 ± 0.4		

$^{16}O(d,p)^{17}O$ (ground state)

Angle (lab.)	E_d = 4.00 MeV		E_d = 4.50 MeV	
	Angle (C.M.)	$\frac{d\sigma}{d\Omega}$ (mb/sr)	Angle (C.M.)	$\frac{d\sigma}{d\Omega}$ (mb/sr)
15.0	16.0	--	16.1	6.17 ± 0.2
20.0	21.3	15.6 ± 0.3	21.4	10.7 ± 0.3
25.0	26.8	24.0 ± 0.4	26.8	15.2 ± 0.4
30.0	32.0	29.5 ± 0.4	32.1	18.3 ± 0.5
35.0	37.3	35.4 ± 0.6	37.4	21.7 ± 0.7
40.0	42.6	35.3 ± 0.8	42.7	21.4 ± 0.8
45.0	47.8	35.1 ± 0.9	47.9	21.6 ± 1.0
50.0	53.1	33.5 ± 0.7	53.2	22.5 ± 0.8
55.0	58.3	30.6 ± 0.7	58.4	21.7 ± 0.7
60.0			63.6	21.1 ± 0.4
65.0	68.6	21.5 ± 0.2	68.8	20.1 ± 0.3
70.0			73.9	20.1 ± 0.3
75.0	78.9	16.8 ± 0.2	79.0	18.7 ± 0.2
80.0			84.1	-- --
85.0	89.0	-- --	89.1	16.2 ± 0.2
90.0			94.2	15.7 ± 0.2
95.0	99.0	15.7 ± 0.2	99.1	14.1 ± 0.3
100.0	103.9	16.5 ± 0.2	104.1	13.2 ± 0.2
105.0	108.9	16.2 ± 0.1	109.0	12.3 ± 0.1
110.0	113.8	16.5 ± 0.1	113.0	11.8 ± 0.1
115.0	118.6	15.9 ± 0.1	118.8	11.8 ± 0.2
120.0	123.5	15.9 ± 0.2	123.6	12.0 ± 0.2
125.0	128.3	14.8 ± 0.2	128.4	11.9 ± 0.2
130.0	133.1	14.4 ± 0.3	133.2	11.8 ± 0.2
135.0	137.8	13.7 ± 0.3	137.9	11.7 ± 0.2
140.0	142.6	13.1 ± 0.2	142.7	11.5 ± 0.2
145.0	147.3	12.6 ± 0.2	147.4	11.3 ± 0.2
150.0	152.0	12.2 ± 0.2	152.1	10.9 ± 0.2
155.0	156.7	11.9 ± 0.1	156.8	-- --
160.0	161.4	11.7 ± 0.1	161.4	-- --
165.0	166.0	11.5 ± 0.1	166.1	-- --
170.0	170.7	11.4 ± 0.1	170.7	-- --

$^{16}O(d,p)^{17}O$ (ground state)

Angle (lab.)	E_d = 5.00 MeV		E_d = 5.25 MeV	
	Angle (C.M.)	$\frac{d\sigma}{d\Omega}$ (mb/sr)	Angle (C.M.)	$\frac{d\sigma}{d\Omega}$ (mb/sr)
15.0	16.1	9.57 ± 0.5		
20.0	21.4	14.9 ± 0.3		
25.0	26.8	22.1 ± 0.4		
30.0	32.1	26.7 ± 0.5	32.1	26.5 ± 0.6
35.0	37.4	30.8 ± 0.6	37.4	29.6 ± 0.7
40.0	42.7	31.7 ± 0.9	42.7	29.2 ± 0.7
45.0	47.9	31.4 ± 0.9	48.0	27.1 ± 0.6
50.0	53.2	26.6 ± 0.7	53.2	22.7 ± 0.8
55.0	58.4	23.7 ± 0.7	58.4	19.2 ± 0.7
60.0	63.6	19.0 ± 0.3	63.6	14.2 ± 0.2
65.0	68.8	15.2 ± 0.2	68.8	11.4 ± 0.2
70.0	73.9	12.5 ± 0.2	73.9	9.08 ± 0.2
75.0	79.0	--	79.1	-- --
80.0	84.1	--	84.1	7.78 ± 0.2
85.0	89.1	8.32 ± 0.2	89.2	7.80 ± 0.1
90.0	94.2	8.07 ± 0.2	94.2	7.83 ± 0.2
95.0	99.1	7.87 ± 0.1	99.2	8.08 ± 0.1
100.0	104.1	7.94 ± 0.1	104.1	8.02 ± 0.1
105.0	109.0	8.34 ± 0.1	109.0	7.89 ± 0.1
110.0	113.9	8.44 ± 0.1	113.9	7.82 ± 0.1
115.0	118.8	8.82 ± 0.2	118.8	7.35 ± 0.2
120.0	123.6	8.93 ± 0.2	123.6	6.99 ± 0.2
125.0	128.4	8.76 ± 0.2	128.4	6.40 ± 0.2
130.0	133.2	8.74 ± 0.2	133.2	6.09 ± 0.2
135.0	137.9	-- --	138.0	5.93 ± 0.1
140.0	142.7	-- --	142.7	5.69 ± 0.1
145.0	147.4	-- --	147.4	5.62 ± 0.1
150.0	152.1	7.65 ± 0.1	152.1	5.64 ± 0.1
155.0	156.8	7.37 ± 0.1	156.8	5.99 ± 0.2
160.0	161.4	7.26 ± 0.1	161.4	6.13 ± 0.2
165.0	166.1	6.88 ± 0.1	166.1	6.60 ± 0.2
170.0	170.7	-- --	170.7	6.56 ± 0.2

$^{16}O(d,p)^{17}O$ (ground state)

Angle (lab.)	E_d = 5.50 MeV		E_d = 6.00 MeV	
	Angle (C.M.)	$\frac{d\sigma}{d\Omega}$ (mb/sr)	Angle (C.M.)	$\frac{d\sigma}{d\Omega}$ (mb/sr)
15.0	16.1	8.42 ± 0.4		
20.0	21.4	15.1 ± 0.3	21.5	16.2 ± 0.6
25.0	26.8	20.8 ± 0.4	26.8	21.1 ± 0.7
30.0	32.2	28.1 ± 0.5	32.1	23.9 ± 0.7
35.0	37.4	31.3 ± 0.5	37.5	28.4 ± 0.7
40.0	42.7	31.5 ± 0.9	42.7	25.8 ± 0.6
45.0	48.0	28.6 ± 0.8	48.0	22.7 ± 0.5
50.0	53.2	24.0 ± 0.6	53.3	19.4 ± 0.4
55.0	58.5	19.8 ± 0.5	58.5	15.0 ± 0.3
60.0	63.7	15.7 ± 0.3	63.7	11.9 ± 0.2
65.0	68.8	12.3 ± 0.2	68.9	10.1 ± 0.2
70.0	74.0	10.3 ± 0.2	74.0	-- --
75.0	79.1	-- --	79.1	7.56 ± 0.1
80.0	84.2	7.70 ± 0.2	84.2	8.98 ± 0.2
85.0	89.2	7.32 ± 0.2	89.3	9.04 ± 0.2
90.0	94.2	7.21 ± 0.2	94.3	10.5 ± 0.1
95.0	99.2	7.06 ± 0.2	99.3	-- --
100.0	104.2	7.09 ± 0.1	104.2	11.9 ± 0.1
105.0	109.1	7.29 ± 0.1	109.1	13.0 ± 0.1
110.0	114.0	7.28 ± 0.2	114.0	12.4 ± 0.1
115.0	118.8	7.05 ± 0.2	118.9	-- --
120.0	123.7	6.87 ± 0.1	123.7	12.9 ± 0.1
125.0	128.5	-- --	128.5	11.6 ± 0.1
130.0	133.2	-- --	133.3	10.6 ± 0.1
135.0	138.0	5.74 ± 0.1	138.0	9.84 ± 0.1
140.0	142.7	5.27 ± 0.1	142.7	8.85 ± 0.1
145.0	147.4	4.89 ± 0.1	147.4	8.39 ± 0.1
150.0	152.1	4.48 ± 0.1	152.1	7.79 ± 0.1
155.0	156.8	4.27 ± 0.1	156.8	6.86 ± 0.1
160.0	161.4	3.94 ± 0.1	161.5	6.66 ± 0.1
165.0	166.1	3.81 ± 0.1		
170.0	170.7	3.47 ± 0.1		

$^{16}O(d,p)^{17}O$ (0.871 MeV)

Angle (lab.)	E_d = 4.00 MeV		E_d = 4.50 MeV	
	Angle (C.M.)	$\frac{d\sigma}{d\Omega}$ (mb/sr)	Angle (C.M.)	$\frac{d\sigma}{d\Omega}$ (mb/sr)
15.0			16.1	87.4 ± 3.
20.0	21.5	104. ± 2.	21.5	44.8 ± 1.
25.0	26.8	58.0 ± 1.	26.9	17.7 ± 0.4
30.0	32.2	26.9 ± 0.7	32.2	5.83 ± 0.2
35.0	37.5	17.0 ± 0.4	37.5	4.03 ± 0.1
40.0	42.8	-- --	42.8	-- --
45.0	48.1	-- --	48.1	-- --
50.0	53.3	18.7 ± 0.7	53.4	16.4 ± 0.6
55.0	58.6	20.5 ± 0.8	58.6	16.8 ± 0.5
60.0			63.8	17.7 ± 0.3
65.0	69.0	16.5 ± 0.4	69.0	16.7 ± 0.3
70.0			74.2	16.4 ± 0.2
75.0	79.2	13.2 ± 0.3	79.3	14.9 ± 0.2
80.0			84.4	15.0 ± 0.2
85.0	89.4	11.8 ± 0.4	89.4	13.6 ± 0.3
90.0			94.4	13.0 ± 0.2
95.0	99.4	12.1 ± 0.4	99.4	11.9 ± 0.2
100.0	104.3	12.6 ± 0.2	104.4	10.6 ± 0.1
105.0	109.2	12.8 ± 0.2	109.3	9.04 ± 0.1
110.0	114.1	13.3 ± 0.2	114.2	7.59 ± 0.1
115.0	119.0	13.0 ± 0.3	119.0	6.02 ± 0.1
120.0	123.8	13.2 ± 0.3	123.8	4.82 ± 0.1
125.0	128.6	12.2 ± 0.3	128.6	3.72 ± 0.1
130.0	133.3	11.9 ± 0.2	133.4	3.01 ± 0.1
135.0	138.1	12.1 ± 0.2	138.1	2.75 ± 0.1
140.0	142.8	11.2 ± 0.1	142.8	2.80 ± 0.1
145.0	147.5	11.0 ± 0.1	147.5	-- --
150.0	152.2	10.7 ± 0.1	152.2	-- --
155.0	156.8	10.8 ± 0.2	156.9	-- --
160.0	161.5	10.6 ± 0.2	161.5	-- --
165.0	166.1	10.7 ± 0.2	166.1	-- --
170.0	170.8	10.7 ± 0.2	170.8	-- --

$^{16}O(d,p)^{17}O$ (0.871 MeV)

Angle (lab.)	E_d = 5.00 MeV		E_d = 5.25 MeV	
	Angle (C.M.)	$\frac{d\sigma}{d\Omega}$ (mb/sr)	Angle (C.M.)	$\frac{d\sigma}{d\Omega}$ (mb/sr)
15.0	16.2	110. ± 4.		
20.0	21.5	57.9 ± 1.		
25.0	26.9	27.7 ± 0.5		
30.0	32.2	14.0 ± 0.3	32.2	14.1 ± 0.3
35.0	37.6	-- --	37.6	11.4 ± 0.4
40.0	42.9	-- --	42.9	12.5 ± 0.4
45.0	48.2	22.2 ± 0.7	48.2	16.3 ± 0.4
50.0	53.4	26.3 ± 0.7	53.4	17.5 ± 0.4
55.0	58.7	23.4 ± 0.7	58.7	18.0 ± 0.3
60.0	63.9	21.9 ± 0.3	63.9	16.9 ± 0.3
65.0	69.1	19.1 ± 0.3	69.1	15.8 ± 0.3
70.0	74.2	17.4 ± 0.3	74.2	14.0 ± 0.3
75.0	79.3	15.1 ± 0.2	79.3	12.9 ± 0.3
80.0	84.4	13.9 ± 0.3	84.4	12.0 ± 0.2
85.0	89.5	12.7 ± 0.3	89.5	10.9 ± 0.2
90.0	94.5	11.9 ± 0.3	94.5	9.71 ± 0.1
95.0	99.5	10.9 ± 0.1	99.5	8.81 ± 0.2
100.0	104.4	10.1 ± 0.1	104.4	7.55 ± 0.1
105.0	109.3	9.13 ± 0.1	109.3	6.70 ± 0.2
110.0	114.2	8.42 ± 0.1	114.2	--
115.0	119.1	7.48 ± 0.1	119.1	--
120.0	123.9	6.66 ± 0.1	123.9	--
125.0	128.7	5.66 ± 0.1	128.7	--
130.0	133.4	5.29 ± 0.1	133.4	--
135.0	138.2	4.70 ± 0.1	138.2	--
140.0	142.9	4.14 ± 0.4	142.9	--
145.0	147.6	-- --	--	--
150.0	152.2	-- --	--	2.16 ± 0.2
155.0	156.9	3.41 ± 0.1	156.9	2.09 ± 0.1
160.0	161.5	3.03 ± 0.1	161.5	1.81 ± 0.1
165.0	166.2	2.93 ± 0.1	166.2	1.51 ± 0.1
170.0	170.8	2.86 ± 0.1	170.8	1.36 ± 0.1

$^{16}O(d,p)^{17}O$ (0.871 MeV)

Angle (lab.)	E_d = 5.50 MeV		E_d = 6.00 MeV	
	Angle (C.M.)	$\frac{d\sigma}{d\Omega}$ (mb/sr)	Angle (C.M.)	$\frac{d\sigma}{d\Omega}$ (mb/sr)
15.0	16.2	115. ± 4.		
20.0	21.5	29.7 ± 0.5	21.6	43.3 ± 2.
25.0	26.9	23.1 ± 0.4	26.9	18.6 ± 0.6
30.0	32.3	8.49 ± 0.2	32.3	-- --
35.0	37.6	6.85 ± 0.2	37.6	-- --
40.0	42.9	11.0 ± 0.3	42.9	11.4 ± 0.3
45.0	48.2	15.1 ± 0.4	48.2	12.5 ± 0.3
50.0	53.5	17.1 ± 0.5	53.5	12.6 ± 0.3
55.0	58.7	17.6 ± 0.5	58.7	11.0 ± 0.2
60.0	63.9	16.3 ± 0.3	63.9	10.6 ± 0.2
65.0	69.1	14.7 ± 0.2	69.1	10.3 ± 0.2
70.0	74.2	13.0 ± 0.2	74.3	11.1 ± 0.2
75.0	79.4	11.4 ± 0.2	79.4	10.7 ± 0.2
80.0	84.5	10.6 ± 0.3	84.5	11.9 ± 0.2
85.0	89.5	9.27 ± 0.2	89.5	12.1 ± 0.2
90.0	94.5	8.29 ± 0.2	94.6	11.9 ± 0.1
95.0	99.5	7.15 ± 0.2	99.5	-- --
100.0	104.4	6.10 ± 0.1	104.5	-- --
105.0	109.4	5.38 ± 0.1	109.4	7.83 ± 0.1
110.0	114.2	4.33 ± 0.1	114.3	6.53 ± 0.1
115.0	119.1	3.66 ± 0.1	119.1	4.80 ± 0.1
120.0	123.9	3.13 ± 0.1	123.9	-- --
125.0	128.7	2.47 ± 0.1	128.7	-- --
130.0	133.5	--	133.5	2.57 ± 0.1
135.0	138.2	--	138.2	2.63 ± 0.1
140.0	142.9	2.19 ± 0.1	142.9	2.77 ± 0.1
145.0	147.6	2.44 ± 0.1	147.6	3.18 ± 0.1
150.0	152.3	2.67 ± 0.1	152.3	3.76 ± 0.1
155.0	156.9	3.01 ± 0.1	156.9	-- --
160.0	161.5	3.29 ± 0.1	161.6	3.86 ± 0.1
165.0	166.2	3.53 ± 0.1		
170.0	170.8	3.91 ± 0.1		

$^{16}O(d,p)^{17}O$ (3.846 MeV)

Angle (lab.)	E_d = 5.25 MeV		E_d = 5.50 MeV	
	Angle (C.M.)	$\frac{d\sigma}{d\Omega}$ (mb/sr)	Angle (C.M.)	$\frac{d\sigma}{d\Omega}$ (mb/sr)
30.0	33.3	-- --	33.2	1.85 ± 0.1
35.0	38.7	1.50 ± 0.1	38.7	-- --
40.0	44.2	1.29 ± 0.08	44.1	1.81 ± 0.2
45.0	49.6	1.02 ± 0.08	49.5	1.74 ± 0.1
50.0	55.0	0.95 ± 0.09	54.9	1.78 ± 0.1
55.0	60.3	-- --	60.2	-- --
60.0	65.6	-- --	65.5	1.07 ± 0.04
65.0	70.9	0.88 ± 0.04	70.8	1.32 ± 0.04
70.0	76.1	0.83 ± 0.04	76.0	1.28 ± 0.05
75.0	81.3	0.80 ± 0.05	81.2	1.21 ± 0.04
80.0	86.4	0.86 ± 0.05	86.3	1.42 ± 0.07
85.0	91.5	0.96 ± 0.04	91.4	1.43 ± 0.06
90.0	96.5	0.97 ± 0.05	96.4	1.53 ± 0.07
95.0	101.5	1.01 ± 0.03	101.4	1.65 ± 0.04
100.0	106.4	1.18 ± 0.05	106.3	1.72 ± 0.04
105.0	111.3	1.21 ± 0.05	111.2	1.88 ± 0.05
110.0	116.1	1.30 ± 0.05	116.0	1.99 ± 0.06
115.0	120.9	1.47 ± 0.06	120.8	-- --
120.0	125.6	-- --	125.5	-- --
125.0	130.3	0.85 ± 0.05	130.2	2.19 ± 0.09
130.0	135.0	-- --	134.9	1.97 ± 0.05
135.0	139.6	-- --	139.5	2.14 ± 0.04
140.0	144.2	1.37 ± 0.05	144.1	2.08 ± 0.04
145.0	148.7	1.43 ± 0.05	148.7	2.19 ± 0.04
150.0	153.2	1.41 ± 0.05	153.2	2.01 ± 0.05
155.0	157.7	1.38 ± 0.06	157.7	2.09 ± 0.05
160.0	162.2	1.47 ± 0.07	162.2	2.03 ± 0.05
165.0	166.7	1.38 ± 0.06	166.6	2.01 ± 0.05
170.0	171.1	1.21 ± 0.06	171.1	2.00 ± 0.05

$^{16}O(d,p)^{17}O$ (3.846 MeV)

Angle (lab.)	E_d = 6.00 MeV	
	Angle (C.M.)	$\frac{d\sigma}{d\Omega}$ (mb/sr)
35.0	38.6	1.05 ± 0.2
40.0	44.0	-- --
45.0	49.4	0.63 ± 0.07
50.0	54.8	-- --
55.0	60.1	-- --
60.0	65.4	1.58 ± 0.09
65.0	70.6	1.54 ± 0.09
70.0	75.9	1.73 ± 0.08
75.0	81.0	1.56 ± 0.07
80.0	86.1	1.98 ± 0.08
85.0	91.2	1.86 ± 0.08
90.0	96.2	2.24 ± 0.05
95.0	101.2	-- --
100.0	106.1	-- --
105.0	111.0	-- --
110.0	115.8	2.38 ± 0.04
115.0	120.6	2.26 ± 0.04
120.0	125.4	2.18 ± 0.04
125.0	130.1	2.37 ± 0.02
130.0	134.8	2.19 ± 0.04
135.0	139.4	2.15 ± 0.04
140.0	144.0	1.86 ± 0.04
145.0	148.6	1.91 ± 0.04
150.0	153.1	1.81 ± 0.04
155.0	157.6	1.61 ± 0.04
160.0	162.1	1.51 ± 0.04

APPENDIX B

There are 2 parts to Appendix B. In part I, the meanings of some terms used frequently in the thesis are given. The purpose is not to give a formal definition of concepts, but to present pictorial ideas suitable for the non-specialist who might happen to read this thesis. In part II of appendix B, a list of the more common symbols is given.

Part I Glossary

(i) Optical Model

The optical model is an attempt to describe the gross features of the interaction of an incident particle with a target nucleus without reference to the internal structure of either object. The name "optical" is used because small particles are frequently observed to have wavelike properties, and thus the behaviour of the scattered particle is somewhat analogous to the scattering of light from a translucent sphere. Some light is reflected at the surface; some is absorbed; some is refracted, and some is diffracted around the sphere. In the cases of medium weight and heavy nuclei, the effects of individual nucleons in the nucleus are not usually of great importance, and the model is amazing useful for systematizing large bodies of data. For lighter nuclei, there are more problems in the application of the optical model, but it is still a very useful tool.

(ii) Direct Interaction

A direct interaction is any type of interaction that proceeds primarily as a one step process. That is, the initial state of the system (target nucleus plus incident particle) passes immediately to the final state (residual nucleus plus outgoing particle) without passing through any well defined intermediate state. The reactions are thus among the simplest of nuclear reactions, and there is some hope of performing calculations which give a fairly accurate account of what is actually happening. The single step nature of the interaction also implies that the reactions proceed quite quickly - in about 10^{-22} seconds.

(iii) Stripping Reaction

This is a special type of direct interaction in which the target nucleus captures part of the incident particle but not all of it. The remainder of the incident particle simply passes by the target, and leaves the vicinity without causing further major effects on the nucleus. Thus there are two types of stripping reactions possible with deuterons. In one, the proton is captured and the neutron escapes, and in the other, the neutron is captured while the proton escapes.

(iv) ℓ-value

Angular momentum is frequently exchanged between the incident particle and target nucleus in a reaction. In the case of direct interactions, the number of units of orbital angular momentum exchanged is known as the ℓ-value. In stripping reactions, the shape of the angular distribution of the outgoing

particles is quite dependent on the ℓ-value of the reaction, and hence, the ℓ-value is easily measured in many cases. Since the parity change between the target nucleus and residual nucleus is $(-1)^{\ell}$, the parity of levels in the residual nucleus is easily measured in many cases.

(v) Spectroscopic Factor

The structure of a nucleus may be considered as the superposition of a number of substructures or configurations. There is thus a certain probability of finding the nucleus with a given configuration as opposed to the many others available to it. A particularly simple substructure is that in which the nucleus looks like a single nucleon orbiting about an inert core. The probability of this type of substructure appearing is known as the spectroscopic factor.

(vi) Compound Nucleus

In some interactions, the entire incident particle is absorbed into the target nucleus. (c.f. stripping reaction). The nucleus consisting of the combined target nucleus and incident particle is known as the compound nucleus. The name is usually restricted to cases in which the compound nucleus subsequently decays by emitting another particle as opposed to a γ-ray. Reactions producing a compound nucleus occur much more slowly than do direct interactions, because the compound nucleus usually requires a relatively long time to decay (10^{-15} to 10^{-20} seconds).

Part II List of Common Symbols Used

a_I	diffuseness parameter of the absorptive well.
a_R	diffuseness parameter of the real well.
a_{SO}	diffuseness parameter of the spin-orbit well.
$C(\varepsilon)$	the autocorrelation function measured as a function of ε.
CN	compound nucleus reaction. Used mainly as a subscript.
D	direct interaction. Used mainly as a subscript.
DWBA	Distorted wave Born approximation. Used in the study of direct interactions in this work.
E	energy of the incident particle.
E_d	incident deuteron energy.
E_x	excitation energy of a level.
exp	experimental. Used as a subscript.
$G(\sigma_1,\sigma_2,\varepsilon)$	the group cross correlation function.
HF	Hauser-Feshbach. Applies to compound nucleus calculations.
I	spin of the target nucleus.
I'	spin of the residual nucleus.
i	spin of the incident particle.
i'	spin of the outgoing particle.
N	the fluctuation damping coefficient.
R(e,E)	instrumental resolution in the analysis of the thick target data. It is also the peak shape of a monoenergetic neutron group of energy e.
r_I	radius parameter of the absorptive well.
r_R	radius parameter of the refractive well.

r_{SO}	radius parameter of the spin-orbit well.
T(E)	the "true" yield curve as measured with a bombarding energy E.
tot	total. Usually used as a subscript.
V	depth of the refractive well.
$V_c(r)$	the Coulomb potential surrounding the nucleus.
V_{pn}	the neutron-proton interaction potential.
V_{SO}	depth of the spin-orbit well.
W_S	depth of the surface-peaked absorptive well.
W_V	depth of the volume absorptive well.
Γ	coherence energy of a yield curve.
γ_d	ratio of the direct interaction cross section to the total cross section for a specific reaction.
ε	in the calculation of the correlation function, the energy difference between energies at which the cross section is compared to its mean value.
σ	the cross section. It is frequently used with the subscripts D, CN etc. to denote the cross section of a particular component of the reaction.